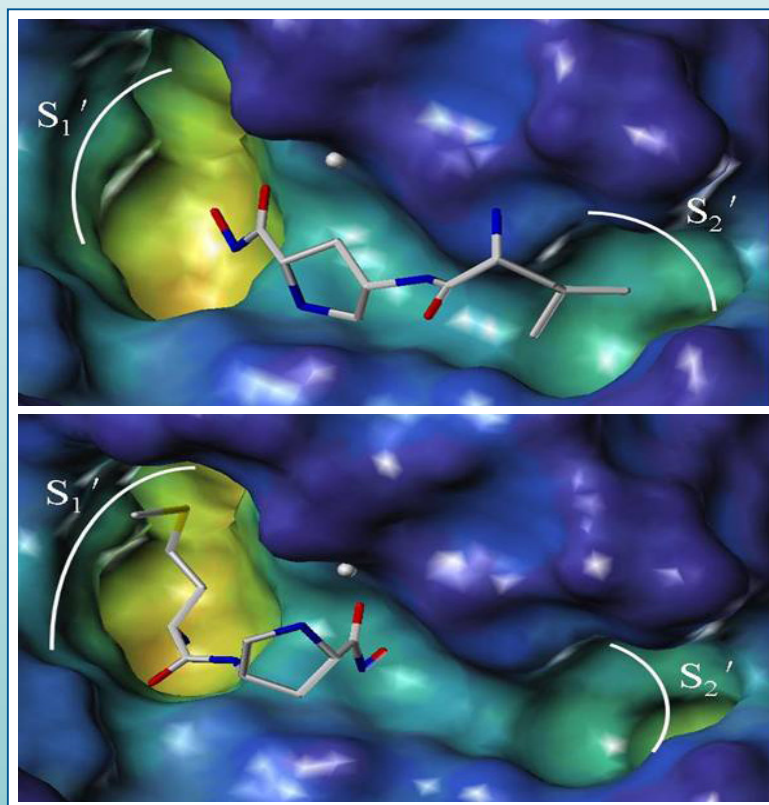


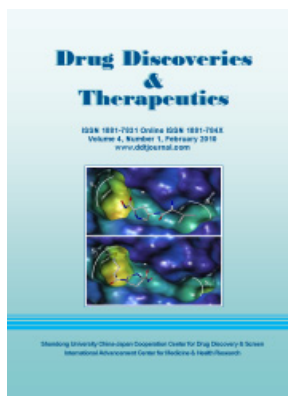
Drug Discoveries & Therapeutics

ISSN 1881-7831 Online ISSN 1881-784X
Volume 4, Number 1, February 2010
www.ddtjournal.com



Shandong University China-Japan Cooperation Center for Drug Discovery & Screen
International Advancement Center for Medicine & Health Research

Drug Discoveries & Therapeutics



Editor-in-Chief:

Kazuhisa SEKIMIZU
(The University of Tokyo, Tokyo, Japan)

Associate Editor:

Norihiro KOKUDO
(The University of Tokyo, Tokyo, Japan)

Drug Discoveries & Therapeutics is a peer-reviewed international journal published bimonthly by *Shandong University China-Japan Cooperation Center for Drug Discovery & Screen* (SDU-DDSC) and *International Advancement Center for Medicine & Health Research Co., Ltd.* (IACMHR Co., Ltd.).

Drug Discoveries & Therapeutics mainly publishes articles related to basic and clinical pharmaceutical research such as pharmaceutical and therapeutical chemistry, pharmacology, pharmacy, pharmacokinetics, industrial pharmacy, pharmaceutical manufacturing, pharmaceutical technology, drug delivery, toxicology, and traditional herb medicine. Studies on drug-related fields such as biology, biochemistry, physiology, microbiology, and immunology are also within the scope of this journal.

Subject Coverage: Basic and clinical pharmaceutical research including Pharmaceutical and therapeutical chemistry, Pharmacology, Pharmacy, Pharmacokinetics, Industrial pharmacy, Pharmaceutical manufacturing, Pharmaceutical technology, Drug delivery, Toxicology, and Traditional herb medicine.

Language: English

Issues/Year: 6

Published by: IACMHR and SDU-DDSC

ISSN: 1881-7831 (Online ISSN 1881-784X)

CODEN: DDTRBX

Editorial and Head Office

Wei TANG, MD PhD
Executive Editor
Drug Discoveries & Therapeutics

TSUIN-IKIZAKA 410,
2-17-5 Hongo, Bunkyo-ku,
Tokyo 113-0033, Japan.
Tel: 03-5840-9697
Fax: 03-5840-9698
E-mail: office@ddtjournal.com
URL: www.ddtjournal.com



Drug Discoveries & Therapeutics

Editorial Board

Editor-in-Chief:

Kazuhisa SEKIMIZU (*The University of Tokyo, Tokyo, Japan*)

Associate Editor:

Norihiro KOKUDO (*The University of Tokyo, Tokyo, Japan*)

Executive Editor:

Wei TANG (*The University of Tokyo, Tokyo, Japan*)

Managing Editor:

Munehiro NAKATA (*Tokai University, Kanagawa, Japan*)

Web Editor:

Yu CHEN (*The University of Tokyo, Tokyo, Japan*)

English Editors:

Curtis BENTLEY (*Roswell, GA, USA*)

Thomas R. LEBON (*Los Angeles Trade Technical College, Los Angeles, CA, USA*)

China Office:

Wenfang XU (*Shandong University, Shandong, China*)

Editorial Board Members:

Yoshihiro ARAKAWA (<i>Tokyo, Japan</i>)	Yuxiu LIU (<i>Nanjing, China</i>)
Santad CHANPRAPAPH (<i>Bangkok, Thailand</i>)	Hongxiang LOU (<i>Jinan, China</i>)
Fen-Er CHEN (<i>Shanghai, China</i>)	Ken-ichi MAFUNE (<i>Tokyo, Japan</i>)
Zhe-Sheng CHEN (<i>Queens, NY, USA</i>)	Norio MATSUKI (<i>Tokyo, Japan</i>)
Zilin CHEN (<i>Wuhan, China</i>)	Tohru MIZUSHIMA (<i>Kumamoto, Japan</i>)
Guanhua DU (<i>Beijing, China</i>)	Abdulla M. MOLOKHIA (<i>Alexandria, Egypt</i>)
Chandradhar DWIVEDI (<i>Brookings, SD, USA</i>)	Masahiro MURAKAMI (<i>Osaka, Japan</i>)
Mohamed F. EL-MILIGI (<i>Cairo, Egypt</i>)	Yoshinobu NAKANISHI (<i>Ishikawa, Japan</i>)
Harald HAMACHER (<i>Tuebingen, Germany</i>)	Yutaka ORIHARA (<i>Tokyo, Japan</i>)
Hiroshi HAMAMOTO (<i>Tokyo, Japan</i>)	Xiao-Ming OU (<i>Jackson, MS, USA</i>)
Xiaojiang HAO (<i>Kunming, China</i>)	Weisan PAN (<i>Shenyang, China</i>)
Waseem HASSAN (<i>Santa Maria, RS, Brazil</i>)	Rakesh P. PATEL (<i>Gujarat, India</i>)
Langchong HE (<i>Xi'an, China</i>)	Shafiqur RAHMAN (<i>Brookings, SD, USA</i>)
David A. HORNE (<i>Duarte, CA, USA</i>)	Shivanand P. PUTHLI (<i>Mumbai, India</i>)
Yongzhou HU (<i>Hangzhou, China</i>)	Adel SAKR (<i>Cincinnati, OH, USA</i>)
Wei HUANG (<i>Shanghai, China</i>)	Abdel Aziz M. SALEH (<i>Cairo, Egypt</i>)
Yu HUANG (<i>Hong Kong, China</i>)	Tomofumi SANTA (<i>Tokyo, Japan</i>)
Hans E. JUNGINGER (<i>Phitsanulok, Thailand</i>)	Yasufumi SAWADA (<i>Tokyo, Japan</i>)
Amrit B. KARMARKAR (<i>Mumbai, India</i>)	Brahma N. SINGH (<i>Commack, NY, USA</i>)
Toshiaki KATADA (<i>Tokyo, Japan</i>)	Hongbin SUN (<i>Nanjing, China</i>)
Gagan KAUSHAL (<i>Charleston, WV, USA</i>)	Benny K. H. TAN (<i>Singapore, Singapore</i>)
Ibrahim S. KHATTAB (<i>Safat, Kuwait</i>)	Renxiang TAN (<i>Nanjing, China</i>)
Hiromichi KIMURA (<i>Tokyo, Japan</i>)	Chandan M. THOMAS (<i>Bradenton, FL, USA</i>)
Shiroh KISHIOKA (<i>Wakayama, Japan</i>)	Murat TURKOGLU (<i>Istanbul, Turkey</i>)
Kam Ming KO (<i>Hong Kong, China</i>)	Zhengtao WANG (<i>Shanghai, China</i>)
Nobuyuki KOBAYASHI (<i>Nagasaki, Japan</i>)	Stephen G. WARD (<i>Bath, UK</i>)
Toshiro KONISHI (<i>Tokyo, Japan</i>)	Takako YOKOZAWA (<i>Toyama, Japan</i>)
Masahiro KUROYANAGI (<i>Hiroshima, Japan</i>)	Liangren ZHANG (<i>Beijing, China</i>)
Chun Guang LI (<i>Victoria, Australia</i>)	Jianping ZUO (<i>Shanghai, China</i>)
Hongmin LIU (<i>Zhengzhou, China</i>)	
Jikai LIU (<i>Kunming, China</i>)	

(as of February 26, 2010)

Brief Report

- 1 - 4** **The direct PAK1 inhibitor, TAT-PAK18, blocks preferentially the growth of human ovarian cancer cell lines in which PAK1 is abnormally activated by autophosphorylation at Thr 423.**
Hisashi Hashimoto, Tamotsu Sudo, Hiroshi Maruta, Ryuichiro Nishimura

Original Articles

- 5 - 12** **Design, synthesis, and primary activity evaluation of pyrrolidine derivatives as matrix metalloproteinase inhibitors.**
Jian Zhang, Xun Li, Huawei Zhu, Qiang Wang, Jinhong Feng, Jiajia Mou, Yonggang Li, Hao Fang, Wenfang Xu
- 13 - 18** **Hypotensive response in rats and toxicological mechanisms induced by shuanghuanglian, an herbal extract mixture.**
Huaishan Wang, Fang Cheng, Yanqiu Shi, Zhonggang Li, Huidi Qin, Zhaoping Liu
- 19 - 25** ***In vitro* modulating effects of glutathione on vascular tension and involvement of extracellular calcium.**
Nattaya Chaothanaphat, Prasan Dhumma-Upakorn, Suree Jianmongkol
- 26 - 32** **Evaluation of *in vitro* dissolution profile comparison methods of sustained release tramadol hydrochloride liquisolid compact formulations with marketed sustained release tablets.**
Amrit B. Karmarkar, Indrajeet D. Gonjari, Avinash H. Hosmani, Pandurang N. Dhabale
- 33 - 43** **Formulation and evaluation of clotrimazole from pluronic F₁₂₇ gels.**
Boushra M. El-Houssieny, Hayam M. Hamouda
- 44 - 53** **Exposure-response modeling and clinical trial simulation of the effect of tolterodine on QT intervals in healthy volunteers.**
Kevin R. Sweeney, Marc R. Gastonguay, Lisa Benincosa, Carol L. Cronenberger, Paul Glue, Bimal K. Malhotra

CONTENTS

(Continued)

Guide for Authors

Copyright

Brief Report

The direct PAK1 inhibitor, TAT-PAK18, blocks preferentially the growth of human ovarian cancer cell lines in which PAK1 is abnormally activated by autophosphorylation at Thr 423

Hisashi Hashimoto^{1,2}, Tamotsu Sudo¹, Hiroshi Maruta^{3,*}, Ryuichiro Nishimura¹

¹Hyogo Cancer Center, Akashi, Hyogo, Japan;

²Ehime University Medical School, Ehime, Japan (Present address);

³NF Cure Japan, Melbourne, Australia.

ABSTRACT: So far no effective therapeutic has been developed for the FDA-approved treatment of ovarian cancer patients. Recently we provided the first evidence indicating that an old antibiotic (anti-parasitic drug) called Ivermectin suppresses the growth of a variety of human ovarian cancer cell lines *in vitro* by inactivating the oncogenic kinase PAK1 somehow (Hashimoto H, *et al. Drug Discov Ther.* 2009; 3:243-246). This kinase is now known to be essential for the growth of more than 70% of all human cancers including breast, prostate, pancreatic, colon, gastric, lung, cervical, thyroid cancers as well as hepatoma, glioma, melanoma, MM (multiple myeloma) and NF (neurofibromatosis) tumors. In this study, using the cell-permeable PAK1-inactivating peptide TAT-PAK18 which blocks the essential PAK1-PIX interaction, we examined the relationship between the sensitivity of ovarian cancer cell lines to this anti-PAK1 peptide and the protein expression/autophosphorylation levels of PAK1 in these cell lines, and found that the more PAK1 is abnormally activated (autophosphorylated at Thr 423), the more their growth is sensitive to this peptide, regardless of their PAK1 expression levels. This observation provides the first direct evidence that ovarian cancers also belong to the PAK1-dependent cancers which represent more than 70% of all human cancers, suggesting that anti-PAK1 drugs would be effective therapeutics for ovarian cancers.

Keywords: TAT-PAK18, PAK1, ovarian cancer, PIX, autophosphorylation

1. Introduction

Among female-specific cancers, breast, ovarian and

cervical cancers are the major three that cause the death of many cancer patients world-wide. Around 75% of breast cancers require estrogen for their growth, and the remaining 25% appears to be estrogen-independent. Thus, in the past the former estrogen-dependent breast cancers have been treated by an estrogen antagonist called Tamoxifen (Tam) with a relatively great success. However, after a prolonged treatment, these breast cancers become Tam-resistant, mainly because the kinase PAK1 is abnormally activated (1). We have shown that the growth of these Tam-resistant breast cancers as well as estrogen-independent breast cancers can be almost completely suppressed by anti-PAK1 drugs such as FK228 and combination of AG 879/GL-2003 and PP1 (2,3) *in vivo* (human cancer xenografts in mice). Similarly, the growth of human ovarian cancer cell lines can be suppressed with FK228, a potent HDAC (histone deacetylase) inhibitor, that eventually inactivates PAK1 (2), at least in cell culture (4), suggesting that some of ovarian cancers require the kinase PAK1 for their growth. However, none of these anti-PAK1 drugs are available on the market as yet. Moreover, Tam is known to be effective in suppressing the growth of only 10% of chemotherapeutics (DNA/MT poisons)-resistant ovarian cancers (5), suggesting that the remaining 90% of these ovarian cancers no longer depend on estrogen for their growth.

Thus, we recently identified a few anti-PAK1 products among those which are already available on the market. One of them is the CAPE (caffeic acid phenethyl ester)-based extract of NZ (New Zealand) propolis called Bio 30. CAPE and a few other anti-cancer ingredients in Bio 30 synergistically work to suppress very strongly the PAK1-dependent growth of breast and pancreatic cancers as well as NF (neurofibromatosis) tumors and glioma *in vivo* (xenografts in mice) (6,7). Another is Ivermectin, an old antibiotic which has been used as a potent anti-parasitic drug that kills mainly the intestinal worms (nematodes) by inhibiting their GABA receptor, but not mammalian counterparts (8). Recently we demonstrated that Ivermectin inactivates the kinase PAK1 in a variety of

*Address correspondence to:

Dr. Hiroshi Maruta, NF Cure Japan, 14 Curtin Avenue, Brunswick West, Australia 3055.

e-mail: julie8860@gmail.com

human ovarian cancer cell lines somehow, and blocks their growth (9), confirming that many ovarian cancers also require this kinase for their growth. However, their sensitivity to Ivermectin varies from one cancer cell line to another for an unknown reason, and the growth of normal cells is not inhibited by this drug at all (9). Interestingly, in many human ovarian cancer cells the PAK1 gene expression was found to be amplified along with a few other genes on 11q13 locus (10,11). In general, however, over-expression of PAK1 protein is a very rare event in human cancers, except for breast and ovarian cancers. In more than 70% of cancer cases, the kinase activity PAK1 is abnormally elevated instead, through the activation of upstream oncogenic signal transducers such as RAS, without any mutation on PAK1 gene itself.

In this study, using one of the direct PAK1 inhibitors called TAT-PAK18 which blocks the PAK1-PIX interaction essential for the PAK1 activation (12,13), we examined the possible relationship between the sensitivity of human ovarian cancer cell lines to TAT-PAK18 and PAK1 expression/its autophosphorylation (at Thr 423) levels, as TAT-PAK18 has been shown to block the autophosphorylation of PAK1 at Thr 423 (14), and inactivate this kinase both *in vitro* and *in vivo* (13,14).

2. Materials and Methods

2.1. Reagents

The peptide TAT-PAK18 (sequence: RKKRRQRRR-G-PPVIAPRPEHTKSVYTRS) was custom-synthesized by Calbiochem. This PAK1-inactivating peptide was synthesized by coupling the specific PAK1 kinase inhibitory domain of 18 amino acids (called PAK18), which blocks the PAK1-PIX interaction (12,13), to a cell-permeable highly basic peptide vector of 9 amino acids called TAT (14,15) through the linker Gly (G).

2.2. Cell lines

Human ovarian cancer cell lines TYK-nu, HTOA, SKOV3, RMUG-S and the control immortalized non-cancerous ovarian surface epithelial cell line HOSE were maintained in DMEM/F12 (Invitrogen, Carlsbad, CA, USA), supplemented with 10% fetal bovine serum and 1% penicillin/streptomycin (Invitrogen), under the standard culture conditions.

2.3. Immuno blot analysis

For whole-cell lysates, samples were lysed in RIPA buffer (20 mM Tris-HCl, pH 7.5, containing 150 mM NaCl, 1 mM Na₂EDTA, 1 mM EGTA, 1% NP-40, 1% sodium deoxycholate, 2.5 mM sodium pyrophosphate, 1 mM beta-glycerophosphate, 1 mM Na₃VO₄, 1 µg/mL

leupeptin, and 1 mM PMSF). Protein samples were separated on 8% SDS-polyacrylamide gels (PAGE) and then transferred to polyvinylidene difluoride. Membranes were probed with antibodies to PAK1, phospho-PAK1 Thr 423, and p-Raf1 (Ser 338) (each diluted at 1:1,000, from Cell Signaling Technology, Danvers, MA, USA) as well as to β-actin (diluted at 1:500, from Santa Cruz Biotechnology, Santa Cruz, CA, USA) overnight at 4°C. After extensive washing with PBS containing 0.1% Tween 20, horseradish peroxidase-conjugated secondary antibodies (Santa Cruz Biotechnology) were used at dilutions of 1:5,000. Proteins were visualized using enhanced chemiluminescence and were normalized to β-actin.

2.4. Cell viability (MTT) assay

2×10^3 cells of each cancer cell line seeded per well were treated with varying concentrations of TAT-PAK18 (0.1-100 µM) for 72 h. Then cells were incubated at 37°C with 1 mg/mL MTT reagent (Sigma, St. Louis, MO, USA) for 3 h. Spectrophotometric absorbance of the samples was determined by the Ultra Multifunctional Microplate Reader (Tecan, Durham, NC, USA) at 595 nm.

2.5. Assay for kinase activity of PAK1 (p-Raf1 levels)

Since the Ser 338 of the kinase Raf1 is the major site to be phosphorylated by PAK1, the kinase activity of PAK1 in cells was routinely monitored by measuring the p-Raf1 level (phosphorylated at Ser 338) through the immuno-blot with the antibody against p-Raf1, which is far more sensitive and direct than measuring the p-PAK1 level (phosphorylated at Thr 423), after culturing the cancer cell lines such as RMUG-S in the presence of TAT-PAK18 (0.1-100 µM) or absence for 48 h as described previously (9).

3. Results and Discussion

3.1. PAK1 expression levels and autophosphorylation at Thr 423 in human ovarian cancer cell lines compared with those in the control non-cancerous cell line

Using the antibody against PAK1, we found that two cancer cell lines HTOA and SKOV3 express the PAK1 protein at a similar level to the non-cancerous cell line HOSE, while the cell line TYK-nu expresses at the significantly lower PAK1 level, and we could hardly detect the expression of PAK1 in the cancer cell line RMUG-S (see Figure 1, top row), although a much longer exposure of the immuno-blot revealed that RMUG-S cells indeed express PAK1, but only a very low level (data not shown). Interestingly, however, using the antibody against p-PAK1 (autophosphorylated at Thr 423), we could detect the p-PAK1 in only in the

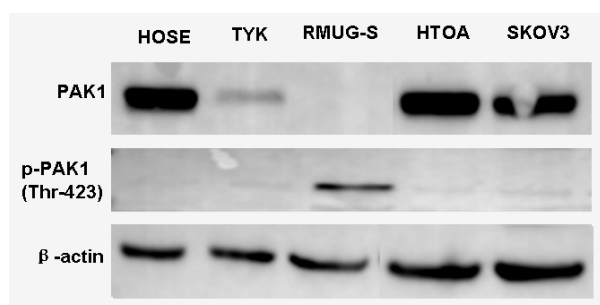


Figure 1. PAK1 protein/autophosphorylation levels in human ovarian cancer cell lines. PAK1 and p-PAK1 (autophosphorylated at Thr 423) levels in human ovarian cancer cell lines were compared with those in the control non-cancerous ovarian cell line (HOSE), using antibodies against PAK1 and p-PAK1, respectively, as described under "Materials and Methods". Only in RMUG-S cancer cells, PAK1 is autophosphorylated (abnormally activated).

cancer cell line RMUG-S, and none in the remaining cancer cell lines and the control non-cancerous cell line (see Figure 1, second row), clearly indicating that among these five human ovarian cell lines, only in RMUG-S cells, PAK1 is autophosphorylated at Thr 423 (abnormally activated), despite the fact that PAK1 (protein) is unexpectedly hypo-expressed in this cancer cell line.

3.2. Sensitivity of ovarian cancer cell lines to TAT-PAK18 in their growth

Although TAT-PAK18 inhibited the growth of all four cancer cell lines, RMUG-S was the most sensitive to this anti-PAK1 peptide (the IC_{50} was lower than 10 μ M), and the IC_{50} of the remaining three cancer cell lines appears to be more than 10 times higher (above 100 μ M) (see Figure 2).

3.3. TAT-PAK18 inhibits the kinase activity of PAK1 in RMUG-S cells

To prove that the effect of TAT-PAK18 on the growth of RMUG-S cell line is mainly due to its inactivation of the autophosphorylated PAK1, we have examined the effect of this peptide (0.1-100 μ M) on the kinase activity of PAK1 in this cell line by monitoring the p-Raf1 (Ser 338) level. As shown in Figure 3, this direct PAK1 inhibitor clearly inactivates the PAK1 in RMUG-S cells around a range of its concentrations (1-10 μ M) which strongly inhibit their growth.

These observations altogether suggest that the more PAK1 is abnormally activated, the more their growth is sensitive to TAT-PAK18. Since unlike FK228 and Ivermectin, TAT-PAK18 both selectively and directly inactivates PAK1, this finding provides the first direct evidence that ovarian cancers also require the kinase PAK1 for their growth. Interestingly, the sensitivity

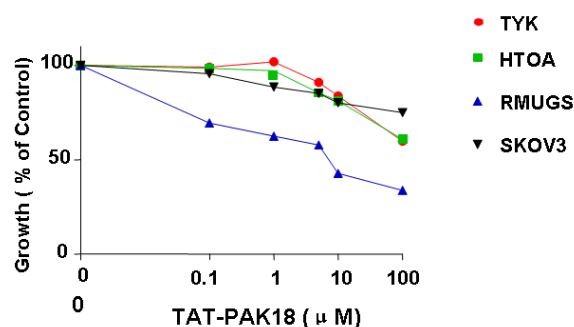


Figure 2. Sensitivity of ovarian cancer cell lines to TAT-PAK18 in their growth. Four ovarian cancer cell lines were treated with TAT-PAK18 at the indicated concentrations for 72 h, and their growth was monitored by MTT methods as described under "Materials and Methods". Among these cell lines, RMUG-S, in which PAK1 is abnormally activated, was the most sensitive to TAT-PAK18 in their growth.

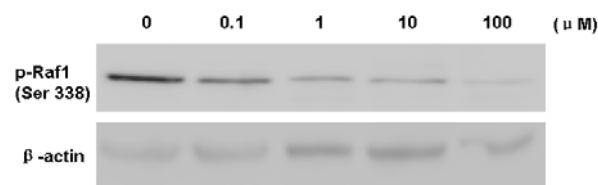


Figure 3. TAT-PAK18 down-regulates p-Raf1 level by inactivating PAK1 in RMUG-S cells. RMUG-S cells were treated with TAT-PAK18 at the indicated concentrations for 48 h, and the p-Raf1 (Ser 338) level was monitored by its antibody as described under "Materials and Methods".

of these cancer cell lines to another anti-PAK1 drug Ivermectin (9) is rather opposite to their sensitivity to TAT-PAK18. The IC_{50} of TYK-nu was around 5 μ M, while the IC_{50} of RMUG-S is around 20 μ M, in both their growth and the kinase activity of PAK1 (monitored by p-Raf1 levels). This might be partly due to the possibility that like FK228, Ivermectin might inactivate another oncogenic kinase called AKT, in addition to the kinase PAK1, perhaps by blocking directly their upstream kinase(s) such as PI-3 kinase. For like FK228, Ivermectin can suppress even the growth of ovarian cancer cell line SKOV3 (9), which is highly resistant to another natural anti-PAK1 drug called menaquinone-7 (vitamin K_2) from a Japanese traditional cuisine called "Natto" (a fermented sticky soy bean product), which does not inactivate AKT (16,17), mainly due to the abnormally activated AKT in this cancer cell line (18). It is also possible that Ivermectin inactivates PAK1 not by blocking its auto-phosphorylation at Thr 423 (= the PAK1-PIX interaction), but by blocking other signaling pathways leading to the PAK1 activation such as Tyrosine phosphorylation of PAK1 by another upstream kinase ETK (3,19).

We previously shown that a combination of two distinct anti-PAK1 drugs, AG 879/GL-2003 and PP1, which block the PAK1-ETK interaction and inactivate

Src family kinases, respectively, almost completely suppresses the PAK1-dependent growth of human pancreatic and breast cancer xenografts in mice, due to their synergy (3,13). In this context, it would be of great interest for us to examine in the future whether Ivermectin and TAT-PAK18 or a few other PAK1 autophosphorylation inhibitors such as CEP-1347, OSU-03012 and Artepillin C (ARC) from Brazilian green propolis (20-22) also show such a synergy to suppress the PAK1-dependent growth of human ovarian cancer xenografts in mice.

References

1. Rayala S, Molli P, Kumar R. Nuclear p21-activated kinase 1 in breast cancer packs off tamoxifen sensitivity. *Cancer Res.* 2006; 66:5985-5988.
2. Hirokawa Y, Arnold M, Nakajima H, Zalberg J, Maruta H. Signal therapy of breast cancers by the HDAC inhibitor FK228 that blocks the activation of PAK1 and abrogates the tamoxifen-resistance. *Cancer Biol Ther.* 2005; 4:956-960.
3. Hirokawa Y, Levitzki A, Lessene G, Baell J, Xiao Y, Zhu H, Maruta H. Signal therapy of human pancreatic cancer and NF1-deficient breast cancer xenograft in mice by a combination of PP1 and GL-2003, anti-PAK1 drugs (Tyr-kinase inhibitors). *Cancer Lett.* 2007; 245:242-251.
4. Khabele D, Son DS, Parl AK, Goldberg GL, Augenlicht LH, Mariadason JM, Rice VM. Drug-induced inactivation or gene silencing of class I histone deacetylases suppresses ovarian cancer cell growth: implications for therapy. *Cancer Biol Ther.* 2007; 6:795-801.
5. Tropé C, Marth C, Kaern J. Tamoxifen in the treatment of recurrent ovarian carcinoma. *Eur J Cancer.* 2000; 36 (Suppl 4):S59-S61.
6. Demestre M, Messerli SM, Celli N, Shahhossini M, Kluwe L, Mautner V, Maruta H. CAPE (caffeic acid phenethyl ester)-based propolis extract (Bio 30) suppresses the growth of human neurofibromatosis (NF) tumor xenografts in mice. *Phytother Res.* 2009; 23:226-230.
7. Messerli S, Li XN, Maruta H. Bio 30, the anti-PAK1 extract of NZ (New Zealand) propolis, blocks the growth of glioma from both adults and children grafted in mice. Submitted, 2010.
8. Wang CC, Pong SS. Actions of avermectin B1a on GABA nerves. *Prog Clin Biol Res.* 1982; 97:373-395.
9. Hashimoto H, Messerli SM, Sudo T, Maruta H. Ivermectin inactivates the kinase PAK1 and block the PAK1-dependent growth of human ovarian cancer and NF2 tumor cell lines. *Drug Discov Ther.* 2009; 3:243-246.
10. Xie D, Yang GF, Chen YQ, Jiang LF, Xiao LZ. Significance and mechanisms of overexpression of PAK1 gene in epithelial ovarian neoplasms. *Zhonghua Zhong Liu Za Zhi.* 2006; 28:911-914. (in Chinese)
11. Brown LA, Kalloger SE, Miller MA, Shih IeM, McKinney SE, Santos JL, Swenerton K, Spellman PT, Gray J, Gilks CB, Huntsman DG. Amplification of 11q13 in ovarian carcinoma. *Genes Chromosomes Cancer.* 2008; 47:481-489.
12. Obermeier A, Ahmed S, Manser E, Yen SC, Hall C, Lim L. PAK promotes morphological changes by acting upstream of Rac. *EMBO J.* 1998; 17:4328-4339.
13. He H, Hirokawa Y, Manser E, Lim L, Levitzki A, Maruta H. Signal therapy for RAS-induced cancers in combination of AG 879 and PP1, specific inhibitors for ErbB2 and Src family kinases, that block PAK activation. *Cancer J.* 2001; 7:191-202.
14. Zhao L, Ma QL, Calon F, Harris-White ME, Yang F, Lim GP, Morihara T, Ubeda OJ, Ambegaokar S, Hansen JE, Weisbart RH, Teter B, Frautschy SA, Cole GM. Role of PAK pathway defects in the cognitive deficits of Alzheimer disease. *Nat Neurosci.* 2006; 9:234-242.
15. Kiosses WB, Hood J, Yang S, Gerritsen ME, Cheresch DA, Alderson N, Schwartz MA. A dominant-negative p65 PAK peptide inhibits angiogenesis. *Circ Res.* 2002; 90:697-702.
16. Liu W, Nakamura H, Yamamoto T, Ikeda N, Saito M, Ohno M, Hara N, Imanishi H, Shimomura S, Yamamoto T, Sakai T, Nishiguchi S, Hada T. Vitamin K₂ inhibits the proliferation of HepG₂ cells by up-regulating the transcription of p21 gene. *Hepatol Res.* 2007; 37:360-365.
17. Shibayama-Imazu T, Sakairi S, Watanabe A, Aiuchi T, Nakajo S, Nakaya K. Vitamin K₂ selectively induced apoptosis in ovarian TYK-nu and pancreatic MIA PaCa-2 cells out of eight solid tumor cell lines through a mechanism different from geranylgeraniol. *J Cancer Res Clin Oncol.* 2003; 129:1-11.
18. Matei D, Chang DD, Jeng MH. Imatinib mesylate (Gleevec) inhibits ovarian cancer cell growth through a mechanism dependent on platelet-derived growth factor receptor alpha and Akt inactivation. *Clin Cancer Res.* 2004; 10:681-690.
19. He H, Hirokawa Y, Gazit A, Yamashita Y, Mano H, Kawakami Y, Kawakami, Hsieh CY, Kung HJ, Lessene G, Baell J, Levitzki A, Maruta H. The Tyr-kinase inhibitor AG879, that blocks the ETK-PAK1 interaction, suppresses the RAS-induced PAK1 activation and malignant transformation. *Cancer Biol Ther.* 2004; 3:96-101.
20. Nheu TV, He H, Hirokawa Y, Tamaki K, Florin L, Schmitz ML, Suzuki-Takahashi I, Jorissen RN, Burgess AW, Nishimura S, Wood J, Maruta H. The K252a derivatives, inhibitors for the PAK/MLK-kinase family, selectively block the growth of RAS transformants. *Cancer J.* 2002; 8:328-336.
21. Porchia LM, Guerra M, Wang YC, Zhang Y, Espinosa AV, Shinohara M, Kulp SK, Kirschner LS, Saji M, Chen CS, Ringel MD. OSU-03012, a celecoxib derivative, directly targets PAK. *Mol Pharmacol.* 2007; 72:1124-1131.
22. Messerli SM, Ahn MR, Kunimasa K, Yanagihara M, Tatefuji T, Hashimoto K, Mautner V, Uto Y, Hori H, Kumazawa S, Kaji K, Ohta T, Maruta H. Artepillin C (ARC) in Brazilian green propolis selectively blocks the oncogenic PAK1 signaling and suppresses the growth of NF tumors in mice. *Phytother Res.* 2009; 23:423-427.

(Received November 6, 2009; Accepted November 22, 2009)

Original Article

Design, synthesis, and primary activity evaluation of pyrrolidine derivatives as matrix metalloproteinase inhibitors

Jian Zhang, Xun Li, Huawei Zhu, Qiang Wang, Jinhong Feng, Jiajia Mou, Yonggang Li, Hao Fang, Wenfang Xu*

Department of Medicinal Chemistry, School of Pharmacy, Shandong University, Ji'nan, Shandong, China.

ABSTRACT: A series of novel pyrrolidine derivatives was designed, synthesized, and assayed to determine the derivatives' activity against matrix metalloproteinase-2 (MMP-2) and aminopeptidase N (APN)/CD13. Preliminary biological tests showed that most compounds inhibit MMP-2 in a highly selective manner compared to APN. Compounds 9d, 9e, and 9g had better inhibitory activity than LY52 and could be used as lead compounds in the future.

Keywords: Matrix metalloproteinase-2, aminopeptidase N, inhibitors, pyrrolidine derivatives, synthesis

1. Introduction

The matrix metalloproteinases (MMPs) are a family of zinc-dependent calcium-containing hydrolytic enzymes that play a crucial role in tissue remodeling and degradation of the extracellular matrix (ECM). More than 20 subfamily members have previously been identified, such as collagenases, stromelysins, gelatinases, and membrane-type MMPs (1,2). Under normal physiological conditions, MMPs are minimally expressed, while their over-expression can lead to a variety of pathological disorders. Among MMPs, MMP-2 has been considered as a potential therapeutic target for cancer due to its high correlation with tumor growth, invasion, and metastasis (2,3).

Recently, the high-resolution X-ray crystal structures of MMP-inhibitor complexes have increasingly been revealed (4). This structural information indicates that besides the conserved catalytic site of Zn²⁺ of the MMP-2 enzyme there are two hydrophobic domains, named the S₁' and S₂' pockets. The S₁' pocket, a deep and narrow channel, is the key domain, and the S₂' pocket is a

solvent-exposed cleft (5,6). In general, a typical inhibitor of MMPs consists of a "zinc-binding group (ZBG)" and a "backbone". In addition, at least one side chain has been reported to effectively interact with enzyme subsites such as the S₁' and S₂' pockets (7).

cis-2-Aminocyclohexylcarbamoylphosphonic acid (*cis*-ACCP; See Figure 1) was designed and synthesized as an efficient MMP inhibitor and can selectively block the proteolytic activity of MMP-2. *cis*-ACCP also significantly inhibited metastasis formation in a murine melanoma model and reduced both local tumor growth and metastasis formation in an orthotopic human prostate tumor model. Moreover, the introduction of amino groups into the molecule enhanced their zinc-binding effect and also improved their inhibitory potency by forming effective hydrogen bonds (8).

The current authors have been developing a pyrrolidine scaffold as an effective MMP inhibitor for many years. Most compounds such as LY52 (See Figure 1) substantially inhibit MMP-2 and display significant anti-cancer activity both *in vitro* and *in vivo* (9,10). Based on this finding, together with the fact that Hyp and Gly residues account for more than 60% of all amino acids in the primary structure of collagen (11), Hyp and Hyp-Gly residues were thus presumed to be the specific recognition sites for effective interaction with MMPs. Additionally, *trans*-*s*-hydroxy-*L*-proline is the main constituent of Hyp and Hyp-Gly residues, so amino acids fragments were introduced into the *trans*-*s*-hydroxy-*L*-proline scaffold to form a new integrated structural pattern (See Figure 1). The R₁ group would be hydroxamate, carboxylate, or ester functioning as an effective ZBG to chelate the active site of catalytic zinc ions. The R₂ group would be introduced with various amino acids as side chains that might occupy the S₁' or S₂' pocket, resulting in effective enzyme interaction.

2. Materials and Methods

2.1. Chemicals

All of the target compounds were designed and synthesized *via* the route shown in Scheme 1. Starting

*Address correspondence to:

Dr. Wenfang Xu, Department of Medicinal Chemistry, School of Pharmacy, Shandong University, 44 Wenhua Road, Ji'nan 250012, Shandong, China. e-mail: wfxu@yahoo.cn

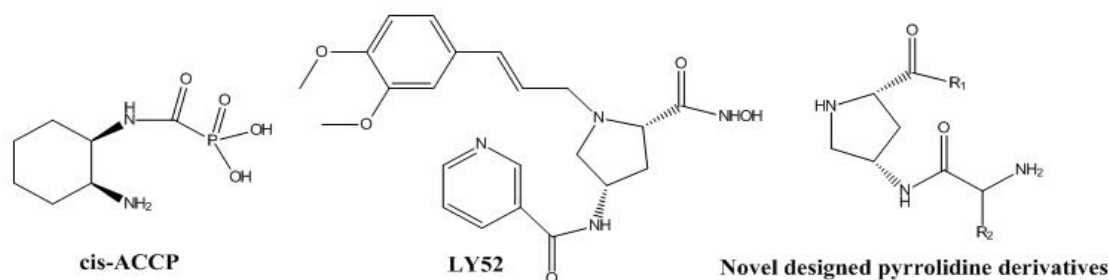
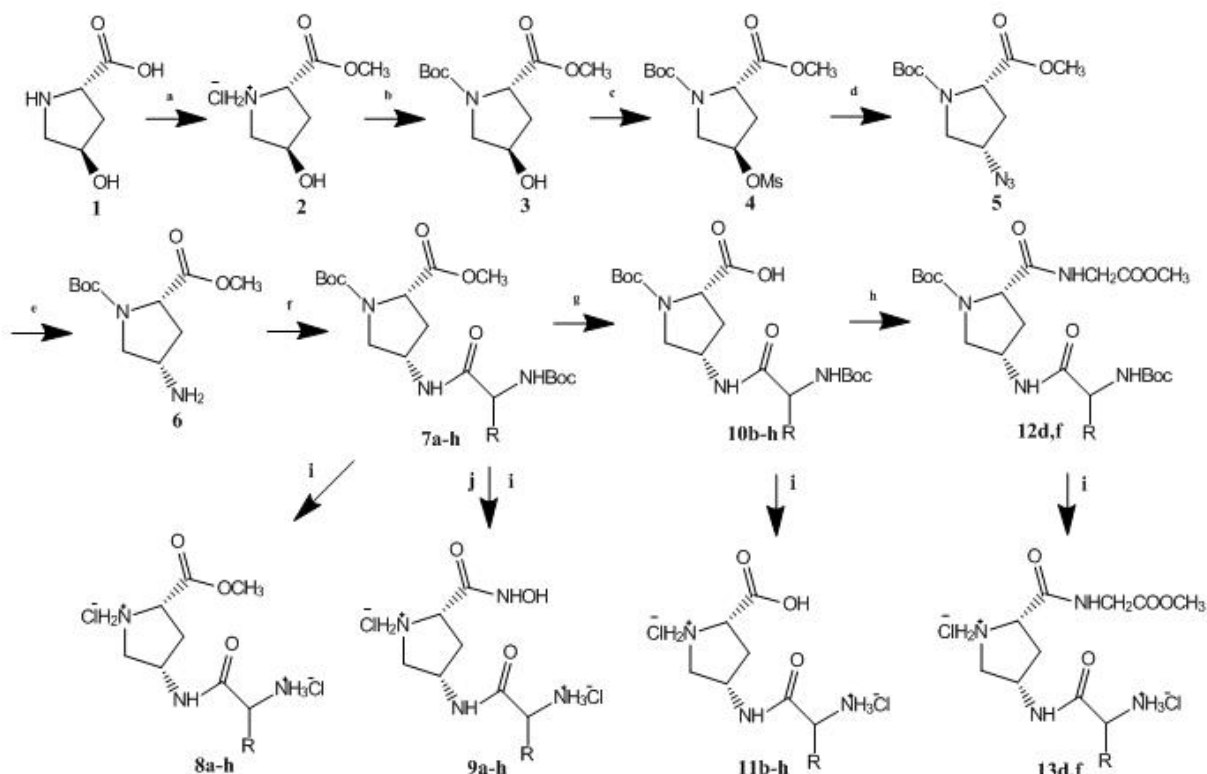


Figure 1. The structures of *cis*-ACCP, LY52, and novel designed pyrrolidine derivatives.



Scheme 1. Reagents and conditions: (a) MeOH, HCl; (b) (Boc)₂O, THF; (c) CH₃SO₂Cl; (d) NaN₃, DMF; (e) 10% Pd-C/H₂; (f) BocNH-CH(R)-COOH; (g) NaOH, CH₃OH/HCl; (h) NH₂CH₂COOCH₃; (i) HCl/EtOAc; (j) NH₂OK, MeOH.

with *trans*-4-hydroxy-L-proline (**1**), the important intermediate (*2S,4S*)-1-*tert*-butyl-2-methyl-4-aminopyrrolidine-1,2-dicarboxylate (**6**) was prepared by esterification, acylation, sulfonation, S_N2 nucleophilic substitution, and catalytic hydrogenation (12). The condensation of compound **6** with various amino acid residues led to compounds **7a-h**, which were directly de-protected or treated with NH₂OK in anhydrous methanol. Subsequent de-protection yielded the target compounds **8a-h** and **9a-h**. Some of the compounds that were selected from **7a-h** were hydrolyzed to obtain compounds **10b-h**, which were also de-protected to obtain the target compounds **11b-h**. Further coupling of compounds **11d** and **f** with glycine methyl ester yielded compounds **12d** and **f**, which were de-protected to

provide the target compounds **13d** and **f**.

2.2. MMP-2 inhibition assay

Gelatinase A (MMP-2) and trinitrobenzene sulfonic acid (TNBS) were purchased from Sigma, St Louis, MO, USA, and the substance was synthesized as described by Vijaykumar *et al.* (13). The pyrrolidine derivatives were assayed for inhibitory activity against MMP-2 in 96-well microtiter plates using succinylated gelatin as the substrate. The gelatinase, substance, and inhibitor were dissolved in sodium borate (pH 8.5, 50 mM) and incubated for 30 min at 37°C, and then 0.03% TNBS was added and the solution was incubated for another 20 min. The resulting solution was detected at a

wavelength of 450 nm to yield OD₄₅₀ values.

2.3. APN inhibition assay

IC₅₀ values against APN were determined using L-Leu-*p*-nitroanilide as the substrate and microsomal aminopeptidase (Sigma) as the enzyme in 50 mM PBS, pH 7.2, at 37°C. The hydrolysis of the substrate was monitored by following the changes in absorbance measured at 405 nm. All solutions of the inhibitors were prepared in the assay buffer, and the pH was adjusted to 7.5 by the addition of 0.1 M HCl or 0.1 M NaOH. All inhibitors were preincubated with APN for 30 min at 37°C. The assay mixture, which contained the inhibitor solution (with its concentration depending on the inhibitor), the enzyme solution (4 µg/mL final concentration), and the

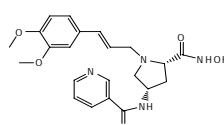
assay buffer, was adjusted to 200 µL.

3. Results and Discussion

All inhibition results are listed in **Table 1**. Similar to MMP-2, APN is also a zinc-dependant metalloproteinase involved in tumor invasion and metastasis. Thus, the assay was performed on both of MMP-2 and APN so as to identify the compounds' selectivity (13,14). **LY52** was used as the positive control.

The pyrrolidine derivatives exhibited better activity against MMP-2 than APN. For example, **9e** had an IC₅₀(APN)/IC₅₀(MMP-2) ratio of 365.46, while **9d** had one of 279.38. To a certain extent, the results confirmed the current strategy of designing effective MMP-2 inhibitors. MMP-2 is a zinc-dependent

Table 1. Compound structure and inhibitory activity against MMP-2 and APN

Compounds	R ₁	R ₂	IC ₅₀ /µM		IC ₅₀ (APN)/IC ₅₀ (MMP-2)
			MMP-2	APN	
8a	OCH ₃	H	54.32	2920.6	53.77
8b	OCH ₃	CH ₃	236.3	132.2	0.56
8c	OCH ₃	CH (CH ₃) ₂	402.7	1615	4.01
8d	OCH ₃	CH ₂ CH (CH ₃) ₂	94.1	317.4	3.37
8e	OCH ₃	CH(CH ₃)CH ₂ CH ₃	262.9	94.4	0.36
8f	OCH ₃	CH ₂ C ₆ H ₅	190.3	343	1.8
8g	OCH ₃	CH ₂ CH ₂ SCH ₃	214.7	1297.4	6.04
8h	OCH ₃	CH ₂ SH	160.5	295.2	1.84
9a	NHOH	H	26	758.1	29.16
9b	NHOH	CH ₃	407.6	92.6	0.23
9c	NHOH	CH (CH ₃) ₂	9.25	377	40.76
9d	NHOH	CH ₂ CH (CH ₃) ₂	4.8	1341	279.38
9e	NHOH	CH(CH ₃)CH ₂ CH ₃	1.83	668.8	365.46
9f	NHOH	CH ₂ C ₆ H ₅	110.6	1495.7	13.52
9g	NHOH	CH ₂ CH ₂ SCH ₃	3.8	317.1	83.45
9h	NHOH	CH ₂ SH	320	/	/
11b	COOH	CH ₃	33	404.4	12.25
11c	COOH	CH (CH ₃) ₂	86.1	1720	19.98
11d	COOH	CH ₂ CH (CH ₃) ₂	45.8	1651.6	36.06
11e	COOH	CH(CH ₃)CH ₂ CH ₃	22.8	1379.2	60.49
11f	COOH	CH ₂ C ₆ H ₅	149	90	0.60
11g	COOH	CH ₂ CH ₂ SCH ₃	332.9	83	0.25
11h	COOH	CH ₂ SH	1515	20.4	0.01
13d	NHCH ₂ COOCH ₃	CH ₂ CH (CH ₃) ₂	76.2	502	6.59
13f	NHCH ₂ COOCH ₃	CH ₂ C ₆ H ₅	16.8	2492.8	148.38
LY52			5.6	578.9	103.75

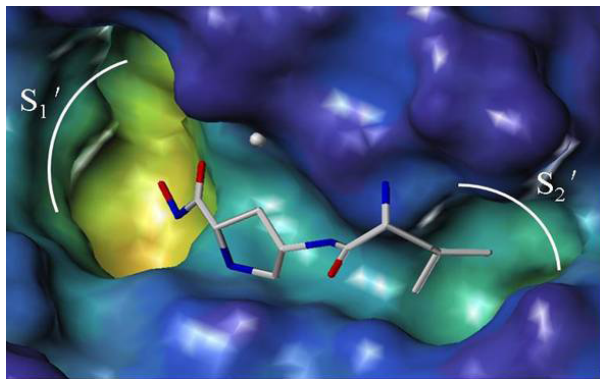


Figure 2. The FlexX Docking of Compound 9e with MMP-2.

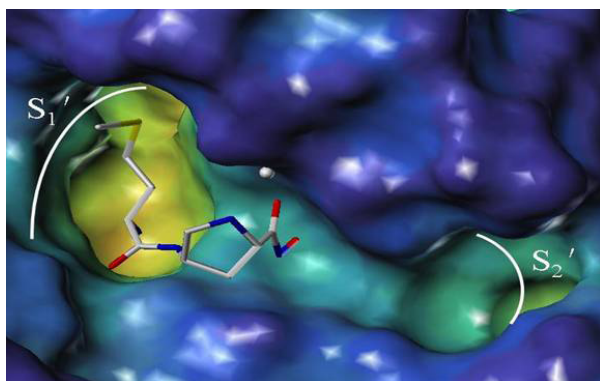


Figure 3. The FlexX Docking of Compound 9g with MMP-2.

endopeptidase that cleaved the peptide from its specific amino acid residue, while APN is a membrane-bound zinc exopeptidase that catalyzed the removal of NH₂-terminal amino acids from the peptide. The differences between the structures of the two enzymes lead to different requirements for their respective inhibitors. Therefore, these compounds are more suitable as MMP-2 inhibitors.

Compounds **9d**, **9e**, and **9g** were more potent MMP-2 inhibitors than the positive control **LY52**. The FlexX docking of compounds **9e** and **9g** with MMP-2 was done using Sybyl 7.0 from Tripos Inc. (St Louis, MO, USA), and the results are shown in Figures 2 and 3, respectively.

Compounds **9a-h** and **11b-h** were more potent than **8a-h**, which might be attributed to the ZBG (R₁). Hydroxamate, carboxylic acid, and carboxylate are the ZBGs for **9a-h**, **11b-h**, and **8a-h**, respectively, all of which chelate zinc ions in the center of the enzyme's catalytic activity. However, the hydroxamate and carboxylic acid groups were more potent ZBGs than carboxylate group, as shown in Table 1.

Compound **13f**, a tripeptide containing Hyp-Gly residues, displayed selective inhibitory activity against MMP-2 with an IC₅₀ (APN)/IC₅₀ (MMP-2) ratio of 148.38. The IC₅₀ (MMP-2) of **13f** was 16.8 μM, which is slightly higher than that of the positive control **LY52** (5.6 μM). The authors are presently working on tripeptides with Hyp-Gly residues in order to obtain more potent compounds.

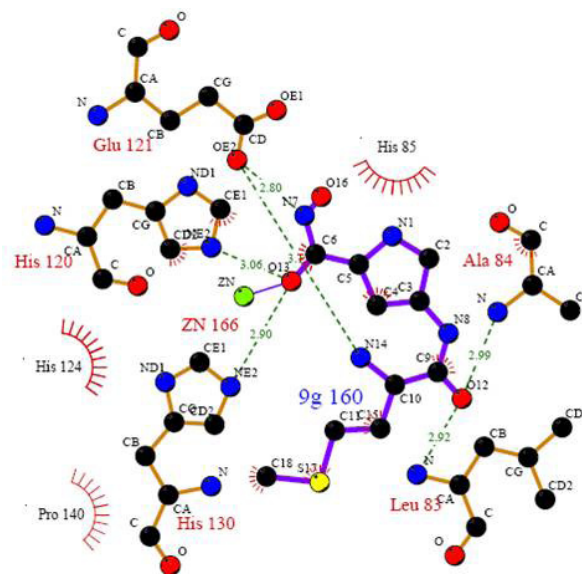


Figure 4. The docking result of **9g** with MMP-2 showed by LIGPLOT. Compound **9g** is shown in violet.

For a further and detailed understanding of the binding mode of **9g** with MMP-2, a 2D picture was also created with the program Ligplot. Hydrophobic and H-bond interactions were visualized between the inhibitor and the residues lining the active site of the protein. Significant hydrophobic interactions can be found between molecule **9g** and amino acid Ala⁸⁴, His¹²⁰ shown in Figure 4. H-bond interactions are formed between the OE2 of Glu¹²¹ and N7 and N14 of **9g**, the N of Leu⁸³ and Ala⁸⁴ and O12 of **9g**, and the NE2 of His¹²⁰, His¹³⁰, and O13 of **9g**.

4. Conclusion

In conclusion, a new series of pyrrolidine derivatives was synthesized as MMP-2 inhibitors. Most of the compounds showed potent activity and selectivity against MMP-2, and **9d**, **9e**, and **9g** in particular were more potent than the positive control **LY52**. Further assays of these compounds in cell cultures and animal models are underway and will be reported in the near future.

Acknowledgements

This work was supported by the National High-Tech Research and Development Program of China (863 project, Grant No. 2007AA02Z314), the National Natural Science Foundation of China (Grant Nos. 30772654 and 90713041), and the Doctoral Foundation of the Ministry of Education of the People's Republic of China (Grant No. 20060422029).

References

- Whittaker M, Floyd CD, Brown P, Gearing AJ. Design and therapeutic application of matrix metalloproteinase inhibitors. *Chem Rev.* 1999; 99:2735-2776.

2. Polette M, Nawrocki-Raby B, Gilles C, Clavel C, Birembaut P. Tumour invasion and matrix metalloproteinases. *Crit Rev Oncol Hematol*. 2004; 49:179-186.
3. Björklund M, Koivunen E. Gelatinase-mediated migration and invasion of cancer cells. *Biochim Biophys Acta*. 2005; 1755:37-69.
4. Rowsell S, Hawtin P, Minshull CA, Jepson H, Brockbank SM, Barratt DG, Slater AM, McPheat WL, Waterson D, Henney AM, Paupit RA. Crystal structure of human MMP9 in complex with a reverse hydroxamate inhibitor. *J Mol Biol*. 2002; 319:173-181.
5. Verma RP, Hansch C. Matrix metalloproteinases (MMPs): chemical-biological functions and (Q)SARs. *Bioorg Med Chem*. 2007; 15:2223-2268.
6. Nagase H, Visse R, Murphy G. Structure and function of matrix metalloproteinases and TIMPs. *Cardiovasc Res*. 2006; 69:562-573.
7. Kontogiorgis CA, Papaioannou P, Hadjipaviou-Litina DJ. Matrix metalloproteinase inhibitors: a review on pharmacophore mapping and (Q)Sars results. *Curr Med Chem*. 2005; 12:339-355.
8. Hoffman A, Qadri B, Frant J, Katz Y, Bhusare SR, Breuer E, Hadar R, Reich R. Carbamoylphosphonate matrix metalloproteinase inhibitors 6: *cis*-2-Aminocyclohexyl-carbamoylphosphonic acid, a novel orally active antimetastatic matrix metalloproteinase-2 selective inhibitor – synthesis and pharmacodynamic and pharmacokinetic analysis. *J Med Chem*. 2008; 51:1406-1414.
9. Li YL, Xu WF. Design, synthesis, and activity of caffeoyl pyrrolidine derivatives as potential gelatinase inhibitors. *Bioorg Med Chem*. 2004; 12:5171-5180.
10. Qu XJ, Yuan YX, Xu WF, Chen MH, Cui SX, Li YL, Makuuchi M, Nakata M, Tang W. Caffeoyl pyrrolidine derivative LY52 inhibits tumor invasion and metastasis *via* suppression of matrix metalloproteinase activity. *Anticancer Res*. 2006; 26:3573-3578.
11. Kramer RZ, Bella J, Mayville P, Brodsky B, Berman HM. Sequence dependent conformational variations of collagen triple-helical structure. *Nat Struct Biol*. 1999; 6:454-457.
12. Abraham DJ, Mokotoff M, Sheh L, Simmons JE. Design, synthesis, and testing of antisckling agents. 2. Proline derivatives designed for the donor site. *J Med Chem*. 1983; 26:549-554.
13. Baragi VM, Shaw BJ, Renkiewicz RR, Kuipers PJ, Welgus HG, Mathrubutham M, Cohen JR, Rao SK. A versatile assay for gelatinases using succinylated gelatin. *Matrix Biol*. 2000; 19:267-273.
14. Lejczak B, Kafarski P, Zygmunt J. Inhibition of aminopeptidases by aminophosphonates. *Biochemistry*. 1989; 28:3549-3555.

(Received October 16, 2009; Accepted November 7, 2009)

Appedix

1. Chemistry: general procedures

All materials were commercial available. All the reactions were monitored by thin-layer chromatography on 0.25 mm silica gel plates

(60GF-254) and visualized with UV light or ferric chloride. 200-300 mesh silica gel was used in column chromatography. Proton NMR spectra were determined on a Bruker DRX spectrometer (600 MHz) with δ in parts per million and J in Hertz; TMS was used as an internal standard. Measurements were made in D₂O solutions. ESI-MS were determined on an API 4000 spectrometer. Melting points were determined on an electrothermal melting point apparatus (uncorrected).

1.1. *trans*-4-Hydroxy-L-proline methylester hydrochloride (2)

26.2 g (200 mmol) *trans*-4-hydroxy-L-proline (1) in methanol (300 mL) was treated with dry hydrogen chloride until homogeneous. The solution was heated to the reflux temperature for 2 h and concentrated *in vacuo*. Upon cooling, the product was crystallized from the solvent, collected by filtration, washed with acetone and ether, and dried to yield *trans*-4-hydroxy-L-proline methylester hydrochloride (2) as white crystals (32.7 g, 90%), mp 159-162°C.

1.2. (4R)-1-(*tert*-Butoxycarbonyl)-4-hydroxy-L-proline methyl ester (3)

10.89 g (60 mmol) *trans*-4-hydroxy-L-proline methylester hydrochloride (2) was dissolved in DCM with Et₃N (18 mL, 126 mmol) and treated with (Boc)₂O (14.4 g, 66 mmol) in 20 mL DCM. The mixture was stirred at room temperature for 12 h, washed with 1 M citric acid, saturated NaHCO₃ solution, and brine, and dried over Na₂SO₄. Evaporation of DCM gave a white solid (3), mp 96-98°C. ESI-MS *m/z*: 246.3 (M+H)⁺.

1.3. (3R,5S)-5-(Methoxycarbonyl)-1-(*tert*-butoxycarbonyl) pyrrolidin-3-ylsulfonates (4)

9.8 g (40 mmol) (4R)-1-(*tert*-butoxycarbonyl)-4-hydroxy-L-proline methyl ester (3) was dissolved in anhydrous DCM with Et₃N (7 mL, 44 mmol) at 0°C and treated with MsCl (3.5 mL, 44 mmol) in 10 mL anhydrous DCM. After 12 h at 0°C, the mixture was washed with 1 M citric acid, saturated NaHCO₃ solution, and brine and then dried over Na₂SO₄. Evaporation of DCM gave compound 4, mp 84-86°C. ESI-MS *m/z*: 324.4 (M+H)⁺.

1.4. (2S,4S)-1-*tert*-Butyl-2-methyl-4-azidopyrrolidine-1,2-dicarboxylate (5)

(3R,5S)-5-(Methoxycarbonyl)-1-(*tert*-butoxycarbonyl) pyrrolidin-3-ylsulfonates (4) (12.92 g, 40 mmol) and 6.5 g NaN₃ (100 mmol) were stirred overnight in DMF (40 mL) at 55-65°C. The mixture was mixed with 20 mL ice water and extracted with ethyl acetate (30 mL × 5).

The organic phase was washed with 0.1 M HCl and brine and dried over Na₂SO₄. Evaporation of EtOAc provided a colorless viscous oil (**5**). ESI-MS m/z: 271.6 (M+H)⁺.

1.5. (2S,4S)-1-*tert*-Butyl-2-methyl-4-aminopyrrolidine-1,2-dicarboxylate (**6**)

(2S,4S)-1-*tert*-Butyl-2-methyl-4-azidopyrrolidine-1,2-dicarboxylate (**5**) (20 mmol) in MeOH (100 mL) was hydrogenated in the presence of a catalytic amount of 10% Pd-C at room temperature and 1 atm of pressure. After 36 h, the catalytic was filtered with a bed of *kieselguhr* on a funnel and the solvent was removed under a vacuum to give (2S,4S)-1-*tert*-butyl-2-methyl-4-aminopyrrolidine-1,2-dicarboxylate (**6**). ESI-MS m/z: 245.5 (M+H)⁺.

1.6. (2S,4S)-1-*tert*-Butyl-2-methyl-4-(2-((*tert*-butoxycarbonyl)amino)acetamido)-pyrrolidine-1,2-dicarboxylate (**7b**)

2-((*tert*-Butoxycarbonyl)amino)-propanoic acid (3.78 g, 20 mmol) and Et₃N (2 equiv.) were dissolved in 100 mL anhydrous DCM. To this stirring solution was added TBTU (1.3 equiv.) followed by compound **6**. The mixture was stirred for 10 h and washed with saturated NaHCO₃ solution, 1 M citric acid, and brine. 2.53 g **7b** was obtained by flash column chromatography, yield 60.8%. ESI-MS m/z: 416.7 (M+H)⁺. ¹H-NMR (DMSO-*d*₆): 1.12 (d, *J* = 6.6 Hz, 3H, CH₃), 1.32 (m, 18H, CH₃), 1.80 (m, 1H), 2.49 (m, 1H), 3.06 (m, 1H), 3.61 (m, 1H), 3.68 (s, 3H, CH₃), 3.86 (m, 1H), 4.21 (m, 2H).

Compounds **7a** and **7c-h** were synthesized following the procedure described above. (2S,4S)-1-*tert*-Butyl 2-methyl 4-(2-((*tert*-butoxycarbonyl)amino)acetamido)-pyrrolidine-1,2-dicarboxylate (**7a**), 2.2 g, 54.6%; (2S,4S)-1-*tert*-butyl 2-methyl 4-(2-((*tert*-butoxycarbonyl)amino)-3-methylbutanamido)pyrrolidine-1,2-dicarboxylate (**7c**), 2.9 g, 65.4%; (2S,4S)-1-*tert*-butyl 2-methyl 4-(2-((*tert*-butoxycarbonyl)amino)-4-methylpentanamido)pyrrolidine-1,2-dicarboxylate (**7d**), 3.12 g, 68.3%; (2S,4S)-1-*tert*-butyl 2-methyl 4-(2-((*tert*-butoxycarbonyl)amino)-3-methylpentanamido)pyrrolidine-1,2-dicarboxylate (**7e**), 3.09 g, 67.6%; (2S,4S)-1-*tert*-butyl 2-methyl 4-(2-((*tert*-butoxycarbonyl)amino)-3-phenylpropanamido)pyrrolidine-1,2-dicarboxylate (**7f**), 3.42 g, 69.5%; (2S,4S)-1-*tert*-butyl 2-methyl 4-(2-((*tert*-butoxycarbonyl)amino)-4-(methylthio)butanamido)pyrrolidine-1,2-dicarboxylate (**7g**), 2.92 g, 61.3%; (2S,4S)-1-*tert*-butyl 2-methyl 4-(2-((*tert*-butoxycarbonyl)amino)-3-mercaptopropanamido)pyrrolidine-1,2-dicarboxylate (**7h**), 2.36 g, 52.7%.

1.7. (2S,4S)-Methyl 4-(2-aminoacetamido)pyrrolidine-2-carboxylate (**8a**)

0.2 g compound **7a** in 20 mL EtOAc saturated with HCl gas was stirred at room temperature for 6 h. The mixture was filtered to obtain the target compound **8a** (0.12 g). Yield 87.4%, mp 75-77°C. ¹H-NMR (DMSO-*d*₆): 2.04 (m, 1H), 2.59 (m, 1H), 3.12 (m, 1H), 3.45 (m, 1H), 3.53 (s, 2H, CH₂), 3.78 (s, 3H, CH₃), 4.40 (m, 1H), 4.48 (m, 1H), 8.24 (s, 2H, NH₂).

Compounds **8b-h** were synthesized following the procedure described above.

(2S,4S)-Methyl 4-(2-aminopropanamido)pyrrolidine-2-carboxylate (**8b**)

White solid, yield 82.6%, mp 137-139°C. ¹H-NMR (DMSO-*d*₆): 1.36 (d, *J* = 6.6 Hz, 3H, CH₃), 2.04 (m, 1H), 2.61 (m, 1H), 3.14 (m, 1H), 3.44 (m, 1H), 3.78 (s, 3H, CH₃), 3.80 (d, *J* = 5.4 Hz, 1H), 4.39 (m, 1H), 4.48 (m, 1H), 8.24 (s, 2H, NH₂).

(2S,4S)-Methyl 4-(2-amino-3-methylbutanamido)pyrrolidine-2-carboxylate (**8c**)

White solid, yield 80.2%, mp 146-148°C. ¹H-NMR (DMSO-*d*₆): 0.93 (d, *J* = 6.6 Hz, 6H, CH₃), 2.06 (m, 1H), 2.09 (m, 1H), 2.62 (m, 1H), 3.10 (m, 1H), 3.49 (m, 1H), 3.57 (s, 1H), 3.78 (s, 3H, CH₃), 4.41 (m, 1H), 4.48 (m, 1H), 8.24 (s, 2H, NH₂).

(2S,4S)-Methyl 4-(2-amino-4-methylpentanamido)pyrrolidine-2-carboxylate (**8d**)

White solid, yield 86.3%, mp 148-150°C. ¹H-NMR (DMSO-*d*₆): 0.90 (t, 6H, CH₃), 1.59 (m, 2H), 1.64 (m, 1H), 2.09 (m, 1H), 2.61 (m, 1H), 3.12 (m, 1H), 3.45 (m, 1H), 3.72 (t, 1H), 3.78 (s, 3H, CH₃), 4.39 (m, 1H), 4.48 (m, 1H), 8.24 (s, 2H, NH₂).

(2S,4S)-Methyl 4-(2-amino-3-methylpentanamido)pyrrolidine-2-carboxylate (**8e**)

White solid, yield 85.7%, mp 154-156°C. ¹H-NMR (DMSO-*d*₆): 0.88 (m, 6H, CH₃), 1.09 (m, 1H), 1.50 (m, 1H), 1.84 (m, 1H), 2.09 (m, 1H), 2.61 (m, 1H), 3.09 (m, 1H), 3.48 (m, 1H), 3.60 (s, 1H), 3.78 (s, 3H, CH₃), 4.41 (m, 1H), 4.48 (m, 1H), 8.24 (s, 2H, NH₂).

(2S,4S)-Methyl 4-(2-amino-3-phenylpropanamido)pyrrolidine-2-carboxylate (**8f**)

White solid, yield 83.5%, mp 159-161°C. ¹H-NMR (DMSO-*d*₆): 1.96 (m, 1H), 2.61 (m, 1H), 2.85 (m, 1H), 3.04 (m, 1H), 3.09 (m, 1H), 3.34 (m, 1H), 3.89 (s, 3H, CH₃), 3.98 (m, 1H), 4.34 (m, 1H), 4.45 (m, 1H), 7.27, 7.28, 7.29, 7.32, 7.35 (5H, C₆H₆), 8.24 (s, 2H, NH₂).

(2S,4S)-Methyl 4-(2-amino-4-(methylthio)butanamido)pyrrolidine-2-carboxylate (**8g**)

White solid, yield 85.8%, mp 151-153°C. ¹H-NMR (DMSO-*d*₆): 1.99 (m, 1H), 2.07 (s, 3H, CH₃), 2.10 (m, 2H, CH₂), 2.12 (m, 1H), 2.51 (m, 1H), 2.61 (m, 1H), 3.17 (m, 1H), 3.47 (m, 1H), 3.78 (s, 3H, CH₃), 3.84 (m, 1H), 4.40 (m, 1H), 4.49 (m, 1H), 8.24 (s, 2H, NH₂).

(2S,4S)-Methyl 4-(2-amino-3-mercaptopropanamido)pyrrolidine-2-carboxylate (8h)

White solid, yield 63.2%, mp 174-176°C. ¹H-NMR (DMSO-*d*₆): 1.87 (m, 1H), 2.60 (m, 1H), 2.65, 2.76 (q, 2H, CH₂), 3.07 (m, 1H), 3.41 (m, 1H), 3.43 (d, *J* = 6 Hz, 1H), 3.78 (s, 3H, CH₃), 3.84 (m, 1H), 4.12 (m, 1H), 4.40 (m, 1H), 8.53 (s, 2H, NH₂).

1.8. (2S,4S)-4-(2-Aminoacetamido)-N-hydroxypyrrolidine-2-carboxamide (9a)

To a solution of compound **7a** (0.4 g, 1 mmol) in 10 mL anhydrous methanol at room temperature was added dropwise a solution of NHOK (3 mmol) in methanol (1.7 mL). The mixture was stirred for 12 h and the solvent was evaporated *in vacuo*. De-protection of Boc group as the synthesis of **8a** provided the target compound **9a** (0.07 g). Yield 39%, mp 124-126°C. ¹H-NMR (DMSO-*d*₆): 1.80 (m, 1H), 2.58 (m, 1H), 3.07 (m, 1H), 3.43 (m, 1H), 3.53 (d, *J* = 3.6 Hz, 2H, CH₂), 4.11 (m, 1H), 4.40 (m, 1H), 8.21 (s, 2H, NH₂).

Compounds **9b-h** were synthesized following the procedure described above.

(2S,4S)-4-(2-Aminopropanamido)-N-hydroxypyrrolidine-2-carboxamide (9b)

White solid, yield 43.2%, mp 167-169°C. ¹H-NMR (DMSO-*d*₆): 1.84 (m, 1H), 2.60 (m, 1H), 3.08 (m, 1H), 3.44 (m, 1H), 3.82 (d, *J* = 5.4 Hz, 1H), 4.11 (m, 1H), 4.37 (m, 1H), 8.31 (s, 2H, NH₂).

(2S,4S)-4-(2-Amino-3-methylbutanamido)-N-hydroxypyrrolidine-2-carboxamide (9c)

White solid, yield 47.8%, mp 170-172°C. ¹H-NMR (DMSO-*d*₆): 0.93 (d, *J* = 7.2 Hz, 3H, CH₃), 1.85 (m, 1H), 2.09 (m, 1H), 2.59 (m, 1H), 3.03 (m, 1H), 3.48 (m, 1H), 3.54 (d, *J* = 5.4 Hz, 1H), 4.10 (m, 1H), 4.41 (m, 1H), 8.24 (s, 2H, NH₂).

(2S,4S)-4-(2-Amino-4-methylpentanamido)-N-hydroxypyrrolidine-2-carboxamide (9d)

White solid, yield 41.8%, mp 176-178°C. ¹H-NMR (DMSO-*d*₆): 0.90 (t, 3H, CH₃), 1.57 (m, 2H, CH₂), 1.63 (m, 1H), 1.83 (m, 1H), 2.59 (m, 1H), 3.05 (m, 1H), 3.46 (m, 1H), 3.73 (t, 1H), 4.10 (m, 1H), 4.41 (m, 1H), 8.31 (s, 2H, NH₂).

(2S,4S)-4-(2-Amino-3-methylpentanamido)-N-hydroxypyrrolidine-2-carboxamide (9e)

White solid, yield 46.5%, mp 171-173°C. ¹H-NMR (DMSO-*d*₆): 0.90 (t, 3H, CH₃), 1.12 (m, 2H, CH₂), 1.51 (m, 1H), 1.87 (m, 1H), 2.61 (m, 1H), 3.05 (m, 1H), 3.40 (m, 1H), 3.63 (t, 1H), 4.11 (m, 1H), 4.41 (m, 1H), 8.23 (s, 2H, NH₂).

(2S,4S)-4-(2-Amino-3-phenylpropanamido)-N-hydroxypyrrolidine-2-carboxamide (9f)

White solid, yield 42.7%, mp 182-184°C. ¹H-NMR (DMSO-*d*₆): 1.78 (m, 1H), 2.60 (m, 1H), 2.75 (m, 1H), 3.05 (d, *J* = 6.6 Hz, 2H, CH₂), 3.30 (m, 1H), 3.98 (t, 1H), 4.09 (m, 1H), 4.37 (m, 1H), 7.26, 7.29, 7.34 (5H, C₆H₆), 8.37 (s, 2H, NH₂).

(2S,4S)-4-(2-Amino-4-(methylthio)butanamido)-N-hydroxypyrrolidine-2-carboxamide (9g)

White solid, yield 45.4%, mp 158-160°C. ¹H-NMR (DMSO-*d*₆): 1.87 (m, 1H), 1.99 (m, 2H, CH₂), 2.07 (s, 3H, CH₃), 2.60 (m, 1H), 2.65, 2.74 (q, 2H, CH₂), 3.07 (m, 1H), 3.49 (m, 1H), 3.84 (m, 1H), 4.11 (m, 1H), 4.40 (m, 1H), 8.38 (s, 2H, NH₂).

(2S,4S)-4-(2-Amino-3-mercaptopropanamido)-N-hydroxypyrrolidine-2-carboxamide (9h)

White solid, yield 33.6%, mp 142-145°C. ¹H-NMR (DMSO-*d*₆): 1.87 (m, 1H), 2.60 (m, 1H), 2.65, 2.76 (q, 2H, CH₂), 3.07 (m, 1H), 3.41 (m, 1H), 3.43 (d, *J* = 6 Hz, 1H), 3.84 (m, 1H), 4.12 (m, 1H), 4.40 (m, 1H), 8.58 (s, 2H, NH₂).

(2S,4S)-4-(2-Aminopropanamido)pyrrolidine-2-carboxylic acid (11b)

Compound **7a** (0.42 g, 1mmol) in 10 mL methanol was treated with 1 M NaOH (3 mL), and stirred for 3 h at room temperature. The solvent was evaporated in a *vacuum* and the residue was adjusted to pH 2-3 with 1 M HCl. The mixture was extracted 3 times by EtOAc. The organic phase was dried over Na₂SO₄. Evaporation of EtOAc provided compound **10b**. De-protection of Boc group as the synthesis of **8a** provided the target compound **11b** (0.11g). Yield 54.8%, mp 195-198°C. ¹H-NMR (DMSO-*d*₆): 1.37 (d, *J* = 7.2 Hz, 3H, CH₃), 2.07 (m, 1H), 2.60 (m, 1H), 3.13 (m, 1H), 3.43 (m, 1H), 3.81 (d, *J* = 6.6 Hz, 1H), 4.36 (m, 1H), 4.48 (m, 1H), 8.33 (s, 2H, NH₂).

Compounds **11c-h** were synthesized following the procedure described above.

(2S,4S)-4-(2-Amino-3-methylbutanamido)pyrrolidine-2-carboxylic acid (11c)

White solid, yield 57.4%, mp 201-203°C. ¹H-NMR (DMSO-*d*₆): 0.94 (d, 3H, CH₃), 1.85 (m, 1H), 2.04 (m, 1H), 2.12 (m, 1H), 2.63 (m, 1H), 3.09 (m, 1H), 3.46 (m, 1H), 3.59 (d, *J* = 4.8 Hz, 1H), 4.40 (m, 1H), 4.47 (m, 1H), 8.37 (s, 2H, NH₂).

(2S,4S)-4-(2-Amino-4-methylpentanamido)pyrrolidine-2-carboxylic acid (11d)

White solid, yield 61.8%, mp 207-209°C. ¹H-NMR (DMSO-*d*₆): 0.90 (t, 3H, CH₃), 1.57 (m, 2H, CH₂), 1.63 (m, 1H), 2.01 (m, 1H), 2.62 (m, 1H), 3.08 (m, 1H), 3.46 (m, 1H), 3.73 (t, 1H), 4.32 (m, 1H), 4.41 (m, 1H), 8.38 (s, 2H, NH₂).

(2S,4S)-4-(2-Amino-3-methylpentanamido)pyrrolidine-2-carboxylic acid (11e)

White solid, yield 56.3%, mp 203-205°C. ¹H-NMR (DMSO-*d*₆): 0.90 (t, 3H, CH₃), 1.09 (m, 1H), 1.49 (m, 1H), 1.84 (m, 1H), 2 (m, 1H), 2.61 (m, 1H), 3.06 (m, 1H), 3.47 (m, 1H), 3.60 (d, *J* = 4.2 Hz, 1H), 4.33 (m, 1H), 4.41 (m, 1H), 8.29 (s, 2H, NH₂).

(2S,4S)-4-(2-Amino-3-phenylpropanamido)pyrrolidine-2-carboxylic acid (11f)

White solid, yield 62.7%, mp 215-218°C. ¹H-NMR (DMSO-*d*₆): 1.90 (m, 1H), 2.57 (m, 1H), 2.78 (m, 1H), 3.04 (d, *J* = 6 Hz, 2H, CH₂), 3.29 (m, 1H), 3.97 (t, 1H), 4.29 (m, 1H), 4.36 (m, 1H), 7.26, 7.29, 7.33 (5H, C₆H₆), 8.36 (s, 2H, NH₂).

(2S,4S)-4-(2-Amino-4-(methylthio)butanamido)pyrrolidine-2-carboxylic acid (11g)

White solid, yield 57.6%, mp 193-196°C. ¹H-NMR (DMSO-*d*₆): 1.87 (m, 1H), 2.02 (m, 2H, CH₂), 2.07 (s, 3H, CH₃), 2.60 (m, 1H), 2.65, 2.74 (q, 2H, CH₂), 3.07 (m, 1H), 3.44 (m, 1H), 3.84 (d, *J* = 6 Hz, 1H), 4.11 (m, 1H), 4.47 (m, 1H), 8.46 (s, 2H, NH₂).

(2S,4S)-4-(2-Amino-3-mercaptopropanamido)pyrrolidine-2-carboxylic acid (11h)

White solid, yield 41.2%, mp 181-185°C. ¹H-NMR

(DMSO-*d*₆): 2.05 (m, 1H), 2.61 (m, 1H), 3.08 (m, 1H), 3.16 (m, 1H), 3.43 (m, 1H), 4.11 (m, 1H), 4.35 (m, 1H), 4.42 (m, 1H), 8.58 (s, 2H, NH₂).

1.9. Methyl 2-((2S,4S)-4-(2-amino-4-methylpentanamido)pyrrolidine-2-carboxamido)acetate (12d)

0.94 g **10d** (2 mmol) and Et₃N (2 equiv.) were dissolved in 30 mL anhydrous DCM. To this stirring solution was added TBTU (1.3 equiv.) followed by methyl 2-aminoacetate. The mixture was stirred for 10 h and washed with saturated NaHCO₃ solution, 1 M citric acid, and brine. 0.57 g of **12d** was obtained by flash column chromatography. Yield 55.2%, mp 54-57°C. ESI-MS *m/z*: 515.6 (M+H)⁺.

Compound **12f** was synthesized following the procedure described above.

(2S,4S)-tert-Butyl 4-(2-((tert-butoxycarbonyl)amino)-3-phenylpropanamido)-2-((2-methoxy-2-oxoethyl)carbamoyl)pyrrolidine-1-carboxylate (12f)

White solid, yield 58.7%, mp 62-64°C. ESI-MS *m/z*: 549.6 (M+H)⁺.

1.10. Methyl 2-((2S,4S)-4-(2-amino-4-methylpentanamido)pyrrolidine-2-carboxamido) acetate (13d)

Compound **13d** was obtained following the synthesis of **8a** described above. White solid, yield 83.5%, mp 164-167°C. ¹H-NMR (DMSO-*d*₆): 0.90 (s, 6H, CH₃), 1.58 (m, 2H), 1.64 (m, 1H), 1.87 (m, 1H), 2.76 (m, 1H), 3.07 (m, 1H), 3.46 (m, 1H), 3.66 (s, 3H, CH₃), 3.75 (t, 1H), 3.97 (m, 2H, CH₂), 4.33 (m, 1H), 4.40 (m, 1H), 8.43 (s, 2H, NH₂).

Compound **13f** was synthesized following the procedure described above.

Methyl 2-((2S,4S)-4-(2-amino-3-phenylpropanamido)pyrrolidine-2-carboxamido) acetate (13f)

White solid, yield 83.5%, mp 172-175°C. ¹H-NMR (DMSO-*d*₆): 1.71 (m, 1H), 2.43 (m, 1H), 2.72 (m, 1H), 2.94 (m, 1H), 3.58 (m, 2H, CH₂), 3.62 (s, 3H, CH₃), 3.82 (m, 1H), 3.93 (m, 1H), 4.13 (m, 1H), 4.18 (m, 1H), 7.27, 7.28, 7.29, 7.32, 7.35 (5H, C₆H₆), 8.24 (s, 2H, NH₂).

Original Article**Hypotensive response in rats and toxicological mechanisms induced by shuanghuanglian, an herbal extract mixture**Huaishan Wang^{1,2}, Fang Cheng², Yanqiu Shi², Zhonggang Li^{1,2}, Huidi Qin^{1,2}, Zhaoping Liu^{2,*}¹ School of Pharmaceutical Sciences, Shandong University, Ji'nan, China;² Center for New Drugs Evaluation, Shandong University, Ji'nan, China.

ABSTRACT: Shuanghuanglian (SHL), an extract mixture isolated from three medicinal herbs, has been used in China as an injection in traditional Chinese medicine to treat viral or bacterial infection. This study examined the hypotensive response in rats induced by SHL and its possible mechanisms. Mean arterial pressure (MAP) and electrocardiograms (ECGs) were studied after intravenous injection of histamine and SHL. Diphenhydramine, an H₁ receptor antagonist, the compound 48/80, a promoter of histamine release, and cromolyn, a histamine release inhibitor, were also used to investigate the potential mechanisms of that response. In addition, the histamine level in plasma was measured after administration of SHL and compound 48/80. Both SHL and histamine led to a MAP reduction immediately but did not affect ECGs when initially administered in a similar manner, though this reduction was partially attenuated by diphenhydramine. Pretreatment blocked the rats' reaction to compound 48/80 but not to SHL. The plasma histamine level in rats was also elevated by SHL. SHL can induce severe hypotension through histamine release upon initial administration. In combination with the direct effects of its histamine-like substances on target tissue, SHL likely has the potential to cause an anaphylactoid reaction.

Keywords: Herbal extract mixture, shuanghuanglian, mean arterial pressure, anaphylactoid reaction, histamine

1. Introduction

Shuanghuanglian (SHL) is an extract mixture isolated from three medicinal herbs: Radix scutellariae (root

of *Scutellaria baicalensis* Georgi), Flos lonicerae japonicae (flower of *Lonicera japonica* Thunb.) and Fructus forsythiae (fruit of *Forsythia suspensa* Thunb. Vahl). SHL has been used for over 40 years as an injection in traditional Chinese medicine to treat viral or bacterial infection. This medicine is commercially available and widely used to treat upper respiratory infections, pharyngitis, acute bronchitis, tonsillitis, and pneumonia in China because of its strong antiviral and bacteriostatic activity and ability to enhance immune function. However, adverse effects have frequently been reported with the extensive clinical use of SHL (1), and a patient who used SHL died, according to the State Food and Drug Administration (SFDA), in February and September 2009 (2).

Nearly 10% of hospitalized patients and over 7% of the general population suffer adverse drug reactions, including hypersensitivity reactions (HSRs) (3). HSRs fall into two categories, anaphylaxis and anaphylactoid reactions (4,5). Anaphylaxis is a specific immunoglobulin IgE-mediated antigen-induced reaction to various allergens resulting in the release of a mediator such as histamine, tryptase, or leukotrienes (6). The incidence of anaphylaxis is unknown but is estimated to be 1/6,000-1/20,000, or 1/10,000 of the general population (5). Anaphylactoid reactions have an identical clinical presentation but involve mediators besides IgE and are caused by various mechanisms (7). Recent estimates suggest that these non-IgE-mediated anaphylactoid reactions may account for as much as 77% of all immune-mediated hypersensitivity reactions (8). The occurrence of HSRs induced by SHL is very high (1), which may be related to anaphylactoid reactions. Mediator measurement combined with symptom monitoring is the primary means of studying anaphylactoid reaction. Sitter *et al.* (9) sought to investigate anaphylactoid reactions by detecting the plasma histamine level, heart rate, mean arterial pressure (MAP), and skin reaction in humans and dogs (4), and they indicated that the plasma histamine level and MAP may be sensitive indices. Histamine release from mast cells, stimulated by the compound 48/80, for instance, is considered to

*Address correspondence to:

Dr. ZhaoPing Liu, Center for New Drugs Evaluation, Shandong University, 44[#] Wen Hua Xi Road, Ji'nan 250012, Shandong, China.

e-mail: liuzhaopingdu@gmail.com

be a cause of anaphylactoid reactions. Cromolyn has also been shown to stabilize mast cells and prevent histamine release (10). Hypotension, which often occurs with an anaphylactoid reaction, can be induced by histamine or histamine-like substances that are usually blocked by histamine receptor antagonists (e.g. diphenhydramine) (9). The current study sought to examine changes in the plasma histamine level and MAP after intravenous administration of SHL and histamine in rats in order to determine the possible cause of HSRs induced by SHL and their correlation with anaphylactoid reactions.

2. Materials and Methods

2.1. Animals

Male Wistar rats (Center for New Drugs Evaluation of Shandong University) used in tests weighed 250-350 g, were housed for 7 days at a room temperature of $23 \pm 1^\circ\text{C}$, and were given free access to food and water. Each group tested consisted of 5 rats. All experiments were performed in accordance with the Care and Use of Laboratory Animals of the US Department of Health and Human Services. The study protocol was approved by the local "Animal Ethics Committee".

2.2. Drugs and Chemicals

SHL as is officially registered in the Chinese Pharmacopoeia (CP) was provided by the Second Traditional Chinese Medicine Factory of the Harbin Pharmaceutical Group (Harbin, China). According to the CP, the quality controls for SHL (freeze-dried powder, mg/600 mg) are baicalin 128-173, chlorogenic acid 8.5-11.5, and forsythine 1.4-2.1, respectively (Figure 1) (11). SHL was required to have a consistent fingerprint (12). Compound 48/80, histamine dihydrochloride, diphenhydramine hydrochloride, and cromolyn were purchased from Sigma (St. Louis, MO, USA). A histamine ELISA kit was purchased from Rapid Bio Lab (Calabasas, CA, USA).

2.3. Effects of histamine, compound 48/80, SHL, diphenhydramine, and cromolyn on MAP

Rats were anesthetized with sodium pentobarbital. After a trachea tube was inserted, a carotid artery was isolated and catheterized with an Angio-set IV catheter system for MAP measurement (Biopac MP System). MAP was recorded every 10 sec (13,14). In a separate study, blood samples used for determining plasma histamine levels were collected from the carotid artery (15).

The jugular vein was isolated and used for intravenous administration. In experiments involving multiple doses or involving both an injection and an infusion, both jugular veins were exposed prior to the initiation of the experiment and used alternatively. All bolus injections were delivered in 30 sec in a volume of 0.5 mL. The infusion rate used for cromolyn was 0.5 mL/min (13,15). A saline vehicle was employed for all compounds, and concentrations of dosing solution were dependent upon the concentration required to deliver 0.5 mL injections and a 0.5 mL/kg/min dose for infusions.

To determine the effect of SHL or histamine on MAP, 100 to 400 mg/kg of SHL (according to the CP, the adult dose of SHL for clinical use is 60 mg/kg) (11) or 0.1 to 5.0 mg/kg of histamine (13) was given *via* the jugular vein ($n = 5$). Saline served as the vehicle for the control group.

To investigate the effects of repetitive treatments, 1.0 mg/kg of histamine ($n = 5$) or 200 mg/kg of SHL ($n = 5$) in saline was given by bolus injection *via* the jugular vein. If the MAP returned to the baseline, a second treatment with the same dose was given 15 min later. The maximum reduction in MAP and duration of hypotension were used to compare the responses induced by the two treatments.

To determine the effects of diphenhydramine on the response induced by histamine and SHL, 0.1 mg/kg of histamine, or 200 mg/kg of SHL was given *i.v.* by bolus injection. Fifteen minutes later, diphenhydramine (4.6 mg/kg) was injected as a bolus. Fifteen minutes later, histamine or SHL was given again in the same dose as before ($n = 5$).

To determine the effects of cromolyn on the response induced by compound 48/80 and SHL, animals were infused with saline (0.1 mL/min) or cromolyn (4 mg/kg/min) for 5 min and then treated with 0.1 mg/kg of compound 48/80 or 200 mg/kg of SHL *i.v.* (bolus) immediately after saline or cromolyn infusion ($n = 5$) (13,15).

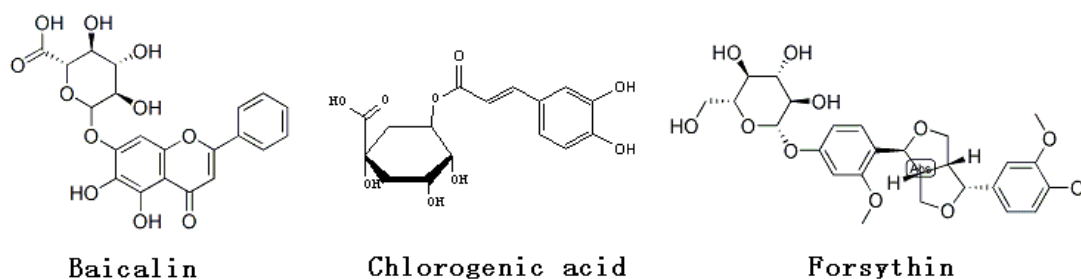


Figure 1. Natural product structures of major components in SHL. Quality controls for SHL (freeze-dried powder, mg/600 mg) were baicalin 128-173, chlorogenic acid 8.5-11.5, and forsythine 1.4-2.1, respectively.

2.4. Histamine release

In a separate experiment to determine the effects on histamine release, animals ($n = 5$) were treated with saline, compound 48/80 (0.1 mg/kg), or SHL (400 mg/kg) as described above. Blood samples (1 mL) were collected from the carotid artery into EDTA vacutainers 5 min after the treatment. Plasma samples were stored at -20°C until assay (15). Histamine concentration was measured using an ELISA kit.

2.5. Statistical analysis

All results are expressed as mean \pm S.E.M. Experimental groups were compared using a Student's paired t test, with $p < 0.05$ considered to indicate a significant difference.

3. Results

3.1. Responses to histamine, SHL, diphenhydramine, compound 48/80, and cromolyn

Intravenous bolus injection of SHL resulted in a decrease in MAP in the dose range of 100 to 400 mg/kg in anesthetized rats but did not influence ECGs (data not shown); this decrease was not dose-dependent (Figure 2A). The decrease in MAP was observed immediately after the initiation of injection, and MAP returned to its baseline level about 2 to 3 min later. To investigate the hypotensive response induced by SHL, the effects of histamine on MAP were determined. Following bolus injection of 0.1 mg/kg of histamine *i.v.*, MAP decreased approximately 50% and then returned to its pretreatment level within 2 min (Figure 2B). Increasing doses of histamine from 0.1 to 1.0 mg/kg prolonged the duration of action but not the maximum effect. At a dose of 5 mg/kg, the MAP decreased more sharply and did not return to its normal level until the

end of monitoring.

When SHL was given twice, 15 min apart, to the same rat in a dose of 200 mg/kg *i.v.* (bolus), the hypotensive response was similar (Figure 3A). Repetitive dosing with 1.0 mg/kg of histamine did not alter the maximum effect and hypotensive duration, resembling the effects of SHL (Figure 3B).

To investigate the effect of diphenhydramine on the hypotensive response induced by histamine, animals were treated with 1.0 mg/kg of histamine, 4.6 mg/kg of diphenhydramine, and 1.0 mg/kg of histamine in turn in intervals of 15 min. The hypotensive response induced by the second injection of histamine was found to be much weaker than the first, as the changes in MAP from its baseline to nadir were 69.1 ± 9.6 mmHg and 15.3 ± 2.8 mmHg, respectively ($p < 0.0004$) (Figure 4A). This demonstrates that diphenhydramine partially blocked the hypotensive response induced by histamine. When rats were given 200 mg/kg of SHL, 4.6 mg/kg of diphenhydramine, and 200 mg/kg of SHL in turn in intervals of 15 min, the hypotensive response induced by the second treatment of SHL was partially blocked by diphenhydramine, with a change in MAP of 38.1 ± 4.6 mmHg, compared to 60.3 ± 14.3 mmHg for the first treatment with SHL ($p < 0.05$) (Figure 4B).

To assess the effect of cromolyn on hypotension induced by the compound 48/80 in this model, saline or cromolyn was given to rats prior to the injection of the compound 48/80 (Figure 5A). When saline was infused (0.1 mL/kg/min, 5 min) prior to the compound 48/80, MAP decreased significantly from 162.8 ± 12.4 mmHg to the nadir of 104.5 ± 12.0 mmHg ($p < 0.003$). When the compound 48/80 was used after the infusion of cromolyn, the slight change in MAP from its baseline to 16 min demonstrated that cromolyn significantly inhibited the response of the compound 48/80. This demonstrates that cromolyn significantly attenuated the hypotension induced by the compound 48/80 (change in MAP from its baseline to 16 min, saline vs.

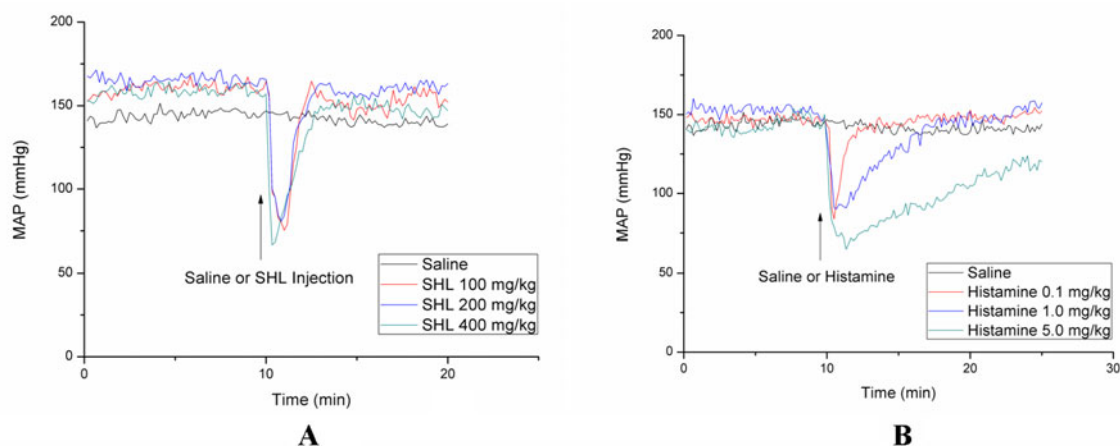


Figure 2. Effect of SHL (A) and histamine (B) on MAP. (A) SHL was injected (100, 200 and 400 mg/kg) *via* the jugular vein 10 min after the initiation of MAP monitoring. Results are presented as the average from five rats. (B) Histamine was injected (0.1, 1.0, and 5.0 mg/kg) *via* the jugular vein 10 min after the initiation of MAP monitoring. Results are presented as the average from five rats.

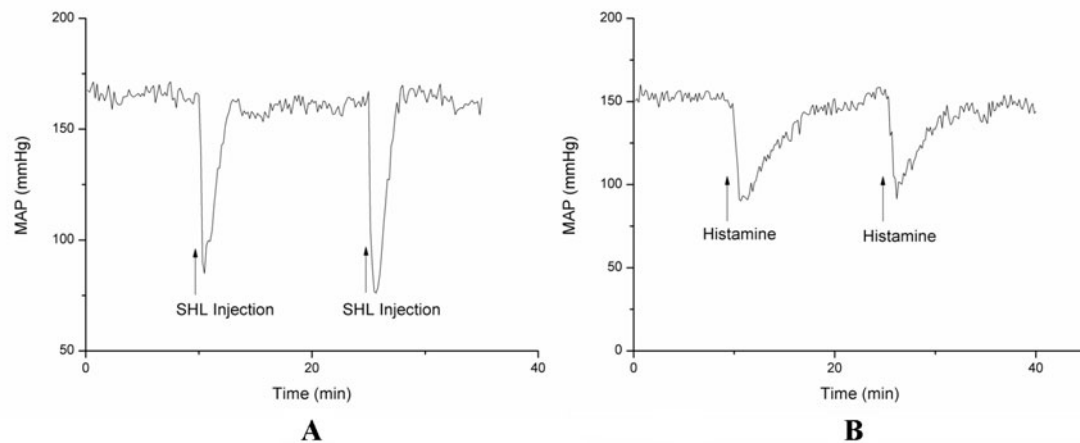


Figure 3. Effect of SHL (A) and histamine (B) on MAP. (A) SHL was injected (200 mg/kg) *via* the jugular vein 10 min and 25 min after the initiation of MAP monitoring. Results are presented as the average from five rats. (B) Histamine was injected (1.0 mg/kg) *via* the jugular vein 10 min and 25 min after the initiation of MAP monitoring. Results are presented as the average from five rats.

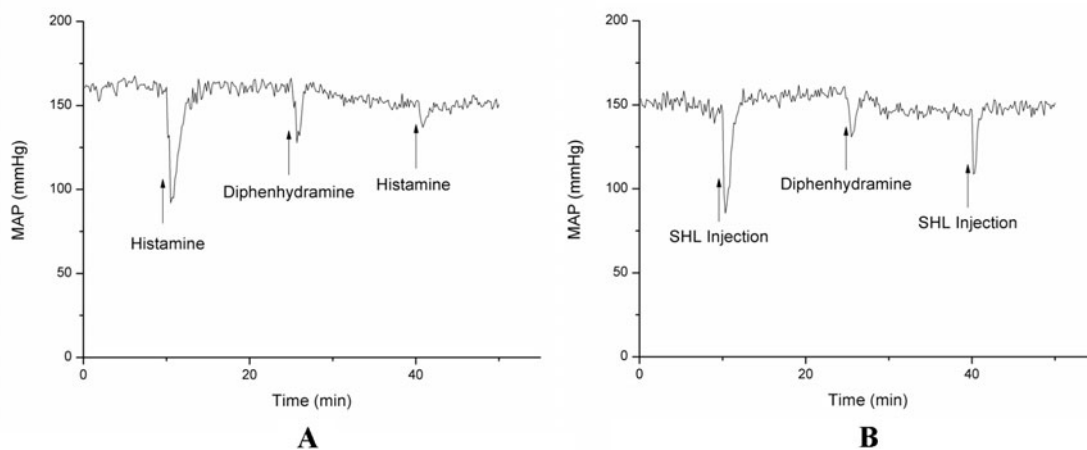


Figure 4. Effects of diphenhydramine and histamine (A) and SHL (B) on MAP. (A) Histamine was given in a dose of 200 mg/kg *i.v.* by bolus injection. Fifteen minutes later, diphenhydramine (4.6 mg/kg) was injected as a bolus. Fifteen minutes later, histamine was given again in the same dose as before. Results are presented as the average from five rats. (B) SHL was given in a dose of 200 mg/kg *i.v.* by bolus injection. Fifteen minutes later, diphenhydramine (4.6 mg/kg) was injected as a bolus. Fifteen minutes later, SHL was given again in the same dose as before. Results are presented as the average from five rats.

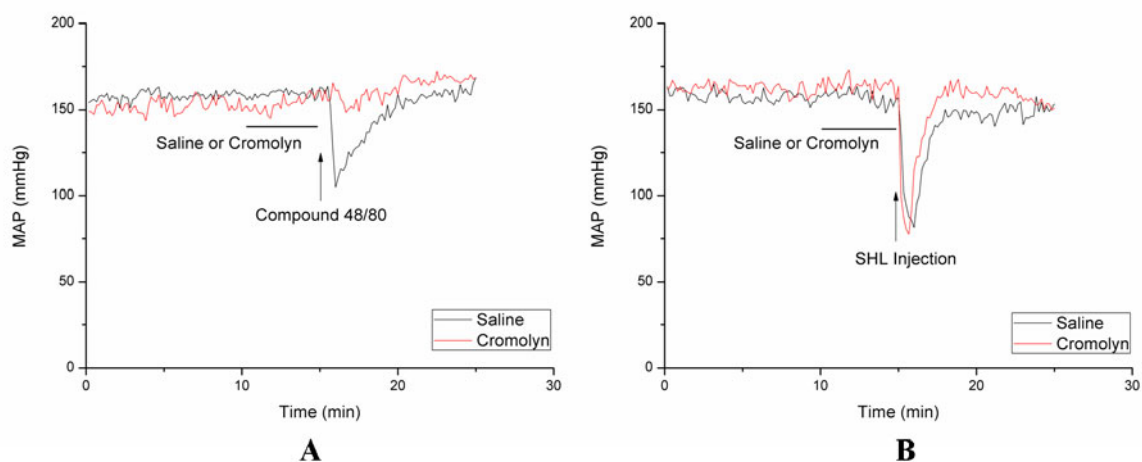


Figure 5. Effect of Cromolyn/saline and Compound 48/80 (A) and SHL (B) on MAP. (A) Cromolyn in a dose of 4 mg/kg/min or saline in a dose of 0.1 mL/min ($n = 5$) was infused for 5 min *via* the jugular vein. Compound 48/80 in a dose of 0.1 mg/kg *i.v.* was given (bolus) immediately after the cromolyn or saline infusion. Results are presented as the average from five rats. (B) Cromolyn in a dose of 4 mg/kg/min or saline in a dose of 0.1 mL/min ($n = 5$) was infused for 5 min *via* the jugular vein. SHL in a dose of 200 mg/kg *i.v.* was given (bolus) immediately after the cromolyn or saline infusion. Results are presented as the average from five rats.

cromolyn, $p < 0.003$). Figure 5B shows the effect of cromolyn on the hypotensive response induced by SHL. When saline was used (0.1 mL/kg/min, 5 min) prior to the injection of SHL (200 mg/kg), MAP decreased rapidly from 156 ± 4.6 mmHg to 81 ± 6.9 mmHg ($p < 0.00005$). Pretreatment with cromolyn did not attenuate the hypotensive response induced by SHL, as evident by 77.6 ± 4.6 mmHg vs. baseline 163.4 ± 4.6 mmHg ($p < 0.0002$) (change in MAP from its baseline to 16 min, saline vs. cromolyn, $p = 0.16$).

3.2. Histamine release

In a separate experiment, blood samples were collected 5 min after the injection (bolus) of saline, compound 48/80, or SHL in order to detect plasma histamine levels. The compound 48/80 and SHL both resulted in an increase in plasma histamine levels (Figure 6).

4. Discussion

As is well-known, the direct release of histamine may cause an anaphylactoid reaction, and physicians consider the plasma histamine level to be the 'golden standard' in gauging such reactions in clinical settings. To determine if an anaphylactoid reaction is imminent, measurement of the plasma histamine level has to be combined with observation of symptoms, *e.g.* skin reaction, tachycardia or bradycardia, hypertension or hypotension, bronchospasms, vomiting, diarrhea, and heart attack or myocardial infarction; such a combination of techniques is commonly used in diagnostic trials and preclinical studies (13,16). The current study injected a standard form of exogenous histamine and SHL in order to determine whether SHL causes an anaphylactoid reaction and explore possible mechanisms of that reaction.

Intravenous administration of SHL led to an elevated plasma histamine level and significant

hypotension (Figures 2A and 6). When SHL was given to rats intravenously, the MAP decreased rapidly. Increasing doses of SHL from 100 to 400 mg/kg did not increase the extent of hypotension (Figure 2A). Similarly, the injection of histamine led to a MAP reduction immediately after administration. The extent of hypotension was not affected by doses of histamine from 0.1 to 1.0 mg/kg, as was found in a previous study of histamine-mediated hypotension (13). Though the response caused by histamine lasts longer than that caused by SHL, the responses are quite similar. Furthermore, the hypotension induced by histamine and SHL was partially inhibited by diphenhydramine, an H_1 receptor antagonist, in a similar manner. Given characteristics identical to the hypotension produced by histamine and evidence of an elevated plasma histamine level after intravenous administration, the hypotension caused by SHL may be histamine-mediated, and the underlying mechanism may be the stimulation of histamine release, which then subsequently induces a hypotensive response. That said, the hypotension induced by SHL was not completely blocked by diphenhydramine (Figure 4), suggesting that other mechanisms that lower the MAP may be at work besides a histamine-related anaphylactoid reaction.

The compound 48/80, a polybasic substance, is known to induce hypotension by stimulating histamine release (17), and this hypotension can be attenuated by cromolyn through inhibition of mast cell degranulation (10). In the current study, hypotension was attenuated when cromolyn was given prior to administration of the compound 48/80, which did not occur prior to administration of SHL (Figure 5). Presumably, the mechanisms by which SHL and compound 48/80 reduce the MAP differ. Certain substances in the SHI injection may induce a hypotensive response, similar to that induced by histamine, that cannot be blocked by cromolyn. This histamine-like reaction may enhance the hypotensive effects of histamine release (Figure 6). Iizuka T *et al.* found that an extract isolated from the leaves of *Forsythia viridissima* has a vasorelaxant effect (18), and this may play a role in the hypotensive response induced by SHL. The molecule mechanisms responsible are being investigated.

In conclusion, SHL can induce severe hypotension through histamine release in combination with the direct effects of its histamine-like substances on target tissue. An elevated plasma histamine level and hypotension are both observed after intravenous administration, so SHL likely has the potential to cause an anaphylactoid reaction.

Acknowledgements

This study was supported by the "Eleventh Five-year Plan" of the Ministry of Science and Technology of China (2006BAI14B05).

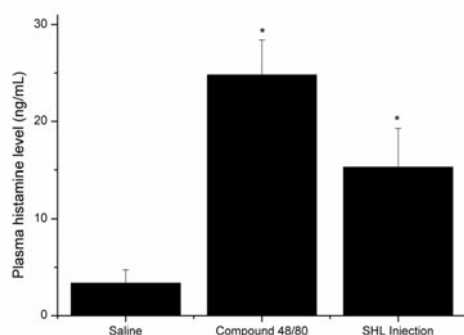


Figure 6. Plasma histamine level. Animals ($n = 5$) were treated with saline, compound 48/80 (0.1 mg/kg), or SHL (400 mg/kg). Blood samples were collected 5 min after the administration. Histamine concentration was measured using an ELISA kit. Results are presented as the average from five rats. * $p < 0.01$, vs. saline group.

References

1. Wu B, Wang Q, Wang HL. Analysis of adverse drug reactions/events caused by Shuanghuanglian Injection. Chinese Journal of Pharmacovigilance. 2008; 5:283-285.
2. <http://www.sda.gov.cn/WS01/CL0051/35856.html> (accessed Feb. 5, 2009).
3. Gomes ER, Demoly P. Epidemiology of hypersensitivity drug reactions. Curr Opin Allergy Clin Immunol. 2005; 5:309-316.
4. Szebeni J. Complement activation-related pseudoallergy: A new class of drug-induced acute immune toxicity. Toxicology. 2005; 216:106-121.
5. Wa E, Jm B. Anaphylactic and anaphylactoid reactions. Clin Anat. 2007; 9:358-360.
6. Estelle F, Simons R. Anaphylaxis. J Allergy Clin Immunol. 2008; 121:S402-S407.
7. Robinson S, Sivanandan I. Anaphylactic and anaphylactoid reactions. Anaesth Intens Care. 2004; 5:298-300.
8. Demoly P, Lebel B, Messaad D, Sahla H, Rongier M, Daures JP, Godard P, Bousquet J. Predictive capacity of histamine release for the diagnosis of drug allergy. Allergy. 1999; 54:500-506.
9. Sitter H, Torossian A, Duda D, Sattler J. Classification of perioperative histamine-related reactions. Inflamm Res. 2004; 53:S164-S168.
10. Norris AA. Pharmacology of sodium cromoglycate. Clin Exp Allergy. 1996; 26:5-7.
11. Pharmacopoeia of the People's Republic of China. People's Medical Publishing House, Beijing, China, 2005. (in Chinese)
12. Ma BP, Zhang J, Kang LP, Xiong CQ, Jia JM. Establishment and application of fingerprints of Shuanghuanglian Powder-Injection by HPLC. Chin Traditional Patent Med. 2006; 28:157-161. (in Chinese)
13. Blom JD, Yang PC, Nicholson NS, Case BL, Parlow JJ, South MS, Wegner CD. A method for determining whether hypotension caused by novel compounds in preclinical development results from histamine release. J Pharmacol Toxicol Methods. 2004; 49:31-37.
14. Koppada R, Norozian FM, Torbati D, Kalomiris S, Ramachandran C, Totapally BR. Physiological effect of a novel immune stimulator drug, (1,4)- α -D-Glucan, in rats. Basic Clin Pharmacol Toxicol. 2009; 105:217-221.
15. Diehl KH, Hull R, Morton D, Pfister R, Rabemampianina Y, Smith D, Vidal JM, van de Vorstenbosch C; European Federation of Pharmaceutical Industries Association and European Centre for the Validation of Alternative Methods. A good practice guide to the administration of substances and removal of blood, including routes and volumes. J Appl Toxicol. 2001; 21:15-23.
16. Levy JH, Kettlekamp N, Goertz P, Hermens J, Hirshman CA. Histamine release by vancomycin: a mechanism for hypotension in man. Anesthesiology. 1987; 67:122-125.
17. Lagunoff D, Martin TW, Read G. Agents that release histamine from mast cells. Annu Rev Pharmacol Toxicol. 1983; 23:331-351.
18. Iizuka T, Sakai H, Moriyama H, Suto N, Nagai M, Bagchi D. Vasorelaxant effects of forsythide isolated from the leaves of Forsythia viridissima on NE-induced aortal contraction. Phytomedicine. 2009; 16:386-390.

(Received October 23, 2009; Accepted December 24, 2009)

Original Article**In vitro modulating effects of glutathione on vascular tension and involvement of extracellular calcium**Nattaya Chaothanaphat¹, Prasan Dhumma-Upakorn², Suree Jianmongkol^{2,*}¹ Graduate Program in Biopharmaceutical Sciences, Chulalongkorn University, Bangkok, Thailand;² Department of Pharmacology and Physiology, Faculty of the Pharmaceutical Sciences, Chulalongkorn University, Bangkok, Thailand.

ABSTRACT: This study investigated the involvement of endothelium and extracellular calcium on the vasorelaxant activity of glutathione (GSH) using *in vitro* model of isolated rat aorta. The aortic tensions upon treatment with GSH in the presence and absence of endothelium were compared in various conditions. In phenylephrine-precontracted aortic rings, GSH (2-8 mM) significantly induced vasorelaxation in concentration-dependent manner. The influence of endothelium was demonstrated in determining the responses of aortic muscle toward GSH treatment. GSH (up to 5 mM) caused a higher loss of vascular tensions in the endothelium-intact aortic rings than those in the endothelium-denude preparations. The vasorelaxant effect of GSH in endothelium-intact rings was inhibited by glibenclamide (3 μ M), methylene blue (10 μ M) and *N*-nitro-L-arginine methyl ester (10 μ M), indicating the involvement of membrane K⁺ channels and NO-cGMP pathway. In the endothelium-denude preparations, only glibenclamide inhibited the modulating effect of GSH on aortic tension. Furthermore, the endothelium-dependent vasorelaxation of GSH was abolished in Ca²⁺-free medium containing EGTA, but not in the medium containing BAPTA-AM (10 μ M). Taken together, our findings suggested that vasorelaxant activity of GSH depended on influx of extracellular Ca²⁺ to activate NO production in endothelium cells. In addition, other possible mechanisms included its hyperpolarizing actions in vascular muscle cells.

Keywords: GSH, vasorelaxation, extracellular calcium, isolated rat aorta

*Address correspondence to:

Dr. Suree Jianmongkol, Department of Pharmacology and Physiology, Faculty of the Pharmaceutical Sciences, Chulalongkorn University, Praya-Thai Road, Bangkok 10330, Thailand.
e-mail: sureejmk@yahoo.com

1. Introduction

Glutathione (GSH), a known endogenous sulfhydryl redox agent, has been demonstrated its roles for protecting endothelium functions and regulating vascular tone (1,2). Several studies have linked the vascular protective effects of GSH to its antioxidative activities, resulting in an increase of nitric oxide (NO) bioavailability and vasodilatation (3-5). It was demonstrated that the vasorelaxing activity of aortic preparations isolated from spontaneous hypertensive rats (SHR) improved in the GSH treatment group, possibly via endothelium-dependent mechanisms (6). Moreover, *in vivo* depletion of GSH enhanced contraction and attenuated endothelium-dependent relaxation (7,8). Beyond the antioxidative mechanisms, an alteration of redox status of endothelium or smooth muscle membrane might directly affect the vascular tension through several mechanisms including oxidative modification of receptors and ion channels. In particular, it was demonstrated that GSH could relax tension of isolated guinea pig tracheas due to activation of potassium (K⁺) channels, not to the NO-mediated mechanism (9). Furthermore, the vasorelaxant effects of other sulfhydryl reducing agents such as *N*-acetylcysteine (NAC) were linked to the activities of membrane K⁺ channels (10).

The change in intracellular Ca²⁺ concentration is very crucial for the regulation of vascular tension. Rising of intracellular Ca²⁺ in endothelium triggers several mechanisms of vasorelaxation including synthesis and release of NO as well as K⁺ channel-activating endothelium-derived hyperpolarizing factors (11-13). Generally, the sources of Ca²⁺ could be from internal stores as well as from extracellular Ca²⁺ pool. To this end, we investigated the vasorelaxing action of extracellular GSH and its involvement with Ca²⁺ handling in the blood vessels. In addition, we further elucidated the influence of endothelium and mechanisms of GSH-induced vasorelaxation in endothelium-intact and endothelium-denude blood vessels, using the functional analysis model of isolated rat thoracic aorta.

2. Materials and Methods

2.1. Chemicals

Glutathione (GSH) and other principal compounds such as phenylephrine (PE), acetylcholine (Ach), glibenclamide, methylene blue, sodium nitroprusside (SNP), *N*-nitro-L-arginine methyl ester (L-NAME), bis(o-aminophenoxy) ethane-*N,N,N',N'*-tetraacetic acid (BAPTA-AM), ethyleneglycol-bis-(β -aminoethylether)-*N,N'*-tetraacetic acid (EGTA) were purchased from Sigma Chemical Company (St. Louis, MO, USA). All other chemicals were reagent grade or the highest-grade commercial available.

2.2. Preparations of isolated aorta

The experiments were approved by the Institutional Animal Ethic Committee of the Faculty of Pharmaceutical Sciences, Chulalongkorn University, Thailand. The thoracic aorta were excised from male Wistar rats (250-300 g), and cut into segments of approximately 0.3 cm long. The aortic rings were mounted with an isotonic force transducer (Model MLT 050/A, AD Instruments, Australia) under a resting tension of 1.0 g in Krebs-Henseleit solution (KHS) (content in mM; NaCl 118, KCl 4.7, CaCl₂ 2.52, MgSO₄ 1.64, KH₂PO₄ 1.18, NaHCO₃ 7, and glucose 5.5) at 37°C and bubbled with 95% O₂/5% CO₂. The tension was recorded through the computerized system equipped with software Chart 5.0 of Powerlab 4/SP data acquisition (AD Instruments, Australia).

The presence of functional endothelium were tested by priming the aortic rings with PE (10 μ M), followed by addition of Ach (10 μ M) when the contraction reached the plateau state. The relaxation response of at least 60% was considered endothelium-intact rings for further experiments. In certain experiments, endothelium was removed by gentle rubbing the lumen with cotton swab. The absence of the endothelium was suggested by less than 10% relaxation response to Ach.

2.3. Vasorelaxant effects of glutathione

The contraction of aortic rings was provoked by PE (1 μ M). When the contraction reached plateau state, GSH was added cumulatively to produce relaxation. The tension was recorded and expressed as the percentage of the maximum contraction induced by PE. In our studies, L-valine (at the equal concentrations to those of GSH) was applied as the control group.

In addition, the vasorelaxant property of GSH was further investigated with the uses of known vasorelaxant inhibitors including ibuprofen (10 μ M), propranolol (10 μ M), atropine (10 μ M), L-NAME (10 μ M), methylene blue (10 μ M), and glibenclamide (10

μ M). These inhibitors were incubated with the rings for 30 min prior to the relaxation experiment as described above.

2.4. Potentiation effects of GSH on the Ach- or SNP-induced vasorelaxation

After the resting tension of the endothelium-intact rings was stable, the contraction was provoked by addition of KCl (60 mM). When the contraction reached a plateau state, Ach (0.01-100 μ M) or SNP (0.001-10 μ M) were added cumulatively to induce relaxation. The potentiation effects of GSH were tested by pre-incubating the rings with GSH for 5 min prior to addition of KCl. The relaxation responses were calculated as a percentage in relative to the contraction provoked by KCl (60 mM) in the absence of GSH.

2.5. Involvement of calcium in GSH-induced vasorelaxation

The involvement of extracellular Ca²⁺ in GSH-induced vasorelaxation was functional determined in the endothelium-intact aortic rings, using the method previously described by Yang *et al.* (14). In these studies, either BAPTA-AM (10 μ M) or EGTA (0.2 M) was employed to chelate Ca²⁺ during the relaxation process. In brief, when the PE-induced contraction reached the plateau state, BAPTA-AM (10 μ M), a known permeable Ca²⁺ chelating agent, was added and incubated with the tissue for 15 min prior to cumulative addition of GSH. In another experiment, the aortic rings were equilibrated in Ca²⁺-free KHS containing EGTA (0.2 M) for 90 min before addition of PE to start the experiment as described above.

2.6. Statistical analysis

Results were presented as the mean \pm S.E.M., obtained from 6 separated experiments ($n = 6$). Statistic comparisons were performed either by Student's *t*-test or one-way ANOVA followed by a post-hoc Dunnett *t*-test where appropriate. Significances were considered at $p < 0.05$.

3. Results

3.1. Vasorelaxant effects of GSH

As shown in Figure 1, GSH caused vasorelaxation in concentration-dependent manner on both endothelium-intact and -denude rat aortic rings, but with different degree of relaxation. GSH at the low concentrations of 2 and 4 mM induced relaxation of the intact preparations at higher degree than those of the denude preparations (Figure 2). Interestingly, it appeared that

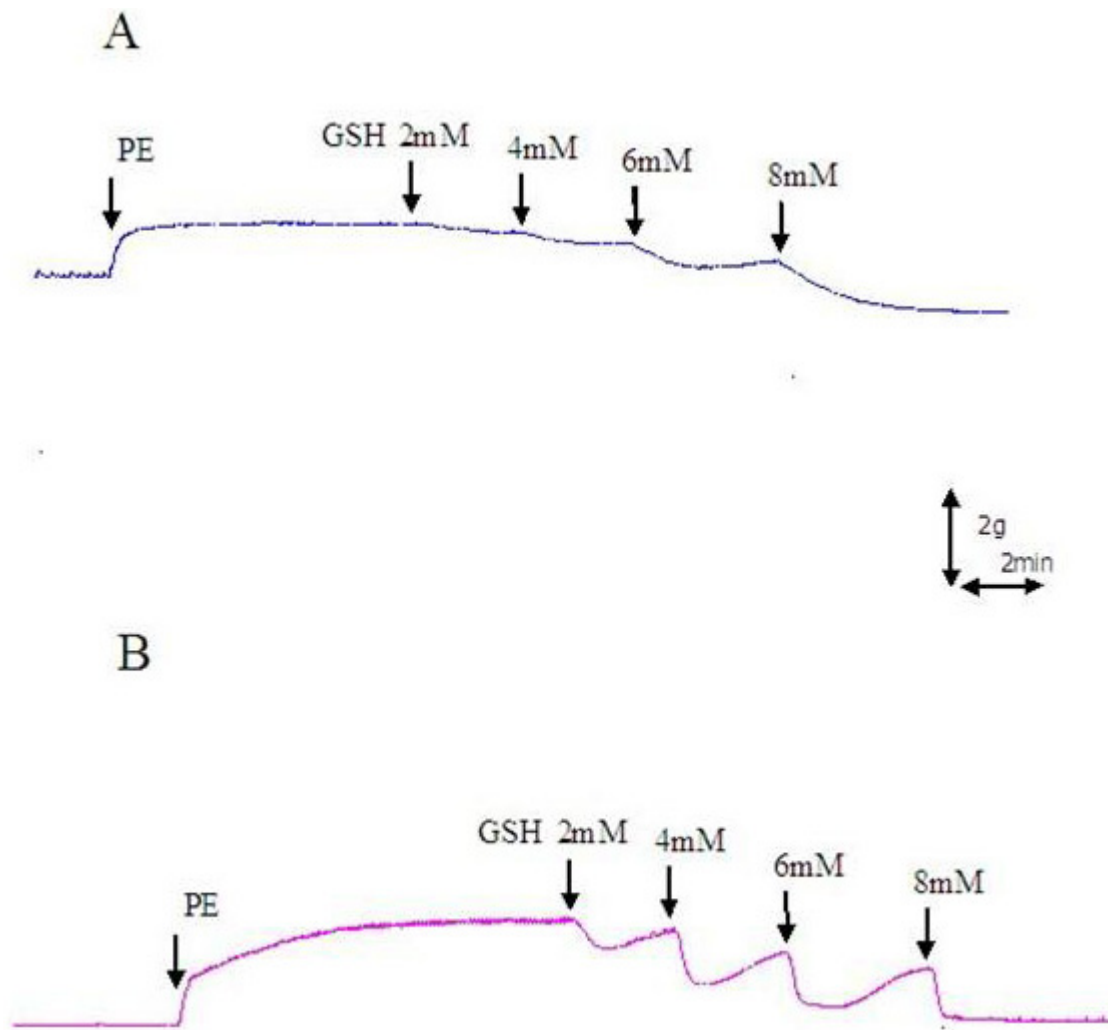


Figure 1. The representative tracing of GSH-induced relaxation in endothelium-denude (A) and endothelium-intact (B) rat aortic rings. The aortic rings were precontracted with PE (1 μ M), followed by addition of GSH cumulatively.

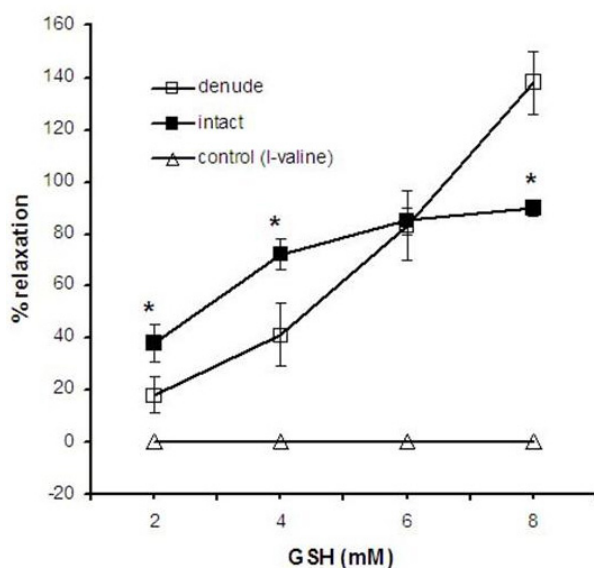


Figure 2. The vasorelaxant effects of GSH in endothelium-intact and endothelium-denude aortic rings. Data are mean \pm S.E.M. ($n = 6$), expressed as the percentage of the vascular tension induced by PE 1 μ M. * $p < 0.05$ vs. the endothelium-denude group.

the modulating effect of GSH on vascular tension could be saturated in the presence of endothelium. Removal of endothelium allowed the vascular smooth muscle to further relax beyond the initial resting tension in response to the high concentration of GSH (8 mM).

The single treatment of GSH (5 mM) was able to suppress PE-induced contraction by 20% and 80% in endothelium-denude and -intact preparations, respectively (Figure 3). Pretreatment with either L-NAME, methylene blue or glibenclamide, but not ibuprofen, atropine, and propranolol, significantly inhibited the tension modulating effects of GSH in endothelium-intact rings. On the other hand, only glibenclamide elicited its inhibitory effect on GSH-mediated relaxation in the endothelium-denude rings. These findings suggested that the relaxation effects of GSH involved the NO-cGMP and hyperpolarizing signaling pathways in endothelium-dependent mechanisms. In addition, the activation of K^+ channel-mediated hyperpolarizing effect was linked to endothelium-independent mechanism.

3.2. Potentiation effects of GSH on the Ach- or SNP-induced relaxation

As known, Ach and SNP induced vasorelaxation *via* an increase of cGMP in the NO-cGMP pathway. Ach increased production of NO in endothelium cells whereas SNP directly activated guanylate cyclase in smooth muscle cells. Our result demonstrated that the presence of GSH increased the sensitivity of aortic preparations toward Ach treatment. As seen in Figure 4A, the concentration-response curve of Ach shifted leftward in the presence of GSH. The calculated concentration of Ach that caused 50% relaxation (IC_{50}) decreased approximately 10 folds from 77 μ M to 7.3 μ M in the presence of GSH. On the contrary, GSH had no effects on SNP-mediated vasorelaxation in this study (Figure 4B). These findings suggested that GSH could enhance the function of endothelium in production of NO. The lack of potentiating effect in SNP-induced vasorelaxation might reflect that GSH had no influence on guanylate cyclase activity or contractile elements.

It was noteworthy to mention that the effects of GSH on Ach-induced relaxation depended on the amount of intact endothelium cells. The more numbers of endothelium intacted, the less potentiative effect of GSH on Ach-induced relaxation was observed. In the preparations with 80-90% of intact endothelium, GSH

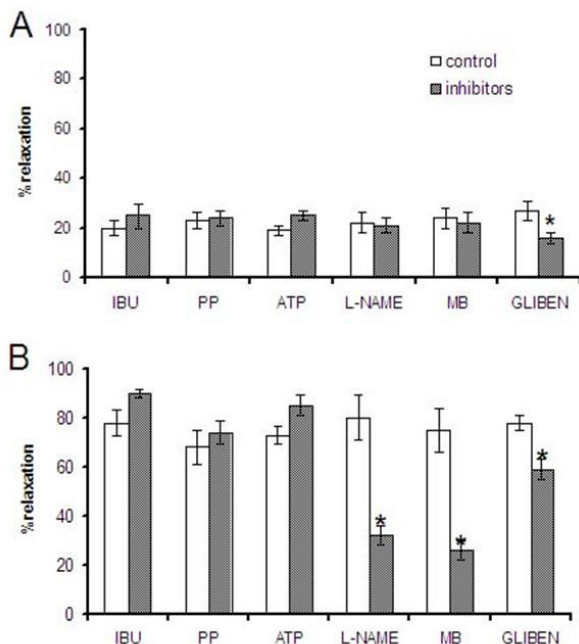


Figure 3. The effects of various vasorelaxant inhibitors on the GSH-induced relaxation in the endothelium-denude (A) and endothelium-intact (B) preparations. IBU, ibuprofen; PP, propranolol; ATP, atropine; L-NAME, *N*-nitro-*L*-arginine methyl ester; MB, methylene blue; GLIBEN, glibenclamide. Data are mean \pm S.E.M. ($n = 6$), expressed as the percentage of the vascular tension induced by PE 1 μ M. * $p < 0.05$ vs. control group.

had no significant potentiative effect of Ach-induced relaxation. However, in those with 60-70% of intact endothelium, GSH elicited its potentiative relaxation significantly.

3.3. Involvement of calcium in GSH-induced endothelium-dependent vasorelaxation

An increase of intracellular Ca^{2+} in the endothelium could activate the NO synthase activity and increased production of NO, resulting in vasorelaxation (11,12). Hence, this study was to examine the influence of intracellular Ca^{2+} on the GSH-induced relaxation by applying Ca^{2+} -free environment to the experiment condition. Upon changing medium from Ca^{2+} -containing solution to Ca^{2+} -free KHS containing EGTA, the contractile response to PE decreased by 80%. However, the PE-induced contraction was still sustainable. Under this condition, the vasorelaxation effects of GSH were compromised significantly (Figure

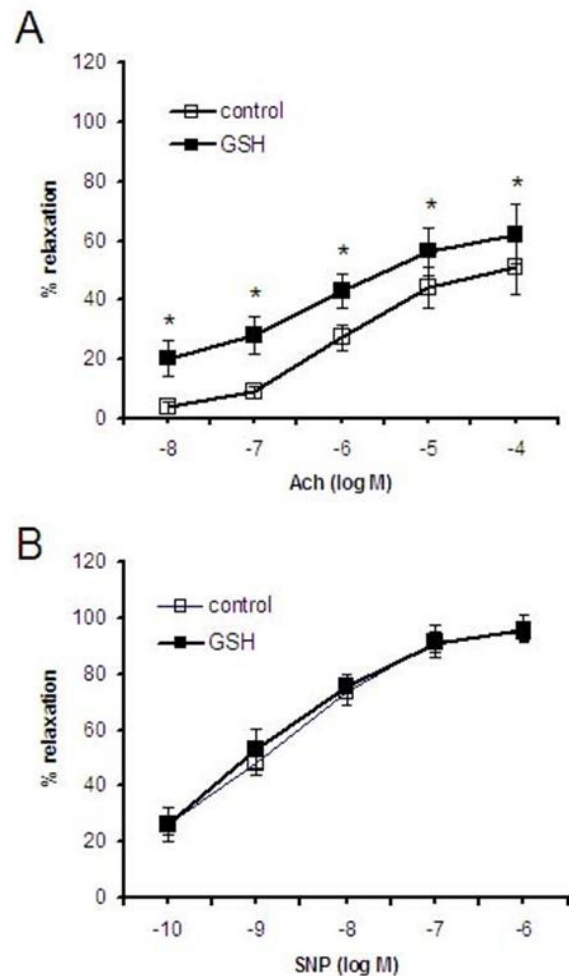


Figure 4. Concentration-response curves for the vasorelaxing action of acetylcholine (Ach) (A) and sodium nitroprusside (SNP) (B) in the presence of GSH (5 mM). Data are mean \pm S.E.M. ($n = 6$), expressed as the percentage of the vascular tension induced by KCl 60 mM. * $p < 0.05$ vs. control group.

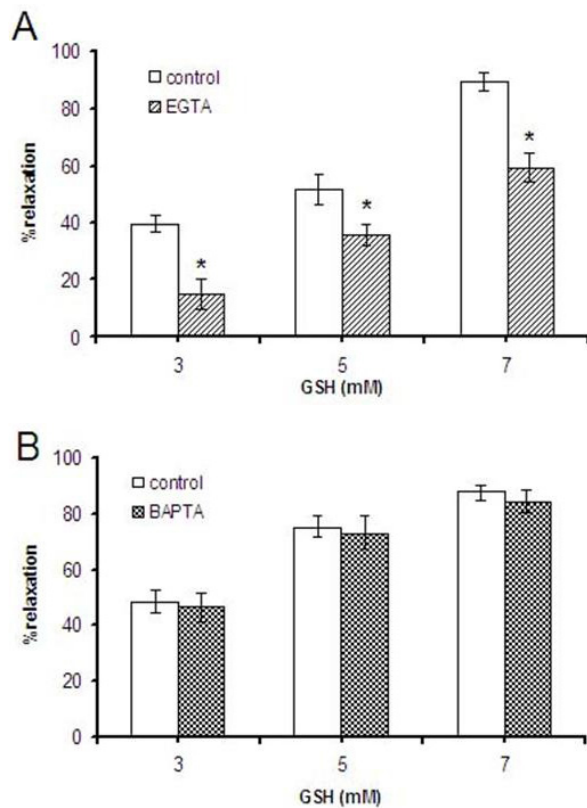


Figure 5. Influence of extracellular Ca^{2+} on the vasorelaxant effects of GSH. The GSH-induced relaxation was determined in the Ca^{2+} -free medium containing 0.2 mM EGTA (A) or in the medium containing 10 μM BAPTA-AM (B). Data are mean \pm S.E.M. ($n = 6$), expressed as the percentage of the vascular tension induced by PE 1 μM . * $p < 0.05$ vs. control group.

5A). On the contrary, BAPTA-AM (10 μM) had no markedly influence on either PE-induced contraction or the degree of GSH-induced relaxation (Figure 5B). These finding suggested that extracellular Ca^{2+} was more critical than intracellular Ca^{2+} in GSH-induced vasorelaxation in the endothelium intact preparation. GSH might affect processes of Ca^{2+} influx, without any interference on activation of Ca^{2+} release from the cellular storage.

4. Discussion and Conclusion

In this study, we were able to demonstrate the vasomotion effects of extracellular GSH in the model of isolated rat thoracic aorta. As known, endothelium protected cells from chemical insults and also control vascular tension. In addition, endothelium may buffer a swift change of vascular tone by balancing between secretion of vasoconstrictors and vasodilators (15). In this study, endothelium certainly contributed its influence in determining the responses of aortic muscle toward GSH treatment. Our results suggested that GSH exerted its vasorelaxant activity through both endothelium-dependent and -independent mechanisms. Removal of endothelium from the aortic

preparations caused the tissue less sensitive to GSH-induced vasorelaxation. However, the removal of endothelium also caused a loss of protective barrier and regulatory control of muscle tension (16,17). Consequently, because of the loss of endothelium buffering system, GSH at high concentration (8 mM) effectively decreased vascular tension of the PE-precontracted aortic smooth muscle beyond the maximum developed tension ($> 100\%$).

The presence of L-NAME and methylene blue, which were inhibitors of nitric oxide synthase (NOS) and guanylate cyclase, respectively, could attenuate GSH-mediated endothelium-dependent vasorelaxation. In agreement with other reports, extracellular GSH exerted its relaxant effects on endothelium cells mainly through activation of the NO-cGMP pathway (2,18,19). In addition, glibenclamide, a known K^+ channel blocker, also inhibited the effect of GSH, although with a lesser degree than L-NAME and methylene blue. Other inhibitors of endothelium-dependent vasorelaxation including atropine, propranolol and ibuprofen had no influence on GSH-induced relaxation. It has been established that an opening of K^+ channels in smooth muscle cells results in membrane hyperpolarization, leading to close of Ca^{2+} channels, and vasodilatation (20,21). Moreover, the inhibitory effect of glibenclamide against GSH-induced vasorelaxation was also observed in endothelium-denude aortic preparations. Taken together, in addition to the NO-cGMP pathway, we suggested that GSH exerted its vasorelaxant activity *via* membrane hyperpolarization as a minor pathway. Furthermore, the vasorelaxant effects of GSH were unlikely to involve with production of PGI_2 , or activation of β_2 -adrenergic and cholinergic receptors (muscarinic receptor).

GSH could potentiate the aortic relaxation induced by acetylcholine (Ach) but not those induced by sodium nitroprusside (SNP). This observation was in agreement with other reports that GSH had no influence on endothelium-independent relaxation induced by NO donors (6,7). Hence, vasorelaxant effects of GSH were unlikely to involve with endothelium-independent activation of guanylate cyclase and cGMP availability. Moreover, methylene blue could not inhibit the GSH-induced relaxation of the endothelium-denude rat aortic rings.

The NO-cGMP pathway could be divided into two sequential steps. The initial step involved the NO production in endothelium and subsequently followed by the cGMP production in vascular smooth muscle cell to induce relaxation. The initial step of NO-cGMP pathway was activated by a rising of intracellular Ca^{2+} . The major source of cytosolic Ca^{2+} are from an influx of extracellular Ca^{2+} and from a release Ca^{2+} of internal stored Ca^{2+} (22,23). In this study, the relationship between the source of Ca^{2+} and the

mechanism of GSH-induced relaxation in endothelium cells were determined. We were able to show that the relaxant effects of GSH were related to inhibition of the Ca^{2+} -free medium containing EGTA but were not inhibited after rapid buffering of intracellular Ca^{2+} in endothelial cell with a membrane-permeable chelator (BAPTA-AM). Hence, the effects of GSH were clearly extracellular Ca^{2+} -dependent.

The sites of extracellular GSH action on endothelium cells have not been reported. It was very unlikely that GSH was rapidly transported into the cells and elicited its actions (24,25). Hence, GSH might affect specific target proteins on plasma membrane which were consequently connected to the process in NOS activation. We were quite certain that GSH had no effect on an increase of intracellular Ca^{2+} through activation of muscarinic receptor because treatment of atropine could not abolish GSH-induced vasorelaxation. It was likely that GSH initiated Ca^{2+} influx from extracellular source to activate NO production in endothelial cells. In addition, a rising of intracellular Ca^{2+} in the endothelium cells could trigger the release of endothelium-derived hyperpolarizing factors, leading to relaxation of vascular smooth muscle (13,26).

In conclusion, the mechanisms of GSH-induced relaxation might involve with the NO-cGMP pathway through an increase in Ca^{2+} influx and NO production in endothelial cells, but not the cGMP production in vascular smooth muscle cell. In addition, other possible mechanisms included the activation of membrane K^+ channels.

Acknowledgements

This work was supported by Graduate Research Fund of Chulalongkorn University, Bangkok, Thailand.

References

- Zhu H, Cao Z, Zhang L, Trush MA, Li Y. Glutathione and glutathione-linked enzymes in normal human aortic smooth muscle cells: chemical inducibility and protection against reactive oxygen and nitrogen species-induced injury. *Mol cell Biochem.* 2007; 301:47-59.
- Prasad A, Andrews NP, Padder FA, Husain M, Quyyumi AA. Glutathione reverses endothelial dysfunction and improves nitric oxide bioavailability. *J Am Coll Cardiol.* 1999; 34:507-514.
- Sommer SP, Gohrbandt B, Fischer S, Hohlfield JM, Warnecke G, Avsar M, Struber M. Glutathione improves the function of porcine pulmonary grafts stored for twenty-four hours in low-potassium dextran solution. *J Thorac Cardiovasc Surg.* 2005; 130:864-869.
- Kim HR, Kim JW, Park JY, Je HD, Lee SY, Huh IH, Sohn UD. The effects of thiol compounds and ebselen on nitric oxide activity in rat aortic vascular responses. *J Auton Pharmacol.* 2001; 21:23-28.
- Vaziri ND, Wang XQ, Oveisi F, Rad B. Induction of oxidative stress by glutathione depletion cause severe hypertension in normal rats. *Hypertension.* 2000; 36:142-146.
- Akpaffiong MJ, Taylor AA. Antihypertensive and vasodilator actions of antioxidants in spontaneously hypertensive rats. *Am J Hypertens.* 1998; 11:1450-1460.
- Ford RJ, Denniss SG, Graham DA, Quadrilatero J, Rush WE. Glutathione depletion *in vivo* enhances contraction and attenuates endothelium-dependent relaxation of isolated rat aorta. *Free Radical Biol Med.* 2006; 40:670-678.
- Wang R, Meng QH, Yan SK, Chang T, Wang H, Wu L. Effects of hydrogen sulfide on homocysteine-induced oxidative stress in vascular smooth muscle cells. *Biochem and Biophys Res Commun.* 2006; 351:485-491.
- Kloek J, Ark I, Blodsmas N, Clerck FD, Nijkamp FP, Folkerts G. Glutathione and other low-molecular-weight thiols relax guinea pig trachea *ex vivo*: interactions with nitric oxide? *Am J Physiol Lung Cell Mol Physiol.* 2002; 283:L403-L408.
- Han WQ, Zhu DL, Wu LY, Chen QZ, Guo SJ, Gao PJ. *N*-acetylcysteine-induced vasodilation involves voltage-gated potassium channels in rat aorta. *Life Sci.* 2009; 84:732-737.
- Dudzinski D, Michel T. Life history of eNOS: partners and pathways. *Cardiovasc Res.* 2007; 75:247-260.
- Buluc M, Demirel-Yilmaz E. Resveratrol decreases calcium sensitivity of vascular smooth muscle and enhances cytosolic calcium increase in endothelium. *Vascul Pharmacol.* 2006; 44:231-237.
- Chen GF, Suzuki H. Calcium dependency of the endothelium-dependent hyperpolarization in smooth muscle cells of the rabbit carotid artery. *J Physiol.* 1990; 421:521-534.
- Yang ZW, Zhang A, Altura BT, Altura BM. Hydrogen peroxide-induced endothelium-dependent relaxation of rat aorta. *Gen Pharmacol.* 1999; 33:325-336.
- Bonetti PO, Lerman LO, Lerman A. Endothelial dysfunction a marker of atherosclerotic risk. *Arterioscler Thromb Vasc Biol.* 2003; 23:168-175.
- Kalinowski L, Malinski T. Endothelial NADH/NADPH-dependent enzymatic sources of superoxide production: relationship to endothelial dysfunction. *Acta Biochimica Polonica.* 2004; 51:459-469.
- Guerci B, Kearney-Schwartz A, Bohme P, Zannad F, Drouin P. Endothelial dysfunction and type 2 diabetes. *Diabetes Metab.* 2001; 27:425-434.
- Kugiyama K, Miyao Y, Sakamoto T, Kawano H, Soejima H, Miyamoto S, Yoshimura M, Ogawa H, Sugiyama S, Yasue H. Glutathione attenuates coronary constriction to acetylcholine in patients with coronary spastic angina. *Am J Physiol Heart Circ Physiol.* 2001; 280:H264-H271.
- Cheung PY, Schulz R. Glutathione causes coronary vasodilation via a nitric oxide and soluble guanylate cyclase-dependent mechanism. *Am J Physiol.* 1997; 273: H1231-H1238.
- Jackson WF. Ion channels and vascular tone. *Hypertension.* 2000; 2:173-178.
- Kühberger E, Kukovetz WR, Groschner K. Cromakalim inhibits multiple mechanisms of smooth muscle activation with similar stereoselectivity. *J Cardiovasc Pharmacol.* 1993; 21:947-954.
- Ungvari Z, Sun D, Huang A, Kaley G, Koller A. Role of endothelial $[\text{Ca}^{2+}]_i$ in activation of eNOS in pressurized arterioles by agonists and wall shear stress. *Am J Physiol*

- Heart Circ Physiol. 2001; 281:H606-H612.
23. Dora KA, Doyle MP, Duling BR. Elevation of intracellular calcium in smooth muscle causes endothelial cell generation of NO in arterioles. Proc Natl Acad Sci U S A. 1997; 94:6529-6534.
 24. Raftos JE, Whillier S, Chapman BE, Kuchel PW. Kinetics of uptake and deacetylation of *N*-acetylcysteine by human erythrocytes. Inter J Biochem Cell Biol. 2007; 39:1698-1706.
 25. Kugiyama K, Hirashima O, Misumi K, Motoyama T, Ogawa H, Ohgushi M, Soejima H, Sugiyama S, Yasue H. Intracoronary infusion of reduced glutathione improves endothelial vasomotor response to acetylcholine in human coronary circulation. Circulation. 1998; 97:2299-2301.
 26. Fukao M, Hattori Y, Kanno M, Sakuma I, Kitabatake A. Sources of Ca²⁺ in relation to generation of acetylcholine-induced endothelium-dependent hyperpolarization in rat mesenteric artery. Br J Pharmacol. 1997; 120:1328-1334.

(Received January 4, 2010; Accepted January 28, 2010)

Original Article

Evaluation of *in vitro* dissolution profile comparison methods of sustained release tramadol hydrochloride liquisolid compact formulations with marketed sustained release tablets

Amrit B. Karmarkar*, Indrajeet D. Gonjari, Avinash H. Hosmani, Pandurang N. Dhabale

Govt. College of Pharmacy, Karad-415124, Dist. Satara, MS, India.

ABSTRACT: The aim of the present work was to prepare and evaluate sustained release liquisolid compact formulations of tramadol hydrochloride. The dissolution profile of the prepared compacts was also compared to that of a marketed preparation. Liquisolid sustained release formulations were prepared by using HPMC K4M as a sustained release agent. Precompression studies of characteristics such as flow properties were also carried out. Liquisolid compacts were evaluated by hardness, friability, and *in vitro* dissolution studies. Comparison of dissolution profiles was carried out by using a model-independent, model-dependent, and statistical approach. The prepared liquisolid compacts are new dosage forms with better sustained release behavior compared to a marketed sustained formulation. The dissolution profile followed the Peppas model as "best fit" model. Two-way ANOVA results revealed a significant difference in dissolution profiles. This systematic approach to producing a formulation was found to help with analyzing the sustained release of tramadol hydrochloride. The use and evaluation of model-dependent methods is more complicated. These methods provide an acceptable model approach that indicates the true relationship between percent drug release and time variables, including statistical assumptions.

Keywords: Liquisolid compacts, tramadol hydrochloride, dissolution, ANOVA

1. Introduction

A sustained release dosage form is mainly designed to maintain therapeutic blood or tissue levels of a drug for an extended period of time with minimized local

or systemic adverse effects. Economy and greater patient compliance are other advantages (1). In recent years, clinical studies on tramadol hydrochloride have demonstrated that this drug is an effective agent for moderate to severe chronic pain (2-5). The half-life of the drug is about 5.5 h and the usual oral dosage regimen is 50 to 100 mg every 4 to 6 h, with a maximum dosage of 400 mg/day (6). A sustained-release formulation tramadol would prove beneficial in reducing the frequent administration of this dosage form and improving patient compliance. The drug is freely water-soluble and hence judicious selection of release-retarding excipients is necessary to achieve a constant *in vivo* input rate of the drug. Various approaches have been used by researchers to sustain drug release in the form of tablets (7-9).

A liquisolid system is a novel technique developed by Spireas *et al.* (10,11). "Liquisolid systems" involve conversion of liquid lipophilic drugs or water-insoluble solid drugs dissolved in non-volatile solvent, and this liquid medication can be converted into free-flowing, non adherent, dry, and readily compressible powders through the use of carrier and coating materials. With water-soluble drugs, sustained release can be obtained (12). The term "liquisolid compacts" as described by Spireas *et al.* refers to immediate or sustained release tablets or capsules that are prepared using the "liquisolid system" technique in combination with inclusion of appropriate adjuvants required for tableting or encapsulation, *e.g.* lubricants, and for rapid or sustained release action, *e.g.* disintegrants and binders (10). Advantages of this technique are its low cost, simplicity of formulation, and applicability to industrial production (13).

In the present study, hydroxy propyl methyl cellulose (HPMC) K4M was used as an adjuvant to sustain drug release from liquisolid compacts. The term "adjuvant" as a sustained release agent is cited by Spireas *et al.* (10,11). Avicel PH 102 and Aerosil 200 were used as carrier and coating materials, respectively. Precompression studies such as determination of the angle of repose, Hausner's ratio, and Carr's index were carried out and stereomicroscopic analysis was also

*Address correspondence to:

Mr. Amrit B. Karmarkar, Govt. College of Pharmacy, Karad-415124, Dist. Satara, MS, India.
e-mail: abkarmarkar@gmail.com

performed. Differences in release profiles to those of marketed tablets of tramadol hydrochloride were determined using a model-independent method f_2 and a statistical approach in the form of two-way repeated-measures ANOVA. Model fitting was also done for different models such as zero-order, first-order, Hixon-Crowell, Peppas, and Matrix models. A new mathematical model for formulation design as described by Spireas *et al.* (10) was used to calculate appropriate amounts of carrier and coating materials based on new fundamental properties of a powder called the flowable liquid retention potential (Φ value) and compressible liquid retention potential (Ψ number) of powder ingredients (previously determined by Spireas *et al.*) (10,11).

2. Materials and Methods

2.1. Materials

Tramadol was generously provided by Panacea Biotech (India). HPMC K4M, Avicel PH 102 and Aerosil 200 were generously provided by Okasa Pharmaceuticals (India). Propylene glycol was purchased from Loba Chemie (India). All other reagents and chemicals were of analytical grade.

2.2. Use of a mathematical model to design liquisolid compacts

The formulation design of liquisolid systems was done in accordance with the new mathematical model described by Spireas *et al.* (10). In this study, propylene glycol was used as a liquid vehicle, and Avicel PH 102 and Aerosil 200 were used as the carrier and coating materials, respectively. The concentration of the drug in propylene glycol was 10, 20, and 30 g% and the carrier: coat ratio ranged from 30 to 40 and 50. According to new theories, the carrier and coating powder materials can retain only certain amounts of liquid while maintaining acceptable flowability and compressibility.

The excipient ratio R of the powder is defined as

$$R = Q / q \quad \text{----- Eq. 1}$$

where R is the ratio of the weight of carrier (Q) and coating (q) materials present in the formulation.

The liquid load factor (L_f) is defined as the ratio of the weight of liquid medication (W) to the weight of the carrier powder (Q) in the system, which should be present in an acceptably flowing and compressible liquisolid system, *i.e.*

$$L_f = W / Q \quad \text{----- Eq. 2}$$

The flowable liquid retention potential (Φ value) of powder excipients was used to calculate the required ingredient quantities. Therefore, powder excipients ratios R and liquid load factors L_f of the formulations are related as follows:

$$L_f = \Phi + \Phi (1 / R) \quad \text{----- Eq. 3}$$

where, Φ and Φ are the Φ values of carrier and coating materials, respectively.

Hence, to calculate the required weights of the excipients used Φ and Φ from Eq. 3 are constants, and thus L_f was calculated according to the ratio of carrier: coating materials (R).

Using the above mathematical model, liquisolid compacts were formulated as summarized in Table 1.

2.3. Determination of solubility

Saturated solutions were prepared by adding excess tramadol to the propylene glycol and shaking on a shaker for 48 h at 25°C with constant vibration. The solutions were filtered through a 0.45 micron filter, diluted with water, and analyzed with a Shimadzu 1700 UV-Vis spectrophotometer at 271.5 nm with respect to a blank sample (the blank sample was a solution containing the same concentration used without the drug). Determination was carried out in triplicate for each sample to calculate the solubility of tramadol.

2.4. Preparation of liquisolid compacts

Calculated quantities of tramadol hydrochloride and propylene glycol were accurately weighed in a 20-mL

Table 1. Formulation design of liquisolid compacts

Formulation batch code	Drug concentration in Propylene glycol (% w/w)	R	L_f	Avicel PH 102 (mg) ($Q = W/L_f$)	Aerosil 200 (mg) ($q = Q/R$)	HPMC K4M (mg)
F1	10	30	0.270	197.5	6.58	100
F2		40	0.243	219.46	5.48	150
F3		50	0.226	235.97	4.71	200
F4	20	30	0.270	395.03	13.10	100
F5		40	0.243	438.93	10.97	150
F6		50	0.226	471.94	9.43	200
F7	30	30	0.270	592.59	19.75	100
F8		40	0.243	658.43	16.46	150
F9		50	0.226	707.96	14.15	200

glass beaker and then heated to 180°C. The resulting hot medication was incorporated into calculated quantities of carrier and coating materials. The mixing process was carried out in three steps as described by Spireas *et al.* (10). In the first, the system was blended at an approximate mixing rate of one rotation per second for approximately one minute in order to evenly distribute liquid medication in the powder. In the second, the liquid/powder admixture was evenly spread as a uniform layer on the surface of a mortar and left standing for approximately 5 min to allow the drug solution to be absorbed inside powder particles. In the third, the powder was scraped off the mortar surface using an aluminum spatula. Then HPMC K4M was added to this mixture and blended in a mortar. This provided the final formulation that was compressed into tablets using a single punch tablet compression machine.

2.5. Precompression studies: Flow properties

Flow properties of liquisolid formulation were studied by angle of repose, Carr's index, and Hausner's ratio (14). Each analysis was carried out in triplicate. Bulk density measurements were carried by placing a fixed weight of powder in a graduated cylinder, and the volume occupied was measured and the initial bulk density was calculated. The cylinder was then tapped at a constant velocity until a constant volume was obtained. The tapped density was then calculated. The angle of repose was calculated by the fixed-height cone method. All studies were done in triplicate.

2.6. Evaluation of liquisolid compacts

The *hardness* of liquisolid compacts was determined using a Pfizer hardness tester (Pfizer). The mean hardness of each formula was determined. The *friability* of prepared liquisolid compacts was determined using a digital tablet friability tester (Roche).

2.7. In vitro drug release studies

Studies were done on a six-station USP dissolution apparatus I (LabIndia). All batches of tablets were evaluated ($n = 3$) using 900 mL of sequential gastrointestinal release medium, *i.e.*, 0.1 N hydrochloric acid (pH 1.2) for the first 2 h, acetate buffer of pH 4.5 for the next 2 h, and then phosphate buffer of pH 7.4 for the remaining 6 h. Temperature was maintained at $37 \pm 0.5^\circ\text{C}$ throughout the study and stirring was done at 50 rpm. Samples were periodically collected, filtered through a 0.45 micron filter, and replaced with dissolution medium. After filtration through Whatman filter paper 41, the concentration of Tramadol hydrochloride was determined spectrophotometrically at 271.5 nm (Shimadzu 1700 UV-Vis Spectrophotometer). The actual amount of released drug was determined

from the calibration curve ($n = 3$).

2.7.1. Model-independent approach

According to US FDA guidance for dissolution data equivalence, a model-independent approach is recommended. This involves use of the similarity factor (f_2), which provides a simple means of comparing data. The similarity factor (f_2) is a logarithmic reciprocal square root transformation of the sum of squared error and is a measurement of the similarity in the percent (%) dissolution between the two curves.

$$f_2 = 50 \times \log\{[1 + (1/n)\sum_{t=1}^n (R_t - T_t)^2]^{-0.5} \times 100\}$$

----- Eq. 4

where n is the number of time points, R is the dissolution value of the reference at time t , and T is the dissolution value of the test at time t .

2.7.2. Model-dependent methods

The drug release from liquisolid compacts was analyzed by various mathematical models such as zero-order, first-order, Hixon-Crowell, Peppas, Hixon-Crowell, and Matrix models.

2.7.3. Statistical methods

Repeated-measures two-way ANOVA was used to determine how dissolution was affected by two factors. The percentage dissolved was the dependent variable and time was a repeated factor.

3. Results and Discussion

3.1. Use of a new mathematical model to design liquisolid systems

Tramadol hydrochloride was selected as model drug for this study as a suitable candidate for sustained release. The liquisolid hypothesis of Spireas *et al.* (18) states that a drug candidate dissolved in a liquid nonvolatile vehicle and incorporated into a carrier material with a porous structure and closely matted fibers in its interior will exhibit both adsorption and absorption. A drug in the form of liquid medication will initially be absorbed in the interior of particles of the carrier and after saturation will be adsorbed into internal and external surfaces of the carrier. Coating materials such as Aerosil 200 that have high adsorptivity and greater surface area allow liquisolid systems to provide desirable flow properties (18).

The mathematical model equation for Avicel PH 102 and Aerosil 200 in propylene glycol is given according to values of Phi (Φ) as cited by Spireas *et al.* (10,11).

$$L_f = 0.16 + 3.31 (1 / R)$$

----- Eq. 5

Based on this equation, L_r is calculated using different R values.

3.2. Solubility of tramadol hydrochloride in propylene glycol

Determination of solubility is most important aspect in formulating liquisolid systems. Solubility may contribute to molecular dispersion of the drug in a non-volatile solvent such as propylene glycol. The solubility of tramadol in propylene glycol was found to be 6.254 ± 0.44 g/10 mL.

3.3. Precompression studies for liquisolid systems: Flow properties

Flow properties are the important aspect of formulation and industrial production of tablet dosage forms. Results of measurements such as the angle of repose, Carr's index, and Hausner's ratio are shown in the Table 2. The angle of repose is characteristic to the flow rate of the powder. In general, an angle of repose $\geq 40^\circ$ indicates a powder with poor flowability (14). The current results were in accordance with that principle. Results of Carr's index and Hausner's ratio also revealed good flow behavior.

3.4. Evaluation of liquisolid compacts

Results of hardness, friability, and disintegration time are shown in Table 3. Tablets should have a certain amount of strength or hardness and resistance to friability so that they do not break during handling. However, these characteristics also affect drug dissolution. The average *hardness* of a liquisolid tablet ranged from 5.11 ± 0.25 to 6.44 ± 0.42 kg/cm². The compactness of tablets may be due to hydrogen bonding between Avicel PH 102 molecules (16). As propylene glycol is an alcoholic compound, it might have hydrogen bonding due to the presence of hydroxyl groups and may contribute to the compactness of compacts. *Friability* of liquisolid compacts was in the range of 0.133% to 0.278%. This indicates that liquisolid compacts had acceptable ability to withstand handling.

3.5. In vitro dissolution studies

In the preparation of liquisolid compacts, liquid medications containing the drug were adsorbed on the surface of carrier materials. When this system is exposed to dissolution medium, the drug on the surface of the compact dissolves quickly and diffuses into the dissolution medium. This can be assumed to be the cause of the burst release effect observed. The concentration of drug in liquid medication is an important aspect as it affects drug release. As was previously proven, an increase in drug concentration in liquid medication leads to a lower drug release rate. This is due to fact that at a higher drug concentration the drug tends to precipitate within silica (Aerosil 200) pores. This finding was also corroborated by Javadzadeh *et al.* (17). A higher amount of Aerosil 200 (Batch F9) was found to result in retarded drug release in comparison to other batches. An increase in the concentration of HPMC K4M might be responsible for the sustained effect. This is reflected in batches F3, F6, and F9. However, the marketed sustained release tablets had faster release than liquisolid sustained release formulations (Figure 1).

3.5.1. Model-independent methods

A model-independent method such as the similarity factor (f_2) provides a simple way to compare dissolution data. US FDA guidance proposes that f_2 values of 50-100 indicate equivalence in dissolution profiles. Table 4

Table 3. Results of hardness and friability tests of sustained release liquisolid tablet formulations

Formulation batch code	Average <i>hardness</i> (kg/cm ²) \pm SD	Percentage <i>friability</i> obtained during friability test (%)
F1	5.11 ± 0.25	0.174
F2	5.78 ± 0.15	0.210
F3	6.14 ± 0.38	0.256
F4	5.74 ± 0.20	0.192
F5	5.96 ± 0.37	0.244
F6	6.26 ± 0.15	0.278
F7	6.32 ± 0.34	0.143
F8	6.44 ± 0.42	0.267
F9	6.29 ± 0.29	0.133

Table 2. Results of flowability parameters of liquisolid powder systems for different formulation batches

Formulation batch code	Average angle of repose (θ) \pm SD	Average Carr's index (%) \pm SD	Average Hausner's ratio \pm SD
F1	40.61 ± 0.54	19.29 ± 0.15	1.23 ± 0.01
F2	38.97 ± 0.57	19.63 ± 0.24	1.26 ± 0.01
F3	38.76 ± 0.24	21.31 ± 0.19	1.28 ± 0.01
F4	39.62 ± 0.52	20.21 ± 0.18	1.24 ± 0.01
F5	38.49 ± 0.97	22.40 ± 0.80	1.27 ± 0.01
F6	38.02 ± 0.12	25.40 ± 0.31	1.30 ± 0.01
F7	39.19 ± 0.46	21.47 ± 0.23	1.27 ± 0.02
F8	38.56 ± 0.11	23.80 ± 0.15	1.32 ± 0.01
F9	37.40 ± 0.32	25.30 ± 0.16	1.34 ± 0.01

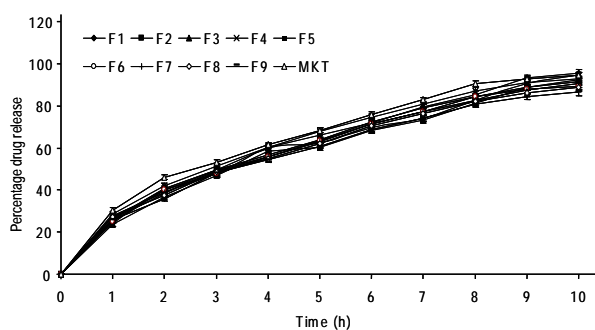


Figure 1. *In vitro* dissolution profile of sustained release tramadol hydrochloride liquisolid compacts (F1-F9) in comparison to a marketed formulation (MKT).

Table 4. Similarity factor (f_2) values of liquisolid compacts in comparison to marketed tablets

Comparison	f_2	Dissolution profile
F1 and MKT	24.52	Dissimilar
F2 and MKT	25.96	Dissimilar
F3 and MKT	11.90	Dissimilar
F4 and MKT	63.30	Similar
F5 and MKT	60.11	Similar
F6 and MKT	56.11	Similar
F7 and MKT	83.12	Similar
F8 and MKT	69.33	Similar
F9 and MKT	64.79	Similar

shows f_2 values of all of the batches. Although the dissolution profile seems to be equivalent to that of the marketed tablets, differences in f_2 values of batches F1 to F3 might be due to a lower concentration of drug present in the formulations. Other batches had f_2 values > 50 , which indicates a similarity in the dissolution profile.

3.5.2. Model-dependent methods

Although model-independent methods are simple and easy to use, they lack scientific justification (18-20). Different models of dissolution profile comparison were used (Tables 5 and 6). The results of these models indicate that all liquisolid compacts followed the Peppas model as "best fit model". This is due to the previously proven R^2 value obtained from model fitting (21). The $T_{50\%}$ of all of the formulations was also determined and indicated that batches F3 and F9 retarded release more. The $T_{50\%}$ value was thus found to increase as the concentration of HPMC K4M increases. The Korsmeyer-Peppas release exponent (n) values of all liquisolid compacts were greater than 0.5, indicating non-Fickian diffusion, *i.e.*, a rapid release initially, the reason for which was previously explained. Different models were characterized based on the plots shown in Figures 2-5.

Table 5. Parameters and determination coefficients of the release profile from sustained release liquisolid compacts (F1-F5)

Model	Parameter	F1	F2	F3	F4	F5
Zero-order	R^2	0.9121	0.9196	0.9223	0.8782	0.8969
	k	11.129	10.788	10.567	11.177	10.843
First-order	R^2	0.9684	0.9655	0.9764	0.9930	0.9933
	k	-0.262	-0.240	-0.223	-0.252	-0.232
Matrix	R^2	0.9975	0.9954	0.9953	0.9991	0.9986
	k	29.885	28.931	28.325	30.155	29.182
Peppas	R^2	0.9990	0.9973	0.9977	0.9991	0.9988
	k	26.469	25.031	24.307	29.121	27.061
Hixon-Crowell	R^2	0.9923	0.9889	0.9908	0.9909	0.9921
	k	-0.062	-0.058	-0.055	-0.061	-0.057
Korsmeyer-Peppas release exponent (n)	n	0.5660	0.5784	0.5828	0.5197	0.5413
$T_{50\%}$ (h)		3.1	3.3	3.4	2.8	3.1

Table 6. Parameters and determination coefficients of the release profile from sustained release liquisolid compacts (F6-F9) and marketed sustained release tablets

Model	Parameter	F6	F7	F8	F9	MKT
Zero-order	R^2	0.9004	0.8936	0.8964	0.8967	0.8636
	k	10.679	10.680	10.513	10.297	11.452
First-order	R^2	0.9959	0.9941	0.9960	0.9967	0.9867
	k	-0.221	-0.222	-0.212	-0.200	-0.274
Matrix	R^2	0.9976	0.9991	0.9986	0.9982	0.9983
	k	28.725	28.756	28.293	27.712	30.941
Peppas	R^2	0.9978	0.9994	0.9989	0.9983	0.9976
	k	26.042	27.512	26.685	25.797	31.230
Hixon-Crowell	R^2	0.9902	0.9904	0.9891	0.9864	0.9892
	k	-0.056	-0.056	-0.054	-0.052	-0.065
Korsmeyer-Peppas release exponent (n)	n	0.5538	0.5235	0.5314	0.5388	0.4954
$T_{50\%}$ (h)		3.2	3.1	3.3	3.4	2.6

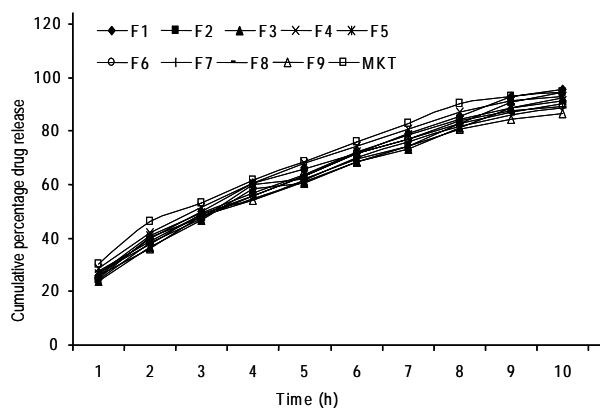


Figure 2. Zero-order plot for liquisolid compacts in comparison to a marketed formulation.

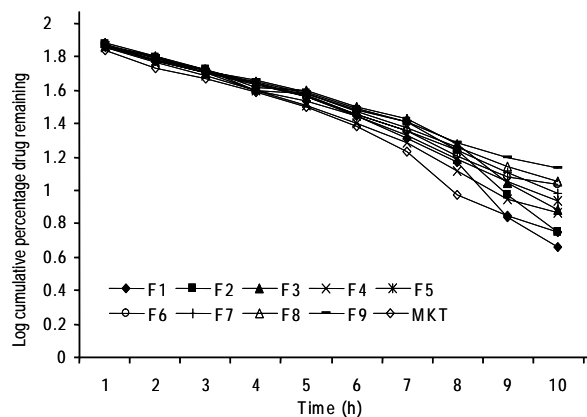


Figure 3. First-order plot for liquisolid compacts in comparison to a marketed formulation.

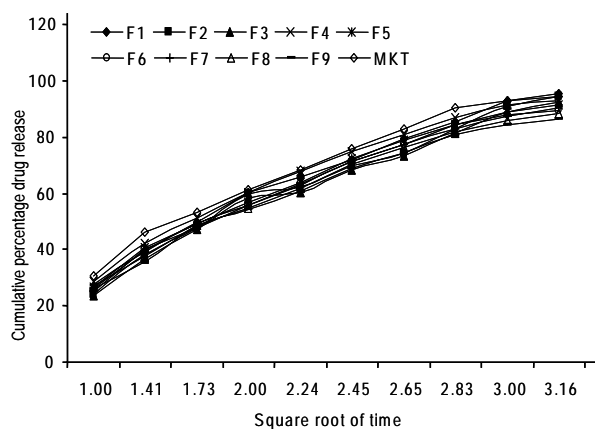


Figure 4. Higuchi plot for liquisolid compacts in comparison to a marketed formulation.

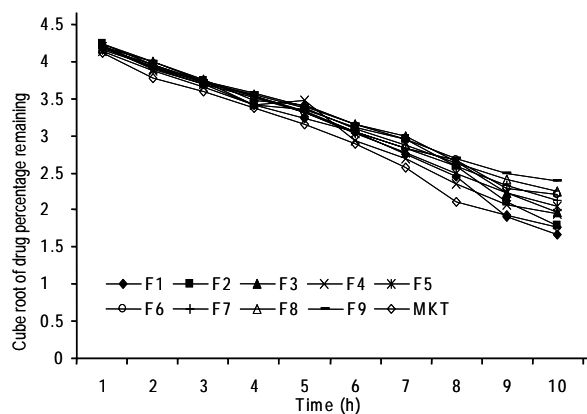


Figure 5. Hixon-Crowell plot for liquisolid compacts in comparison to a marketed formulation.

Table 7. Results of two-way ANOVA

Source of variation	Degrees of freedom	Sum of squares	Mean squares	F value
Column factor	9	441.4	49.05	21.58
Row factor	10	81150	8115	3570.52
Residual (error)	90	204.6	2.273	
Total	109	81800		

3.5.3. Statistical methods

Statistical methods based on ANOVA are the simplest way to determine differences in dissolution profiles. A statistically significant difference was observed in two-way ANOVA (Table 7). This was confirmed by a *p* value of < 0.0001.

4. Conclusion

The present work showed that the liquisolid compact technique can be effectively used to prepare sustained release matrices of water-soluble drugs such as tramadol hydrochloride. Propylene glycol was used as a liquid vehicle. Drug release profiles in model fitting

follow the Peppas model as the best-fit model, which indicates drug release from sustained release dosage forms. Model-independent methods were found to be the simplest way to compare dissolution profiles, but differences in dissolution profiles were noted using a model-dependent approach.

Acknowledgements

The authors wish to thank Mr. Khire, MD, Okasa Pharmaceuticals (India) for providing Avicel PH102, Aerosil 200, and HPMC K4M. The authors also wish to thank Mr. Sudhir Pandya (NuLife Pharmaceuticals) and Dr. S. B. Bhise for their continued encouragement.

References

1. George M, Grass IV, Robinson JR. Sustained and controlled release delivery systems. Marcel Dekker, NY, USA, 1978; pp.124-127.
2. Karmarkar AB, Gonjari ID, Hosmani AH, Dhabale PN, Thite RD. Preparation and *in vitro* evaluation of lyophilized nasal inserts of Tramadol Hydrochloride. Asian Journal of Pharmaceutical Sciences. 2008; 3:276-283.
3. Sunshine A, Olson NZ, Zigelboim I, DeCastro A, Minn FL. Analgesic oral efficacy of tramadol hydrochloride in postoperative pain. Clin Pharmacol Ther. 1992; 51:740-746.
4. Lee CR, McTavish D, Sorkin EM. Tramadol: a preliminary review of its pharmacodynamic and pharmacokinetic properties, and therapeutic potential in acute and chronic pain states. Drugs. 1993; 46:313-340.
5. Ortho-McNeil Pharmaceutical. Ultram[®] (tramadol hydrochloride) tablets prescribing information. Raritan, New Jersey, USA; 2001.
6. Scott LJ, Perry CM. Tramadol: a review of its use in perioperative pain. Drugs. 2000; 60:139-176.
7. Khullar P, Khar RK, Agarwal SP. Evaluation of guar gum in the preparation of sustained release matrix tablets. Drug Dev Ind Pharm. 1998; 24:1095-1099.
8. Mishra B, Seenra J, Singh S, Sankar C. Development and characterization of matrix tablets of ketorolac tromethamine. Indian Pharm. 2003; 2:86-89.
9. Rani M, Mishra B. Effect of admixed polymers on diclofenac sodium release from matrix tablets. Pharm Pharmacol Lett. 2001; 2:76-78.
10. Spireas S, Bolton M. U.S. Patent No. 6096337. 2000.
11. Spireas S. U.S. Patent No. 6423339 B1. 2002.
12. Javadzadeh Y, Musaalrezaei L, Nokhodchi A. Liquefied technique as a new approach to sustain propranolol hydrochloride release form tablet matrices. Int J Pharm. 2008; 362:102-108.
13. Karmarkar AB, Gonjari ID, Hosmani AH, Dhabale PN, Bhise SB. Liquefied tablets: A novel approach for drug delivery. Int J Health Res. 2009; 2:93-98.
14. Staniforth J. Powder flow. In: Pharmaceutics, the Science of Dosage Form Design. 2nd ed. (Aulton M, ed.). Churchill Livingstone, Edinburgh, UK, 2002; pp. 197-210.
15. Banker GS, Anderson NL. Tablets. In: The theory and practice of industrial pharmacy. 3rd ed. (Lachman, L, Liberman HA, Kanig JL, eds.). Varghese Publishing House, Bombay, India, 1987; pp. 293-345.
16. Shangraw RF. Compressed tablets by direct compression. In: Pharmaceutical dosage forms: Tablets. Vol. I, 2nd ed. (Liberman HA, Lachman L, Schwartz JB, eds.). Marcel Dekker, New York, USA, 1989; pp.195-220.
17. Javadzadeh YJ, Jafari-Navimipour B, Nokhodchi A. Liquefied technique for dissolution rate enhancement of high dose water-insoluble drug (Carbamazepine). Int J Pharm. 2007; 34:26-34.
18. Ju HL, Liaw SJ. On the assessment of similarity of drug dissolution profiles – A simulation study. Drug Inf J. 1997; 31:1273-1289.
19. Polli JE, Rekihi GS, Augsburger LL, Shah VP. Methods to compare dissolution profiles and a rationale for wide dissolution specifications for metoprolol tartrate tablets. J Pharm Sci. 1997; 86:690-700.
20. Liu JP, Chow SC. Statistical issues on the FDA conjugated estrogen tablets bioequivalence guidance. Drug Inf J. 1996; 30:881-889.
21. Costa P, Sousa Lobo JM. Modeling and comparison of dissolution profiles. Eur J Pharm Sci. 2001; 13:123-133.

(Received September 27, 2009; Accepted November 7, 2009)

Original Article**Formulation and evaluation of clotrimazole from pluronic F₁₂₇ gels****Boushra M. El-Houssieny^{1,*}, Hayam M. Hamouda²**¹ Department of Pharmaceutics, National Organization for Drug Control and Research (NODCAR), Giza, Egypt;² Department of Microbiology, National Organization for Drug Control and Research (NODCAR), Giza, Egypt.

ABSTRACT: Thermally reversible gels of poly(oxyethylene)-poly(oxypropylene)-poly(oxyethylene)-triblock copolymer, pluronic F₁₂₇ (PF₁₂₇), were evaluated as a vehicle for topical administration of clotrimazole as a model of a broad spectrum antifungal agent against superficial fungal infections. The solubility of clotrimazole was significantly increased as a linear function of pluronic F₁₂₇ concentration at four temperatures. Clotrimazole was highly trapped by the micelles as indicated by a large partition coefficient. The micellar solubilization was a spontaneous ($\Delta G < 0$) and exothermic ($\Delta H < 0$) process which resulted in a less orderly state ($\Delta S > 0$). Different additives were used to enhance drug release from preparations including propylene glycol, polyethylene glycol 400, glycerin, and dimethyl sulfoxide at concentrations of 5 and 10% and polysorbate 80 at concentrations of 1 and 2%. Different formulae were characterized in terms of drug content, pH and particle size measurement, spreadability, rheological properties, drug release, diffusion, and permeation. The formulae showing the best drug release were selected to study the effect of storage on various parameters over a period of 6 months and for microbiological evaluation. The best release enhancers were propylene glycol and polyethylene glycol 400 at a concentration of 10% and polysorbate 80 at a concentration of 2% and the formulae containing it were stable and proved to be effective in inhibition. Furthermore they were tested microbiologically against three fungi as well as yeast. The antimicrobial activities of the tested preparations were compared with the pure drug at the same concentrations and also tested for their antifungal activity. It was found to be effective against *Aspergillus niger*, *A. flavus*, *Candida albicans*,

and *Sacharomyces cerevisiae* with inhibition zones of 39, 39, 35, and 32 mm, respectively.

Keywords: Clotrimazole, pluronic F₁₂₇, solubility, gel formulation, release enhancers, antimicrobial activities

1. Introduction

The delivery of drugs to the skin is recognized as an effective means of therapy for local dermatologic diseases, which is a desirable feature for the relief of local symptoms at a low dose, thereby reducing systemic side effects.

Clotrimazole is a synthetic imidazole derivative shown to be a potent well-tolerated topical antifungal agent. It is active against dermatophytes (the causative organisms of time infections) and yeast (*Candida albicans*) (1,2). Its *in vitro* spectrum includes yeasts, dermatophytes, dimorphic fungi, and dematiaceous species (3). Plempel *et al.* (3,4) reported that it was inhibitory *in vitro* at concentrations of 4 µg or less per mL for most susceptible fungi and that many species, particularly Trichophyton and Candida, were inhibited by 1 µg/mL or less. However, it was said to be fungicidal only at concentrations greater than 20 µg/mL (3). Published data regarding the clinical effectiveness of clotrimazole are limited. In one report (5), it was described as being effective in one patient with pulmonary aspergilloma, in another with bronchial infection due to *Candida krusei*, and in a third with tinea barbae due to *C. albicans*.

According to another report (6), it was effective in treatment of candidiasis in a limited number of pediatric patients. Unpublished data from clinical studies in 87 adults indicated that it was effective in approximately 80% of patients with acute or systemic candidiasis including septicemia, pneumonia, endocarditis, and renal infection.

Efficacy and safety of topical clotrimazole were investigated by El-Gibaly (7) who found that clotrimazole (1%) formulated in an oleaginous or water

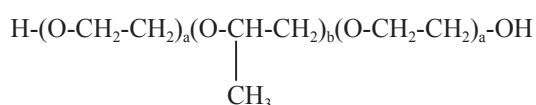
*Address correspondence to:

Dr. Boushra M. El-Houssieny, Department of Pharmaceutics, National organization for Drug Control and Research (NODCAR), Giza, Egypt.
e-mail: dr.boushra@yahoo.com

soluble ointment base was clinically more effective for the treatment of tinea circinate as compared with emulsion bases or its respective vehicles.

Over the last few decades, gels formed from natural, semisynthetic or synthetic polymers have been confirmed as vehicles for different types of pharmaceutical applications. They have good viscosity and satisfactory bioadhesion without irritating or sensitizing actions. Generally, hydrogel bases can be easily washed out and adhered well to mucous membrane or skin, wet with secreting fluid, and thus these are applied to injured skin and also to eyes (8).

Pluronic F₁₂₇ is one in a series of poloxamer ABA block copolymers, the members of which share the chemical formula:



The polymers are produced by condensation of ethylene oxide and propylene oxide. Pluronic F₁₂₇ has a molecular weight of 11,500, 70-79% of which is accounted for by the hydrophilic ethylene oxide portion. It is more soluble in cold water than hot due to increased solvation and hydrogen bonding at lower temperatures. Aqueous solutions of between 20 and 30% (w/w) of PF₁₂₇ have the interesting characteristic of reverse thermal gelation, that is, they are liquid at refrigerated temperatures (4-5°C) but gel upon warming to ambient levels. The gelation is reversible upon cooling (9).

Gelation of PF₁₂₇ is thought to occur due to the hydration of the polymer leading to increased chain friction and entanglement, producing a hydrophilic association (10,11). Reverse thermal gelation and low toxicity have been the basis of research into the use of PF₁₂₇ as a possible drug delivery system in man (12-17).

The present study is concerned with formulation of a topical clotrimazole gel using pluronic F₁₂₇ as a polymer having surface active properties. The prepared gels were investigated to observe the physicochemical phenomena and thermodynamic properties of clotrimazole in PF₁₂₇ and to determine the effects of different penetration enhancers on the micellar solubilization and release of clotrimazole from the vehicle into the receptor medium. Therefore, the aim of the present investigation was also to test the *in vitro* activity of the gel preparations of clotrimazole against pathogenic fungi.

2. Materials and Methods

2.1. Materials

Clotrimazole (molecular weight 344 g/mol, aqueous solubility: 5.5 µmol/L), was purchased from Sigma Chemicals (Steinheim, Germany). Pluronic F₁₂₇ (PF₁₂₇),

propylene glycol, polyethylene glycol 400, semi-permeable cellulose membrane (molecular weight cut off 12,000-14,000), were purchased from Sigma-Aldrich (St. Louis, MO, USA). Citric acid anhydrous, disodium hydrogen phosphate, polysorbate 80, glycerol, dimethyl sulfoxide were from El-Nasr Chemical Industries (Cairo, Egypt). All other chemicals were of analytical reagent grade and used without further purification.

2.2. Organisms

Four isolates of pathogenic fungi, *Aspergillus niger*, *Aspergillus flavus*, *Candida albicans* CAIM 22, and *Saccharomyces cerevisiae* CAIM 14, were used for determination of antifungal activity. All test organisms were kindly supplied by Microbiological Resource Center, Cairo, Mircen-Egypt (CAIM). Potato dextrose agar (PDA, Oxoid) was used as media for fungi and yeasts.

2.3. Equipment

The equipment used was: Ultra-violet Spectrophotometer (Schimadzu, UV 1601, Kyoto, Japan), Electric balance (Satorius, GMBH, Gottingen, Germany), Thermostatically controlled heater with magnetic stirrer (LABINCO BV, Netherlands), pH meter (Cyberscan 10, USA), Cone and plate viscometer (Brookfield Model DV 111, USA), Franz diffusion (Hanson Research Corporation (HRC), USA), Thermostatatically controlled shaking water bath (Gallenkamp. Co., Germany), Laser Scattering particle size distribution analyzer (LA-920, Horiba, USA), USP dissolution tester (Pharma test, type PTW2, Germany).

2.4. Solubility test

An excess amount of clotrimazole was added to 0.1 M cetrophosphate buffer (pH 5.5) containing different amounts of PF₁₂₇ (0-10%, w/w) in glass vials which were continuously shaken for 48 h in a thermostated water bath set at 25, 30, 37, and 40°C (± 1°C). The properly diluted samples were assayed spectrophotometrically at 250 nm after filtration through 0.45 µm Millipore membrane filters. The solubility was established by analyzing serial samples. To minimize the effect of temperature change on solubility, filtration was performed in a temperature-controlled oven. PF₁₂₇ did not interfere with the assay.

2.5. Preparation of pluronic F₁₂₇ gels

Clotrimazole PF₁₂₇ gels were prepared by the cold method as described by Schmolka (9). The required amount of PF₁₂₇ (20%) was dissolved in a buffer solution (0.1 M citrophosphate buffer, pH 5.5) with the aid of a

magnetic stirrer and the solution was left in a refrigerator overnight. When the mixture became a clear solution, an ethanol solution of the drug: ethyl alcohol (1:20) was thoroughly mixed into the PF₁₂₇ solution. The mixture was then left at room temperature until becoming a clear gel. To study the effect of penetration enhancers on the *in vitro* release (namely, propylene glycol, polyethylene glycol 400, glycerin, and dimethyl sulfoxide in concentrations of 5 and 10%, and polysorbate 80 in concentration of 1 and 2%), they were incorporated in the gel either separately or in combination namely, propylene glycol and polyethylene glycol 400 (5% + 5%), propylene glycol and polysorbate 80 (5% + 1%), polyethylene glycol 400 and polysorbate 80 (5% + 1%). The compositions of the gels are summarized in Table 1.

2.6. Evaluation of the physical properties of the prepared gel

All prepared gels (with or without the penetration enhancers) were subjected to the following tests.

2.6.1. Determination of actual drug content in the prepared clotrimazole gels

The actual drug content was determined in each prepared formula as follows: 0.5 g of the gel was dissolved in 100 mL of citrophosphate buffer, pH 5.5, and then filtered through a 0.45 μm membrane filter (No. 40) (18). The concentration of the drug was determined spectrophotometrically at a λ_{max} of 250 nm using the same buffer as a blank.

2.6.2. Determination of pH of the prepared formula

pH of the prepared formulae was determined using the following method: one g of gel was diluted with 9 g distilled water and shaken well (19,20). pH measurement was repeated three times for each formula and the reading was the average of 3 replicates.

2.6.3. Particle size measurement

A particle size distribution analyzer was used,

frequency distribution curve was done by plotting $q^3\%$ against diameter in μm , where $q^3\% = (V_d/V_t) \times 100$. V_d is the volume of particles corresponding to each diameter in μm and V_t is the total volume of particles in the examined sample.

2.6.4. Test for spreadability

A sample of 0.1 g of each formula was pressed between two slides (divided in squares of 5 mm sides) and left for about 5 min where no more spreading was expected (21-24). Diameters of spread circles were measured in cm and were taken as comparative values for spreadability. The results obtained were the average of three determinations.

2.6.5. Rheological measurements and data analysis

Steady shear measurements were conducted where the rheograms of all prepared gels were performed at $25 \pm 0.1^\circ\text{C}$ with spindle 52, with the shear rate ranging from 2 to 400 sec^{-1} corresponding to 1 to 200 rpm with 10 sec between each two successive speeds and then in a descending order. Equilibration of the sample for 5 min was made following loading of the viscometer. Ramp time for each viscosity stage was the reading after 20 sec. All studies were performed in triplicate and the average was taken.

Rheological data was fitted to different models (Bingham, Power law, Casson) to examine the pattern of flow and the presence of yield value (25).

$$\text{Bingham: } \tau = \tau_0 + \eta\dot{\gamma}$$

$$\text{Power law: } \tau = \eta\dot{\gamma}^n$$

$$\text{Casson: } \tau^{1/2} = \tau_0^{1/2} + \eta^{1/2}\dot{\gamma}^{1/2}$$

where τ is the shear stress, τ_0 the yield value, η a constant called the apparent viscosity or the consistency index, $\dot{\gamma}$ the shear rate, and n is the flow index. In the case of Newtonian behavior $n = 1$ and $\tau_0 = 0$, whereas in the case of pseudoplastic (shear thinning) behavior $0 < n < 1$ and $\tau_0 = 0$, for plastic behavior, it is the same as pseudoplastic but with $\tau_0 > 0$ while in the case of dilatant's flow (shear thickening) $n > 1$ (26).

Table 1. Composition of clotrimazole pluronic F₁₂₇ gels

Components	Gel formulae													
	F ₁	F ₂	F ₃	F ₄	F ₅	F ₆	F ₇	F ₈	F ₉	F ₁₀	F ₁₁	F ₁₂	F ₁₃	F ₁₄
Clotrimazole	1	1	1	1	1	1	1	1	1	1	1	1	1	1
Pluronic F ₁₂₇	20	20	20	20	20	20	20	20	20	20	20	20	20	20
Ethyl alcohol	20	20	20	20	20	20	20	20	20	20	20	20	20	20
Propylene glycol	—	5	—	—	—	—	10	—	—	—	—	5	5	—
Polyethylene glycol 400	—	—	5	—	—	—	—	10	—	—	—	5	—	5
Polysorbate 80	—	—	—	1	—	—	—	—	2	—	—	—	1	1
Glycerin	—	—	—	—	5	—	—	—	—	10	—	—	—	—
Dimethyl sulfoxide	—	—	—	—	—	5	—	—	—	—	10	—	—	—
Buffer pH 5.5 to	100	100	100	100	100	100	100	100	100	100	100	100	100	100

2.6.6. *In vitro* release

The study was carried out using the modified USP dissolution apparatus. A sample of 3 g of the preparation was spread on a cellophane membrane previously soaked overnight in the release medium. The loaded membrane was firmly stretched over the edge of a 2 cm diameter glass tube; the membrane was tied with a rubberband to prevent leakage (27). Tubes were then immersed in the dissolution vessel which contained 200 mL of the release medium, citrophosphate buffer, pH 5.5, containing 1% polysorbate 80:ethyl alcohol (1:1) and maintained at $35 \pm 0.5^\circ\text{C}$ (28). The shafts were rotated at 100 rpm and at appropriate intervals, 3 mL aliquots of the release medium were withdrawn and immediately replaced by an equal volume of fresh release medium. The sample was assayed spectrophotometrically at a λ_{max} of 250 nm and the concentration of the drug was determined from the previously constructed calibration curve. Experiments were carried out in triplicate, the results were averaged and blank experiments were carried using plain base.

2.6.7. Diffusion tests

The release of clotrimazole from PF₁₂₇ gels was studied at $35 \pm 0.5^\circ\text{C}$ using a Franz diffusion cell apparatus with a permeation area of 1.77 cm². Cellulose membranes were previously soaked in the release medium consisting of citrophosphate buffer, pH 5.5, containing 1% polysorbate 80:ethyl alcohol (1:1). A constant weight (0.5 g) of each gel formula was added to the donor compartment and 7.5 mL of the release medium were placed in the receptor compartment with constant stirring. At appropriate intervals, 500 μL aliquots of the receptor medium were withdrawn and immediately replaced by an equal volume of fresh receptor solution. The samples were analyzed spectrophotometrically at 250 nm after suitable dilution to determine the drug permeation per unit time.

2.6.8. Kinetic analysis of drug release data

Drug release data generated from the dissolution experiments were fitted to the following power law equation by Peppas, 1985 (29) using logarithmic transformations and least squares regression analysis:

$$M_t/M_x = kt^n$$

where M_t/M_x is the fraction of drug released up to time t , k is the kinetic constant and n is the release exponent indicative of the release mechanism.

The permeation parameters of clotrimazole from gels including permeability coefficient (p , cm/min), diffusion coefficient (D , cm²/min), and apparent steady state flux (J_{ss} , $\mu\text{g}/\text{cm}^2/\text{min}$) were calculated as follows:

The penetration profile conducted by plotting the cumulative amount of permeated drug ($\mu\text{g}/\text{cm}^2$) versus time (min), the flux (J_{ss}) was calculated from the slope of the line.

P : permeability coefficient calculated by dividing (J_{ss}) by the employed concentration of the drug C_0 according to the equation $P = J_{ss}/C_0$.

D : diffusion coefficient was calculated from the slope by plotting the cumulative amount of drug permeated versus square route of time (\sqrt{t} min) and (D) was calculated from the equation: $D = (\text{slope}/2C_0)^2\pi$.

2.7. Stability study on the selected clotrimazole gels

Based on the results from previous studies, formulae prepared with 10% (w/w) propylene glycol, 10% (w/w) polyethylene glycol 400, and 2% (w/w) polysorbate 80 (F_7 , F_8 , and F_9 , respectively) were stored in well stoppered glass container for 6 months at room temperature. Gels were subjected to all the previous tests. The results obtained from the freshly prepared samples and after storage were compared using a Student's t -test and the software utilized was Graphpad Instant ver. 2.04 with a 5% level of significance.

2.8. Evaluation of antimicrobial activity

The antimicrobial activity of the gel preparation against four fungi, *Candida albicans* CAIM 22 and *Saccharomyces cerevisiae* CAIM 14 (kindly supplied by Microbiological Resource Center, Cairo, Mircen-Egypt; CAIM). *Aspergillus niger* and *Aspergillus flavus* obtained from the Microbiology Laboratory, Department of Microbiology, NODCAR. The antimicrobial activity was determined by the pour diffusion method as described in CLSI 2006 (30) using potato dextrose agar plates (PDA, Oxoid) previously inoculated with 18 h spores (10^6 spores/mL fungi) suspension in potato dextrose broth (PDB, Oxoid) of the test organisms. Gel preparation as well as pure drug of the same concentration was applied over each of the culture plates previously seeded with the 10^6 spores/mL of fungi. The experiment was performed in triplicate. Incubations were at 37°C for 24-48 h for *C. albicans* and at room temperature for 72 h for the other filamentous fungi. Following incubation the zones of inhibition formed were measured and the mean diameter obtained. Overall, cultured fungi with 10 mm halos were considered susceptible to the tested compound.

3. Results and Discussion

3.1. Solubility of clotrimazole in pluronic F₁₂₇ solutions

For the development of topical formulations, the solubility of the active ingredient in the vehicle is

often an important factor to determine the applied dose. Clotrimazole is practically insoluble in water, thus, limiting its use in aqueous preparations. Since surfactants have been successfully used to enhance the solubility of drugs in many pharmaceutical formulations, pluronic F₁₂₇ was evaluated for its potential use in formulating an aqueous clotrimazole preparation in this study.

3.1.1. Solubility profile

Figure 1 shows a linear relationship between the amount of clotrimazole solubilized and the concentration of PF₁₂₇ in the medium at four temperatures. The solution properties of the surfactant including the solubilizing activity are generally known to change drastically near the critical micelle concentration (CMC). In the presence of 10% PF₁₂₇, the solubility of clotrimazole increased nearly 100-fold at each of the four temperatures. However, due to the low CMC of PF₁₂₇ (31), the solubilization of drugs in a surfactant solution has been suggested to occur due to the increased partitioning of solute molecules into the micelles which could be considered as a separate, pseudo-phase (27). The linear increase in the solubility of clotrimazole as a function of PF₁₂₇ concentration observed in this study suggested that the total micellar volume into which clotrimazole partitioned was a linear function of the amount of PF₁₂₇ present.

3.1.2. Partition coefficient (17)

The partition coefficient of clotrimazole (k_m) between micellar and aqueous phases was determined by the ratio of the clotrimazole solubility in the micellar phase (S_m) to that in the aqueous phase (S_w) as shown in Table 2. The solubility of clotrimazole in the extramicrocellular phase was assumed to be equal to that in water since colloidal surfactants usually do not change the chemical potential of the solute (32).

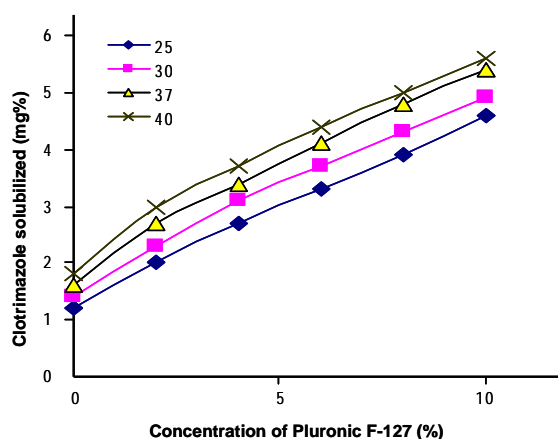


Figure 1. Solubility profile of clotrimazole as a function of pluronic F₁₂₇ concentrations at different temperatures. ♦, 25°C; ■, 30°C; ▲, 37°C; ×, 40°C. *n* = 3.

The S_m values were estimated by extrapolating the solubility of clotrimazole to 100% (w/w) of PF₁₂₇ as previously reported (33).

The large k_m values observed in this study indicated that clotrimazole had highly partitioned into the micelles.

The partition coefficients of clotrimazole were found to be inversely related to temperature. When temperature was increased from 25°C to 40°C, the $\log K_m$ values were decreased from 1.63 to 1.54, despite the higher solubility of clotrimazole in both the micellar and aqueous phases. According to Elworthy and McDonald (34), the size of micelles increased only slightly until a threshold temperature, approximately 20°C below the cloud point of the surfactants, was reached. They showed that beyond this temperature, the micellar volume expanded rapidly and asymmetrically, thus causing increased loading of the drug into the micelles. In this experiment, the highest temperature used was 40°C, far below the cloud point of PF₁₂₇ which was reported to be beyond 100°C (35). Therefore, the reduction of k_m at 40°C as compared to that at 25°C could be attributed to a smaller increase in the solubility of clotrimazole in the micellar phase than to that in the external aqueous phase, probably due to a higher temperature coefficient of the aqueous solubility of clotrimazole.

3.1.3. Thermodynamics

Table 2 summarizes the thermodynamic parameters associated with the solubilization of clotrimazole in the PF₁₂₇ solution. These parameters are practically useful in understanding the thermodynamic phenomena involved in the micellar solubilization of clotrimazole.

A typical Van't Hoff's plot, $\log K_m$ versus $1/T$, which was nearly straight over the employed temperature range as shown in Figure 2, was used to calculate thermodynamic parameters. ΔH , ΔS , and ΔG (apparent enthalpy, entropy and free energy change, respectively) were calculated from temperature dependence of k_m values. The standard free energy change which indicates the spontaneity of the solubilization process was calculated using the equation: $\Delta G = -RT \ln K_m$, where ΔG is the free energy change for the transfer of one mole of clotrimazole from the aqueous phase into

Table 2. Partition coefficient (K_m) and thermodynamic parameters of clotrimazole in pluronic F₁₂₇ at four different temperatures

Temperatures °C	K	K_m	ΔG (kJ/mol)	ΔH (kJ/mol)	ΔS (J/K·mol)
25	298	42.668	-9.29	-0.77944	30.07
30	303	39.82	-9.27	-0.91787	27.56
37	310	36.07	-9.25	-1.10435	26.28
40	313	34.71	-9.24	-1.18059	25.75

K_m , partition coefficient; ΔG , free energy change; ΔH , apparent enthalpy; ΔS , entropy.

the micellar phase; R, the gas constant; T, the absolute temperature, and k_m is the partition coefficient. All the values of ΔG obtained at the four temperatures were found to be negative, indicating that clotrimazole molecules spontaneously partitioned into the micelles.

The standard enthalpy change, ΔH , which was calculated from the slope of the Van't Hoff's plot representing $d \ln k_m/d (1/T) = -\Delta H/R$, was also negative, indicating that the micellar solubilization of clotrimazole was an energetically favored exothermic process. This is in accordance with the negative ΔH values for the solubilization of steroids in the nonionic polyoxyethylene surfactant solution as was previously reported (36).

The standard entropy change for the micellar solubilization of clotrimazole which was calculated using $\Delta S = (\Delta H - \Delta G)/T$ was a positive value (Table 2). Entrapment of clotrimazole molecules within micelles could restrict their activity, causing a decrease in entropy of the system.

3.2. Evaluation of the physical properties of the prepared gels

3.2.1. Clotrimazole content in the prepared gels

Drug content of the prepared gels ranged from 98.9 to

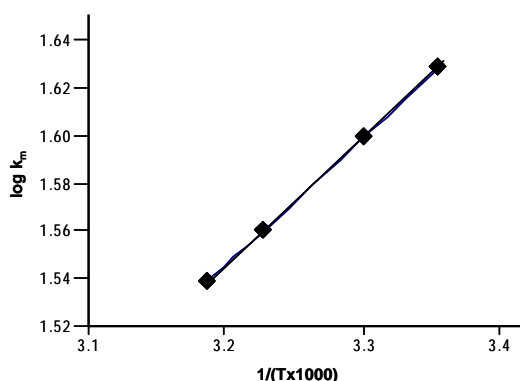


Figure 2. Van't Hoff's plot of clotrimazole in pluronic F₁₂₇.

101.3% of the labeled amount. These results revealed that no interference occurred between different components and clotrimazole in the assay which indicates homogeneity and uniformity of the prepared gels.

3.2.2. Test for spreadability

Results for spreadability testing are shown in Table 3. All prepared gels using different concentrations of different release enhancers were spreadable on the skin surface. It should be mentioned that the addition of propylene glycol, polyethylene glycol 400, and polysorbate 80 improved the physical characteristics including spreadability, consistency and skin feel (37). Also, its addition helped the dissolution of the drug and prevented precipitation upon storage. With each type of release enhancer used, its addition led to a significant increase ($p < 0.05$) in the diameter of the spread circle of the gel.

3.2.3. pH and particle size of the prepared formulae

pH values of the prepared clotrimazole formulae ranged from 5.28-6.05 which is decreased from the pH of the plain base to some extent (Table 3). This pH range allows maximum stability for all release enhancers used and is also suitable for skin.

Relevant to determination of particle size measurement, the mean particle size diameter value ranged from 0.985-6.319 μm where formula F₇ showed the lowest value and F₁ showed the highest value (Table 3).

3.2.4. Rheological measurements and data analysis

The rheological parameters of the prepared formulations, namely, the flow index (n) and the consistency index (η) are shown in Table 4, while their rheograms are shown in Figure 3. Based on the

Table 3. Physical parameters of clotrimazole gels

Formulae	Drug content (%)	Spreadability (cm)	pH	Particle size (μm)
F ₁	98.9	2.3	6.05	1.755 \pm 0.87
F ₂	99.1	3.3	5.89	4.232 \pm 1.548
F ₃	99.6	3.1	5.55	1.637 \pm 0.669
F ₄	99.3	3.0	6	2.577 \pm 0.896
F ₅	99.0	3.2	6	1.581 \pm 0.939
F ₆	100.5	3.1	6.02	5.843 \pm 2.453
F ₇	100.4	4.8	6	1.441 \pm 0.514
F ₈	100.2	3.9	5.28	2.104 \pm 1.233
F ₉	101.3	4.3	5.97	1.291 \pm 0.753
F ₁₀	100.9	3.8	5.92	6.319 \pm 2.506
F ₁₁	101.1	3.4	5.91	0.985 \pm 0.357
F ₁₂	99.7	2.9	5.67	1.465 \pm 0.684
F ₁₃	99.4	2.6	5.91	0.241 \pm 0.139
F ₁₄	99.8	3.0	5.64	1.289 \pm 0.641

values of n , calculated after the power law equation and which were all < 1 as shown in Table 4, it could be confirmed that all the formulations exhibited shear thinning behavior. This is a desirable property in a topical semisolid preparation, since it should thin during application (38). The cause of pseudoplastic flow revealed by gels may be due to progressive rupture of the internal structure of the formulations and its later reconstruction by means of Brownian movement (38,39).

It is obvious that increasing all the penetration enhancer concentrations led to a decrease in the flow index values. This result was explained by the formation of full structured three dimensional polymer lattices due to increased enhancer concentration (40). Also, this effect may be attributed to the plasticizing effect of these compounds. The plasticizer would have the ability to weaken polymeric intermolecular attractions, thus allowing polymer chains to move more readily, improving the flexibility of the polymer. Consequently, the higher relaxation and mobility of the chains provoke greater entanglement and increase gel

viscosity (41).

An important rheological parameter is the apparent viscosity of the gels. It is related to mechanical and physical properties such as spreadability, consistency and hardness of the preparation which in turn are related to ease of product removal from container, ease of application on the skin surface and product feel on the application site.

3.2.5. *In vitro* release and effect of some penetration enhancers on drug release

The percent of clotrimazole released after 6 h, apparent diffusion coefficient, permeability coefficient, and partition coefficient were represented in Table 5 and Figures 4-6. It is clear that 20% pluronic F₁₂₇ gave a very low percent of clotrimazole release after 6 h (34.41%). This may be due to the fact that pluronic F₁₂₇ gels consist of a large population of micelles and the drug is released by diffusion through extra micellar aqueous channels of gel matrix (12,42-44).

The addition of hydrophilic or lipophilic additives into pharmaceutical formulations in order to modulate

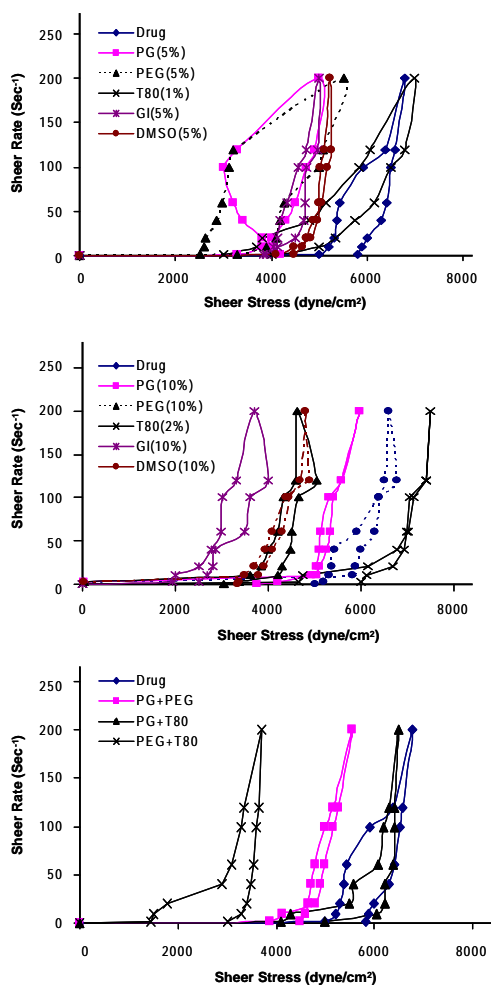


Figure 3. Rheogram of clotrimazole from 20% pluronic F₁₂₇ gels containing different release enhancers. PG, propylene glycol; PEG, polyethylene glycol 400; T80, polysorbate 80; GI, glycerin; DMSO, dimethyl sulphoxide.

Table 4. Rheological parameters of clotrimazole gels

Formulae	Consistency index (η)	Flow index (n) at shear rate 120
F ₁	4,500	0.066
F ₂	3,800	0.048
F ₃	3,200	0.087
F ₄	4,000	0.100
F ₅	3,800	0.050
F ₆	4,220	0.036
F ₇	4,600	0.030
F ₈	3,814	0.038
F ₉	5,963	0.041
F ₁₀	2,555	0.048
F ₁₁	3,722	0.031
F ₁₂	4,350	0.037
F ₁₃	4,730	0.054
F ₁₄	1,390	0.166

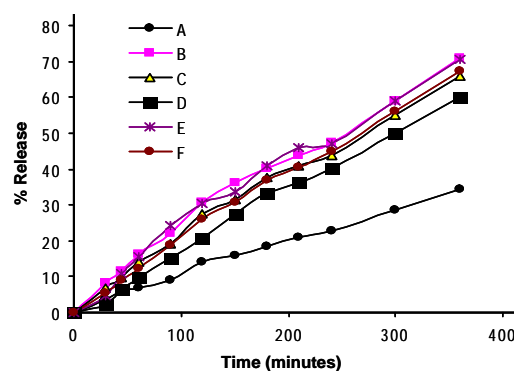


Figure 4. Release profiles of clotrimazole from 20% pluronic F₁₂₇ gels containing different release enhancers. A, drug; B, propylene glycol (5%); C, polyethylene glycol 400 (5%); D, polysorbate 80 (1%); E, glycerin (5%); F, dimethyl sulphoxide (5%).

the release of drugs is most common. Polarity produced by the additives is an important factor that affects drug release. The higher the water solubility of the additives the greater the enhancement of dissolution of the formulation and thereby, the higher rate of drug release and *vice versa* (45). In this study, all the additives used, namely, propylene glycol, polyethylene glycol, glycerin, and dimethyl sulfoxide in concentrations of 5 and 10% (w/w) and also polysorbate 80 in concentrations of 1 and 2% (w/w), showed significant enhancement of the release of clotrimazol in comparison with the additives free base, but to a variable extent. The higher release was obtained from formula (F₇) containing 10% propylene glycol (86.94%) after 6 h in comparison with other additives or their combination, followed by formula (F₉) containing 2% polysorbate 80 (80.415%) and then formula (F₈) containing 10% polyethylene glycol (73.53%).

It has been reported that the addition of polyethylene glycol 400, propylene glycol, and glycerin (in concentrations ranging from 2.5% to 10%) into different polymer bases including pluronic F₁₂₇ significantly

enhanced drug release rate. This was related to the high water solubility of glycols where they readily absorb water and therefore speed up the hydration rate and so the dissolution rate of the polymer into which these hydrophilic agents are incorporated (46-49). The high solubility of these polyhydroxy compounds resulted also in a decrease of the resistance to drug diffusion by increasing the formulation porosity following their dissolution. These results were in accordance with Korsmeyer *et al.* and Jones *et al.* (50,51).

A further advantage of these polyhydroxy compounds is that they act as humectants, to prevent drying and crusting of the vehicles (52).

From the results, it is clear that addition of 10% propylene glycol gave the highest release pattern. This is because propylene glycol may change the microviscosity of the base (47).

Addition of the non-ionic surfactant polysorbate 80 to pluronic F₁₂₇ gels has also enhanced the release rate which could be attributed to increasing the number and dimensions of the aqueous channels available for drug diffusion, thus increasing the effective porosity

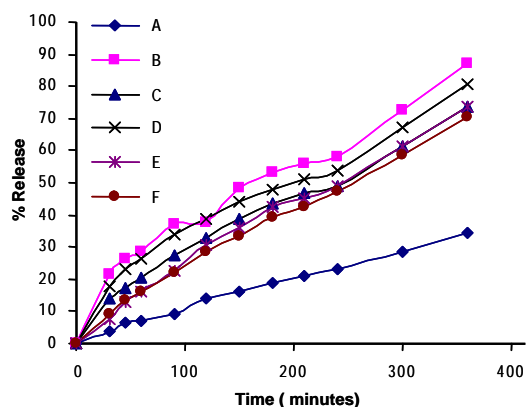


Figure 5. Release profiles of clotrimazole from 20% pluronic F₁₂₇ gels containing different release enhancers. A, drug; B, propylene glycol (10%); C, polyethylene glycol 400 (10%); D, polysorbate 80 (2%); E, glycerin (10%); F, dimethyl sulphoxid (10%).

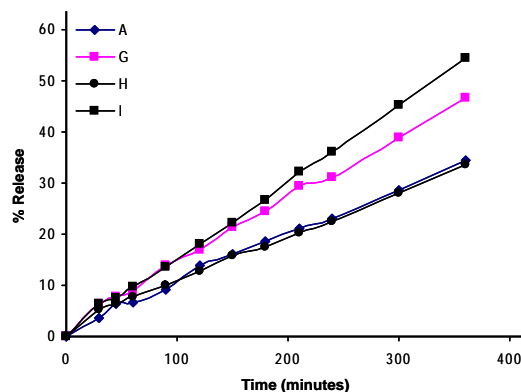


Figure 6. Release profiles of clotrimazole from 20% pluronic F₁₂₇ gels containing different release enhancers. A, drug; G, propylene glycol:polyethylene glycol (5% + 5%); H, propylene glycol:polysorbate 80 (5% + 1%); I, polyethylene glycol:polysorbate 80 (5% + 1%).

Table 5. Effect of different penetration enhancers on the *in vitro* release characteristics of clotrimazole from pluronic F₁₂₇ gels

Formulae	Order of reaction	% clotrimazole released after 6 h	D _{app} (× 10 ⁻³ μg·cm ² ·h ⁻¹)	P _m (× 10 ⁻³ cm·h ⁻¹)	K _p
F ₁	zero	34.41	14.91	10.59	0.1419
F ₂	zero	71	9.45	20.90	0.4425
F ₃	zero	65.93	8.63	19.20	0.4450
F ₄	zero	60.133	13.24	18.30	0.2764
F ₅	zero	70.65	6.55	19.80	0.6047
F ₆	zero	67.38	14.33	20.65	0.2882
F ₇	zero	86.94	4.92	23.11	0.9391
F ₈	zero	73.53	6.35	20.48	0.6449
F ₉	zero	80.415	5.97	22.16	0.74198
F ₁₀	zero	73.53	8.59	21.37	0.4979
F ₁₁	zero	70.64	12.78	21.43	0.3354
F ₁₂	zero	46.73	15.99	14.48	0.1811
F ₁₃	zero	33.69	26.56	10.73	0.0808
F ₁₄	zero	54.34	19.28	18.25	0.0189

D_{app}, apparent diffusion coefficient; P_m, permeability coefficient; K_m, partition coefficient; H, membrane thickness; K_p, P_m × H/D_{app}.

of the gel matrix. Also, polysorbate 80 has emulsifying properties due to increasing formation of intrapolymeric micelles which decrease interpolymeric connections allowing enhanced drug release. This was in accordance with what was reported by Hansson and Lindman (53).

Addition of dimethyl sulfoxide at concentrations of 5 and 10% to pluronic F₁₂₇ gels also enhanced the release rate. The most enhanced effect was found to be dependent on the additive concentration (54).

Kinetic analysis of release data have shown that by trying the three different models, the highest regression coefficient was always obtained with a zero order release model. This result was previously found by Wang *et al.* and Paavola *et al.* (55,56).

3.3. Stability study on selected clotrimazole gels

No significant change ($p > 0.05$) in the measured parameters (spreadability, rheological behavior, and *in vitro* clotrimazole release) were noticed after 6 months of storage, indicating high physical stability of all clotrimazole gels under study.

3.4. Evaluation of antimicrobial activity

Clotrimazole, which is an imidazole derivative antifungal agent, was widely used for treatment of mycotic infections of the genitourinary tract (57).

The results presented here confirm the earlier reports of Plempel *et al.* (3,4) regarding the *in vitro* activity of clotrimazole against pathogenic fungi. This compound is, indeed, a "broad spectrum" antifungal agent; its inhibitory action is seen against systemic and opportunistic pathogenic fungi (Figure 7).

Antifungal activities of plain gels and standing solutions were determined using the pour diffusion method described by CLSI 2006 (30). In this process, the clear zone of inhibition indicated the sensitivity of the organism to the chemical agents (58). *In vitro* antifungal activity of clotrimazole was carried out by the agar diffusion method. Table 6 shows the antifungal activity of clotrimazole in propylene glycol (10%, w/w), polyethylene glycol 400 (10%, w/w) and polysorbate 80 (2%, w/w) as well as in drug form.

The effect of gel against the tested organisms was estimated by the width of the inhibition zone. The clotrimazole plain form exhibited the highest activity against *Aspergillus flavus* with an inhibition zone of 46 mm. On the other hand, clotrimazole gels with release enhancer propylene glycol (10%, w/w) showed antifungal activity against all the tested microorganisms with a zone inhibition of nearly 30 mm. In the case of clotrimazole gels with release enhancer polyethylene glycol 400 (10%, w/w), it was found to be effective against *A. niger*, *A. flavus*, *C. albicans*, and *S. cerevisiae* with inhibition zones of 39, 39, 35, and 32 mm, respectively.

Table 6. Antifungal activity of clotrimazole gels

Organisms tested	Inhibition zones for fungi (mm) ^a				
	PD	PG	PEG	P	SC
<i>Aspergillus flavus</i>	46	44	39	37	40
<i>Aspergillus niger</i>	37	38	39	35	32
<i>Candida albicans</i>	30	35	35	31	42
<i>Saccharomyces cerevisiae</i>	32	30	32	28	32

^aDiameter of inhibition zones from triple readings. Abbreviations: PD, plain drug; PG, propylene glycol (10%, w/w); PEG, polyethylene glycol 400 (10%, w/w); P, polysorbate 80 (2%, w/w); SC, standard clotrimazole.

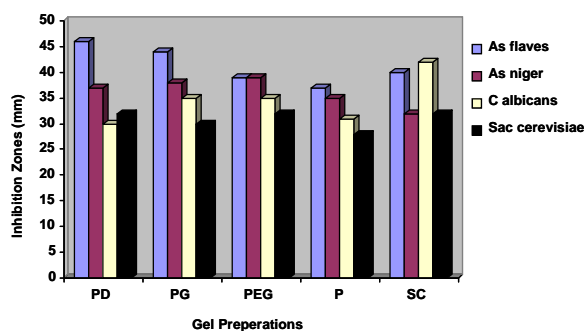


Figure 7. Antifungal activity of tested preparations. PD, plain drug; PG, propylene glycol (10%, w/w); PEG, polyethylene glycol 400 (10%, w/w); P, polysorbate 80 (2%, w/w); SC, standard clotrimazole.

Clotrimazole inhibits biosynthesis of the sterol ergosterol, an important component of fungal cell membranes. Its action leads to increased membrane permeability and apparent disruption of enzyme systems bound to the membrane, resulting in leakage and loss of essential intracellular compounds, and eventually cell lysis.

4. Conclusion

The solubility of clotrimazole was significantly increased in the presence of PF₁₂₇. The micellar solubilization was an energetically favored, spontaneous process resulting in a lower thermodynamic orderliness. The best release enhancers were propylene glycol and polyethylene glycol 400 at a concentration of 10% and polysorbate 80 at a concentration of 2%. The formulae containing it were physically stable and proved to be effective against *A. niger*, *A. flavus*, *C. albicans*, and *S. cerevisiae* with inhibition zones of 39, 39, 35, and 32 mm, respectively. Therefore, it was concluded that these formulae could be a very promising topical alternative for the treatment of skin fungal infections.

Acknowledgements

Dr. Hayam would like to express her profound gratitude and appreciations to Prof. F. H. Ahmed, Professor of Microbiology (NODCAR) for his great help throughout this work.

References

1. Martindale, The Extra Pharmacopoeia, 28th ed. Pharmaceutical Press, London, UK, 1982; pp. 721-722.
2. Spiekermann PH, Young MD. Clinical evaluation of clotrimazole. A broad spectrum antifungal agent. Arch Dermatol. 1976; 112:350-352.
3. Plempel M, Bartmann K, Buchel KH, Regel E. Experimentelle befunde uber ein neucs, oral wirksames antimykoticum mit breitem wirkungsspektrum. Deut Med Wochenschr. 1969; 94:1356-1364.
4. Plempel M, Bartmann K, Buchel KH, Regel E. Bay b 5097, a new orally applicable antifungal substance with broad-spectrum activity. Antimicrob Agents Chemother. 1969; 9:271-274.
5. Oberste-Lehn H, Baggesen I, Plempel M. Erste klinische erfahrungen bei system-mykosen mit einem oralen antimykotikum. DcLnt Med Wochenschr. 1969; 94:1365-1367.
6. Marget W, Adamn D. Erste erfahrungen mit dens breitband-antimykotikum Bay b 5097. Med Klin. 1969; 64:1235-1238.
7. EL-Gibaly I. Formulation and evaluation of some topical antimycotic delivery systems, M. SC. Thesis Assuit University. 1988.
8. Tas C, Ozkan Y, Savaser A, Baykara T. *In vitro* release studies of chlorpheniramine maleate from gels prepared by different cellulose derivatives. Farmaco. 2003; 58:605-611.
9. Schmolka IR. Artificial skin I. Preparation and properties of pluronic F-127 gels for treatment of burns. J Biomed Mater Res. 1972; 6:571-582.
10. Rassing J, Mckenna WP, Bandyopadhyay S, Eyring EM. Ultrasonic and ¹³C-NMR studies on gel formation in aqueous solutions of the ABA block polymer Pluronic F-127. J Mol Liq. 1984; 27:165-178.
11. Vadnere M, Amidon G, Lindenbaum S, Haslam J. Thermodynamic studies on the gel-sol transition of some pluronic polyols. Int J Pharm. 1984; 22:207-218.
12. Chen PC, Frank SG. *In vitro* release of lidocaine from pluronic F-127 gels. Int J Pharm. 1981; 8:89-99.
13. Miyazaki S, Takeuchi S, Yokouchi C, Takada M. Pluronic F-127 gels as a vehicle for topical administration of anticancer agents. Chem Pharm Bull (Tokyo). 1984; 32:4205-4208.
14. Miller SC, Donovan MD. Effect of ploxamer 407 gel on the miotic activity of pilocarpine nitrate in rabbits. Int J Pharm. 1982; 12:147-152.
15. Hadgraft J, Howard JR. Drug release from Pluronic F-127 gels. J Pharm Pharmacol. 1982; 34:3.
16. Collett JH, Tait CJ, Attwood D, Sharma HL, Smith AM. *In vitro* evaluation of polaxamer gels as controlled release systems using gamma scintigraphy. Proc Int Symp Contr Rel Bioact Mater. 1985; 12:28-30.
17. Nalbandian RM, Henry RL, Wilks HS. Artificial skin. II. Pluronic F-127 silver nitrate or silver locate gel in treatment of thermal burns. J Biomed Res. 1972; 6:583-590.
18. Choi HG, Jung HJ, Ryu MJ, Yoon SJ, Oh YK, Kim CK. Development of *in situ*-gelling and mucoadhesive acetaminophen liquid suppository. Int J Pharm. 1998; 165:33-44.
19. Kushula GP. In: Pharmaceutical Dosage Form, Disperse System, Vol II, 2nd ed., (Lieberman HA, Reiger MM, eds.). Marcel Dekker, Inc., New York, USA, 1996; pp. 399-305, and 415.
20. Davis HM. Analysis of creams and lotions in manual of cosmetic analysis. FDA, pp. 32-49.
21. De Martin ML, Cussler EL. Predicting subjective spreadability, viscosity, and stickness. J Pharm Sci. 1975; 64:976-982.
22. Lucero MJ, Vigo J, Leon MJ. Study of shear and compression deformations on hydrophilic gels of tretinoin. Int J Pharm. 1994; 106:125-133.
23. Vennat B, Gross D, Pourrat A. Hydrogels based on cellulose derivatives: validation of the spreading diameter measurements. STP Pharma Sci. 1994; 4:453-357.
24. Contreras MD, Sanchez M. Application of factorial design to the study of the flow behavior, spreadability, transparency of carbopol ETD 2020 gel. Part II. Int J Pharm. 2002; 234:149-157.
25. Abdel-Hamid SM, Abdel-Hady SE, El-Shamy AA, EL-Dessouky HF. Formulation of antispasmodic drug as a topical local anesthetic. Int J Pharm. 2006; 326:107-118.
26. Steffe JF. In: Rheological methods in food process engineering, 2nd edition, Chapter 1, Freeman Press, 1996; pp. 1-91.
27. Chang JY, Oh YK, Choi HG, Kim YB, Kim CK. Development of mucoadhesive and thermosensitive gel containing clotrimazole for prolonged antifungal activity. Int J Pharm. 2002; 241:155-163.
28. Siewert M, Dressman J, Brown CK, Shah VP. FIP/AAPS guidelines to dissolution/*in vitro* release testing of novel/ special dosage forms. AAPS Pharm Sci Tech. 2003; 4: E7.
29. Peppas NA. Analysis of fickian and nonfickian drug release from polymers. Pharm Acta Helv. 1985; 60:110-111.
30. Clinical and Laboratory Standards Institute. Performance Standards for Antimicrobial Susceptibility Testing; 15th Informational Supplement. M100-S15. Clinical and Laboratory Standards Institute (CLSI), Wayne, PA, USA, 2006.
31. Rassing J, Attwood D. Ultrasonic velocity and light scattering studies on the polyoxyethylene-polyoxypropylene copolymer pluronic F127 in aqueous solution. Int J Pharm. 1982; 13:47-55.
32. McBain MEL, Hutchinson E. Solubilization and related phenomena. Academic Oress, New York, USA, 1955.
33. Humphreys KJ, Rhodes CT. Effect of temperature upon solubilization by a series of nonionic surfactants. J Pharm Sci. 1968; 57:79-83.
34. Elworthy PH, McDonald C. Chemistry of non-ionic detergents. Part VII. Variation of the micellar structure of some synthetic non-ionic detergents with temperature. Colloid Polym Sci. 1964; 195:16-23.
35. BASF Company Organic Specialties and Fine Chemicals Department. Technical Data on Pluronic Polyols. Parsippany, NJ, USA, Publication No. OS 796.
36. Barry BW, EL Eini DI. Solubilization of hydrocortisone, dexamethasone, testosterone and progesterone by long-chain polyoxyethylene surfactants. J Pharm Pharmacol. 1976; 28:210-218.
37. Garg A, Aggarwal D, Garg S. Spreading of semisolid formulation. Pharm Tech. 2002; 9:89-105.
38. Pena LE, Lee BI, Sternes JF. Structural rheology of model ointment. Pharm Res. 1994; 11:875-881.
39. Dolz M, Herraes M, Gozalez F, Diez O. Flow behavior of carbopol 940 hydrogels, the influence of concentration

- and agitation time. Pharmazie. 1998; 53:126-130.
40. Fresno MJ, Ramírez AD, Jiménez MM. Systematic study of the flow behaviour and mechanical properties of Carbopol Ultrez 10 hydroalcoholic gels. Eur J Pharm Biopharm. 2002; 54:329-335.
 41. Llabot JM, Palma SD, Manzo RH, Allemandi DA. Design of novel antifungal mucoadhesive films. part I. Pre-formulation studies. Int J Pharm. 2007; 330:54-60.
 42. Miyazaki S, Yokouchi C, Nakamura T, Hashiguchi N, Hou WM, Takada M. Pluronic F-127 gels as a novel vehicle for rectal administration of indomethacin. Chem Pharm Bull (Tokyo). 1986; 34:1801-1808.
 43. Gilbert J, Hadgraft J, Bye A, Brookes L. Drug release from pluronic F-127 gels. Int J Pharm. 1986; 32:223-228.
 44. Chi SC, Jun HW. Release rates of Ketoprofen from poloxamer gels in memberaneless diffusion cell. J Pharm Sci. 1991; 80:280-283.
 45. Desai SD, Blanchard J. *In vitro* evaluation of pluronic F127-based controlled-release ocular delivery systems for pilocarpine. J Pharm Sci. 1998; 87:226-230.
 46. Dibiasse MD, Rhodes CT. Formulation and evaluation of epidermal growth factor in pluronic F-127 gels. Drug Dev Ind Pharm. 1996; 22:823-831.
 47. Hadgraft J. Percutaneous absorption: possibilities and problems. Int J Pharm. 1983; 16:255-270.
 48. Mitchell K, Ford JL, Armstrong DJ, Elliott PNC, Rostron C, Hogan JE. The influence of additives on the cloud point, disintegration and dissolution of hydroxypropylmethyl cellulose gels and matrix tablets. Int J Pharm. 1990; 66:233-242.
 49. Buckton G, Tawburic S. Triblock copolymers in aqueous solution studies by static and dynamic light scattering and oscillatory shear measurements; Influence of relative block sizes. J Phys Chem. 1992; 96:6038-6044.
 50. Krossemeyer RW, Gurny R, Doelker E, Buri P, Peppas NA. Mechanisms of solute release from porous hydrophilic polymers. Int J Pharm. 1983; 15:25-35.
 51. Joens DS, Woolfson AD, Djokic J, Coulter WA. Development and mechanical characterization of bioadhesive semi-solid polymeric systems containing tetracycline for the treatment of periodontal diseases. Pharm Res. 1996; 13:1732-1736.
 52. Miller SC, Drabik BR. The rheological properties of ploxamer vehicles. Int J Pharm. 1984; 18:269-276.
 53. Hansson P, Lindman B. Surfactant-polymer interactions. Curr Opin Colloid Interface Sci. 1996; 1:604-613.
 54. Rahman MS, Babar A, Patel NK, Plakogiannis FM. Medicament release from ointment bases: V. Naproxen *in-vitro* release and *in-vivo* percutaneous absorption in rabbits. Drug Dev Ind Pharm. 1990; 16:651-672.
 55. Wang YY, Hong CT, Chiu WT, Fang JY. *In vitro* and *in vivo* evaluation of topically applied capsaicin and nonivamide from hydrogels. Int J Pharm. 2001; 224:89-104.
 56. Paavola A, Yliruusi J, Rosenberg P. Controlled release and dura mater permeability of lidocaine and ibuprofen from injectable poloxamer-based gels. J Control Rel. 1998; 52:169-178.
 57. Ning M, Guo Y, Pan H, Chen X, Gu Z. Preparation, *in vitro* and *in vivo* evaluation of liposomal/nisomal gel delivery system for clotrimazole. Drug Dev Ind Pharm. 2005; 31:375-383.
 58. Prescott SC, Dunn CG. Industrial Microbiology. McGraw-Hill Book company, Inc., 1959; p. 10.

(Received October 29, 2009; Accepted December 22, 2009)

Original Article**Exposure-response modeling and clinical trial simulation of the effect of tolterodine on QT intervals in healthy volunteers****Kevin R. Sweeney^{1,*}, Marc R. Gastonguay², Lisa Benincosa³, Carol L. Cronenberger¹, Paul Glue⁴, Bimal K. Malhotra⁵**¹ Pfizer Inc., Groton, CT, USA;² Metrum Research Group LLC, Tariffville, CT, USA;³ Hoffmann-La Roche Inc., NJ, USA;⁴ Dunedin School of Medicine, Dunedin, New Zealand;⁵ Pfizer Inc., New York, NY, USA.

ABSTRACT: The objective of this analysis was to explore exposure-response modeling of data from a thorough QT (TQT) study of tolterodine in CYP2D6 extensive (EMs) and poor metabolizers (PMs). Crossover treatments of the TQT study included the recommended (2 mg twice daily) and suprathreshold (4 mg twice daily) doses of tolterodine, moxifloxacin (400 mg once daily), and placebo. The concentration-response relationships for the QTc effects of moxifloxacin and tolterodine were described using a linear model with baseline effect, placebo effect, and a drug effect. The mixed effects modeling approach, using the first order conditional estimation method, was implemented in NONMEM. Simulated data from 250 trial replicates were used for limited predictive check and to describe the expected extreme responders in this study, under the derived model and point estimates. Modeling results for tolterodine showed linear concentration-dependent increases in QTc interval, with no difference in slopes between EMs and PMs. Model-predicted QTc prolongations for tolterodine and moxifloxacin were consistent with their respective observed mean results. No subjects were predicted to have increases of > 60 milliseconds (ms); the predicted incidence of borderline QTc increases (> 30 and ≤ 60 ms) remained low at the suprathreshold tolterodine dose in both PMs (9.1%) and EMs (3.9%). In conclusions, this analysis supports our clinical experience that tolterodine does not have a clinically significant effect on QT interval.

Keywords: Tolterodine, QTc prolongation, exposure-response modeling

*Address correspondence to:

Dr. Kevin Sweeney, Pfizer Inc., 50 Pequot Avenue MS6025-A2242, New London, CT 06320, USA.

e-mail: kevin.sweeney@pfizer.com

1. Introduction

Tolterodine is an antimuscarinic agent approved for the treatment of overactive bladder (1-3). Metabolism by cytochrome P450 (CYP) 2D6 and 3A4 isoenzymes represents the major route of elimination of tolterodine (4,5). Since CYP2D6 is involved in tolterodine metabolism, both extensive (EMs) and poor metabolizers (PMs) of tolterodine have been identified (6,7). Metabolism of tolterodine by CYP2D6 in EMs results in the formation of an equipotent pharmacologically active metabolite, 5-hydroxymethyltolterodine (DD01), which has been documented to be comparable to tolterodine in its antimuscarinic activity (8,9). In PMs, however, CYP3A4 is involved in the formation of an inactive metabolite.

Systemic exposure to tolterodine following the recommended 4 mg daily dose is substantially different due to the aforementioned metabolism profiles in EMs and PMs. In EMs, the systemic exposures to tolterodine and DD01 are approximately similar, while in PMs, tolterodine concentrations are higher with virtually no detectable DD01 in serum. The observed pharmacologic effects are attributable to both tolterodine and DD01 in EMs and to tolterodine alone in PMs. The unbound fraction of tolterodine and DD01 is 3.7% and 36%, respectively (10,11), and the combined exposure of unbound active moieties is similar in EM and PM subjects (7). Since antimuscarinic activity is not dependent on metabolizer status, a dosage adjustment is not recommended based on CYP2D6 metabolizer status (7). With respect to drug-drug interactions, in CYP2D6 PMs, there is approximately a doubling of exposure following administration of potent CYP3A4 inhibitors, with a recommendation that dose administration be halved (2 mg daily) (8).

An *in vitro* study of the effects of tolterodine on cardiac ion channels showed that tolterodine is a potent inhibitor of both human ether a-go-go-related

gene (HERG) cardiac potassium and L-type calcium channels (12). The HERG inhibitory concentration 50% value (IC_{50}) was reported to be 17 nM, with some inhibition evident at concentrations as low as 3 nM (12). These activities resulted in a prolongation of action potential duration, but not to the extent observed with dofetilide, a pure HERG blocker (12). For drugs like tolterodine and verapamil, it has been hypothesized that blocking the cardiac L-type calcium channel, at least in part, serves to counteract the QT prolonging effects of HERG potassium channel blockade (12).

Despite extensive post-registration clinical experience and a lack of cardiac arrhythmic events potentially related to QT interval prolongation, a thorough QT (TQT) study was deemed to be important for a definitive assessment of the effects of this agent on the QT interval in view of the positive results in the preclinical HERG assay. With few exceptions, regulatory agencies now require a TQT study not only for drug candidates in clinical development, but also for marketed drugs (13). Therefore, a TQT study was performed in healthy subjects to evaluate the potential of tolterodine to alter cardiac electrical conductivity using the recommended and twice the recommended doses.

The results of this tolterodine TQT study have been previously published (14). There were four treatment arms in this crossover study in both CYP2D6 EM and PM subjects: 1) tolterodine immediate release (IR) tablets at the recommended dose (2 mg BID); 2) tolterodine IR at a supratherapeutic dose (4 mg BID); 3) moxifloxacin (400 mg QD) as a positive control and 4) placebo. The supratherapeutic tolterodine dose was selected to provide systemic exposures consistent with the increases in exposures observed following CYP3A4 inhibition. This current work details the exposure-response modeling of data collected as part of this TQT assessment of tolterodine.

2. Materials and Methods

2.1. Study design

This was a positive- and placebo-controlled, multiple-dose, 4-way crossover study conducted at 2 centers. This study evaluated the single-dose and steady-state QTc effects of the recommended (2 mg twice daily) and supratherapeutic (4 mg twice daily) doses of tolterodine IR and the positive control, moxifloxacin (400 mg once daily), each compared with placebo. Treatments were administered for 4 days (morning dose only on Day 4), with a washout period of ≥ 5 days between periods. Moxifloxacin was included as a positive control to confirm the sensitivity of the study to detect small increases in the QTc interval. Moxifloxacin is frequently used in TQT studies because it has a well-defined QTc prolongation effect, usually about 6 to 12 ms.

A total of 48 subjects were enrolled for this study. At the time of study enrollment, subjects were categorized as either extensive metabolizers (EM, $N = 26$) or poor metabolizers (PM, $N = 22$) for CYP2D6, as assessed by genotyping (14). Eligible study participants were men and women between the ages of 18 and 55 years, with a body mass index of 18 to 30 kg/m². All subjects reported to the clinic two days prior to initiation of dosing in each treatment period. During each period, baseline and on-treatment ECGs were obtained in triplicate at pre-specified time points, with the consecutive replicates about 2 min apart.

Electrocardiograms were obtained within 1-hour predose on the mornings of Days 1-4 in each period. In addition, ECGs were obtained at 0.5, 1, 2, and 4 h postdose on Day 1 and at steady state (Day 4) at 0.5, 1, 2, 3, 4, 6, 9, and 12 h postdose. Baseline ECGs were performed on Day 0 at the same times of the day (time-matched) as those on Day 4. All ECG data used in the PK/PD analysis were machine-read (GE Marquette's MAC 1200[®] ECG recorders, GE Medical Systems, Milwaukee, WI, USA), and obtained in triplicate. Malhotra *et al.* have published additional information on ECG collection and study conduct (14).

2.2. ECG data

An initial graphical assessment was performed to assure that pre- and post-treatment heart rate (HR) distributions were similar prior to generation of heart rate adjusted data. After verifying the similarity of the distributions, corrected QT interval (QTc), period- and subject-specific baseline-subtracted QTc interval (Δ QTc or Δ QTc) data were generated.

All QT intervals were adjusted to a HR of 60 beats/minute (bpm). Methods used to generate heart rate corrected QTc values from QT and RR intervals were the Fridericia ($QTcF = QT/RR^{0.33}$), Bazett ($QTcB = QT/RR^{0.50}$), and study-specific population ($QTcP = QT/RR^{0.41}$) correction formulae (15), where RR equals 60/HR and 0.41 represents the mean study-specific correction factor across the four baseline periods. The exponent for RR in the study-specific population correction formula was determined as the slope of the regression of $\ln(QT)$ versus $\ln(RR)$. In addition to the population-specific correction factor, an individual-specific correction factor was generated. This factor was obtained in similar fashion to the population-specific factor outlined above except that a correction factor was generated from each individual's baseline data. Therefore, this correction factor is individual-specific and period-specific. QTcI denotes the heart-rate adjusted QT interval using the individual correction.

Following application of the correction formulae to pre- and post-treatment QT interval data, Δ QTc data were derived as corrected QT interval minus the period- and subject-specific, time-matched baseline data. Plots

of corrected QT interval (QTcF, QTcB, QTcP and QTcI) versus HR data were constructed to assess the adequacy of each heart rate correction factor. Acceptable correction was defined as no apparent relationship between corrected QT interval and heart rate.

2.3. Concentration data

During each treatment, 2 sets of blood samples were obtained at the same time point as the ECGs. One set of samples was processed for the analyses of tolterodine and DD01 in serum and the other for moxifloxacin in plasma, as described by Malhotra *et al.* (14).

Since pharmacologic activity is a function of unbound drug concentration, and there is a significant difference in the free fraction of active moieties (16), period- and subject-specific unbound fractions for tolterodine ($f_{u,Tolterodine}$) and DD01 ($f_{u,DD01}$) were calculated from alpha₁-acid glycoprotein (AAG) concentrations using the following formulae (17):

$$f_{u,Tolterodine} = 1/(1 + (2100 \cdot AAG/42))$$

$$f_{u,DD01} = 1/(1 + (130 \cdot AAG/42))$$

Individual concentration-time data for tolterodine, DD01 and moxifloxacin on Days 1 and 4 were analyzed by a standard non-compartmental approach using WinNonlin Enterprise (Pharsight Co., Mountain View CA, Version 3.2) (14). Maximum observed concentrations (C_{max}) and time of C_{max} (T_{max}) were obtained by direct observation of the experimental data. Area under the concentration-time curve (AUC) was calculated using the linear-log trapezoidal rule.

2.4. Concentration-ΔQTc analysis

The concentration-response relationships for moxifloxacin and tolterodine were modeled using machine-read QT interval data which were collected at baseline (Day 0), after the first dose (Day 1), pre-dose on Days 2 and 3, and at steady state (Day 4). This dataset provided the most complete and comprehensive range of exposures for modeling the concentration-response relationships. For heart-rate correction, the population-corrected ΔQTcP data were used as the population correction appeared to best eliminate the QT dependence on heart rate, as evidenced by the slope closest to zero in Figure 1. This model characterized the relationship between ΔQTcP interval and concentration, accounting for placebo, baseline, and drug effects. For the tolterodine-ΔQTcP effect modeling, contributions to the observed QTc prolongation were assumed from both the parent drug and its primary active metabolite, DD01.

Since there is an approximately 10-fold difference in unbound fraction of DD01 compared with tolterodine, the pharmacokinetic/pharmacodynamic (PK/PD)

analysis was performed using the sum of unbound serum concentrations along with a modeled relative potency factor of IKr-channel antagonism *in vivo* by both tolterodine and DD01. A similar model was fitted to ΔQTcP interval versus moxifloxacin total plasma concentration data. Because there was no apparent nonlinearity when the data were graphically displayed, a population mixed effects modeling approach using linear models was employed to characterize the concentration-ΔQTcP relationship. The mixed effects modeling approach was implemented in NONMEM Version V Level 1.1 (ICON Development Solutions, Ellicott City, MD, USA and NONMEM Project Group, UCSF, San Francisco, CA, USA) using the first order conditional estimation method.

2.5. ΔQTc model definition

The relationship between ΔQTcP interval and tolterodine/DD01 serum concentration was described using a linear model with baseline effect, placebo effect, and a drug effect. The placebo parameter (PCBO_i) describes the average offset of ΔQTcP that can be attributed to the placebo treatment. The baseline parameter (BSLN_i) describes the average ΔQTcP interval in the absence of any drug-induced effect for each individual contributing data (predose, Day 0 data). The slope parameter (SLP_i) describes the dependence of ΔQTcP interval on serum concentration for each individual following tolterodine administration. The potency (POT) parameter accounts for the potential difference between tolterodine and DD01 metabolite in ability to block IKr channels. The model with BSLN_i, PCBO_i, SLP_i and POT parameters, and associated variances, is presented below:

$$PCBO_i = \theta_1 + \eta_1$$

$$BSLN_i = \theta_2 + \eta_1$$

$$SLP_i = \theta_3 + \eta_2$$

$$POT = \theta_4$$

$$\Delta QTcP_{i,j} = PCBO_i + BSLN_i + SLP_i \times (C_{tolterodine_{i,j}} + POT \times C_{DD01_{i,j}}) + \epsilon_{i,j}$$

In these equations, ΔQTcP_{i,j} is the jth ΔQTcP observation for the ith individual, θ₁ represents the population mean estimate of the placebo effect, θ₂ represents the population mean estimate of the baseline ΔQTcP, θ₃ represents the population mean estimate of the slope describing concentration effect, θ₄ represents the population mean estimate of the relative potency between tolterodine and DD01 metabolite, η₁ represents the inter-individual random effect for the placebo and baseline parameters, assumed to be a normal, independent, identically distributed random variable with zero mean and variance ω₁² (~NIID(0, ω₁²)), and η₂ represents the inter-individual random effect of the slope parameter (~NIID(0, ω₂²)). The ε_{i,j}

parameter represents the j^{th} residual error for the i^{th} individual and is assumed to be a normal, independent, identically distributed random variable with zero mean and variance σ^2 ($\sim \text{NIID}(0, \sigma^2)$). An additive model (constant variance) was used for the inter-individual random effect distributions, allowing for these effects on ΔQTcP interval to be positive or negative across individuals.

A similar analysis was conducted on the observed $\text{DQTcP}_{i,j}$ versus moxifloxacin plasma concentration data. The difference from the model presented above is that total concentration of moxifloxacin was used, as there is no active metabolite. The equation used is as follows:

$$\begin{aligned}\text{PCBO}_i &= \theta_1 + \eta_1 \\ \text{BSLN}_i &= \theta_2 + \eta_1 \\ \text{SLP}_i &= \theta_3 + \eta_2 \\ \Delta\text{QTcP}_{i,j} &= \text{PCBO}_i + \text{BSLN}_i + \text{SLP}_i \times (C_{\text{MOXI},i,j}) + \varepsilon_{i,j}\end{aligned}$$

In this equation, all terms are as defined above, with the difference that $\Delta\text{QTcP}_{i,j}$ values are associated with the respective moxifloxacin concentration and no potency parameter was necessary since there is no active metabolite of moxifloxacin.

2.6. Model evaluation

A linear model was fitted to ΔQTcP data using the first order conditional method of estimation. Bootstrap analysis was employed to generate a 95% CI constructed about each of the parameters in the final model. Model estimates and associated CI were used to characterize the magnitude and estimate confidence (precision) of parameters in the linear model, even those that may be associated with "no effect".

Model performance was assessed by performing a predictive check using the final model and final parameter estimates, generating distributions of simulated maximum ΔQTcP values by tolterodine dose and genotype status, with the respective observed mean maximum ΔQTcP value by tolterodine dose level and genotype status superimposed onto the appropriate distribution. A total of 250 replicates of this study were simulated.

A variety of QTc-derived ECG indices may be analyzed to evaluate the effect of a drug on ventricular repolarization and the potential clinical risk of torsades de pointes (TdP). In addition to the population-based mean increase in placebo-corrected maximal QTc interval, a frequently used index is the number of subjects with a > 60 ms increase in QTc interval from baseline (13,19). Therefore, a second simulation with uncertainty around all parameter estimates was performed to provide insight into extreme responder individuals (e.g. individuals identified with ΔQTcP values defined as borderline or prolonged) and to make

a statement about model performance. To address the question of extreme responder individuals, the median percentage of individuals with ΔQTcP values in the following categories were tabulated by tolterodine dose level and genotype status:

- ≤ 30 ms (Normal)
- > 30 and ≤ 60 ms (Borderline)
- > 60 ms (Prolonged)

These categories were selected based on the recommendations in the ICH-E14 guidance (13). Additionally, the 95% confidence interval for each of these values was also generated and reported.

3. Results

3.1. Tolterodine and DD01 exposures

Tolterodine was quickly absorbed and systemic exposure increased proportionally between the 2 and 4 mg doses. The tolterodine C_{max} and AUC were approximately 3-5 and 10 times greater, respectively, in PMs than in EMs. In EMs, DD01 exposure increased proportionally with dose, consistent with exposure of tolterodine. The systemic exposure of DD01 in PMs was 6-7 times less than that of EMs (14).

3.2. Corrected QT interval

The observed heart rates in baseline (Day 0) and respective treatment periods were similar in range and distribution. The range of heart rates for baseline ($n = 1,286$), placebo ($n = 752$), tolterodine 4 mg/day ($n = 768$) and tolterodine 8 mg/day ($n = 768$) and moxifloxacin ($n = 543$) groups were 41-105, 45-101, 45-97, 40-97 and 43-101 bpm, respectively. Correction methods previously described (15) were applied to the QT data in an effort to eliminate the QT interval dependence on heart rate, and permit the use of a linear model for analysis. Graphical representation of baseline QTc interval versus baseline heart rate is presented for each correction method (Figure 1).

The study-specific population correction (bottom left panel) appeared to best correct QT interval over the observed heart rate range. All other correction methods did not appear to adequately correct the observed dependence of QT interval on heart rate. This is represented by the non-horizontal pattern of the data.

Following the regression of $\log(\text{QT})$ on $\log(\text{HR})$, the population correction factors for each of the four Day 0 baseline periods were: Period 1, 0.414; Period 2, 0.423; Period 3, 0.407; and Period 4, 0.394. These period-specific correction factors were then used to generate heart rate adjusted QTc interval data using the population correction method described previously, and appropriate baseline data were then used to

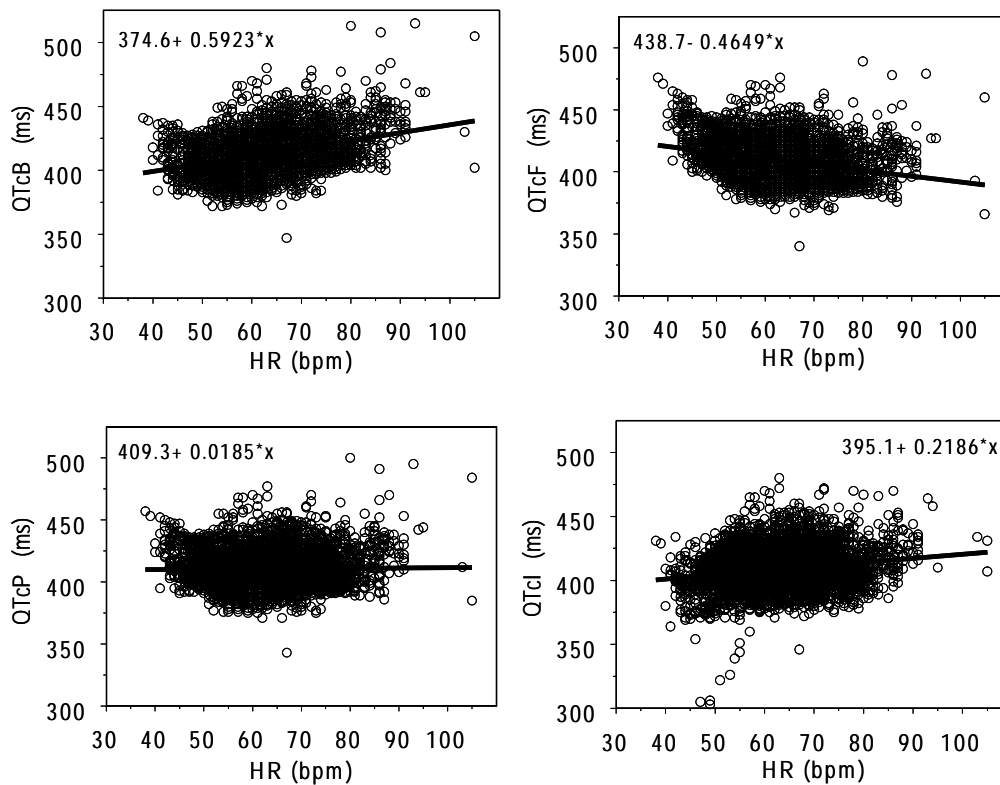


Figure 1. Corrected baseline (Day 0) QT interval (fridericia, bazett, population and individual correction) versus baseline (Day 0) heart rate.

generate Δ QTcP. Analysis of the effect of tolterodine/DD01 concentration on Δ QTcP was performed and conclusions drawn from subsequent results.

3.3. Moxifloxacin plasma concentration- Δ QTcP analysis

Moxifloxacin was included in this study as a positive control to validate the ability to detect a positive signal when present (13). The slope (%SE) from this analysis was 0.00300 (0.000475) ms/ng/mL, with a 95% CI constructed about slope of 0.00207 to 0.00393 ms/ng/mL. Given the exclusion of zero in this CI and the good precision of the parameter estimate (%SE = 15.8), the slope estimate was sufficiently robust for making clinical inferences. The observed C_{max} on Day 4 was 3,610 ng/mL, translating to a Δ QTcP prolongation of 10.8 ms, consistent with historical data describing the effects of moxifloxacin on QT interval prolongation.

3.4. Tolterodine/DD01 serum concentration- Δ QTcP analysis

Results from the concentration- Δ QTc model fitted to the Δ QTcP interval versus unbound serum concentration data are provided in Table 1. As a measure of precision of model estimates, the asymptotic relative standard errors (%SE) of the placebo, baseline, slope and potency, and associated inter-individual variance (IIV)

Table 1. Modeling results of the study-specific population Δ QTcP interval vs. unbound serum tolterodine and DD01 concentration analysis

Parameter	Parameter Estimate	%SE ^a	95% CI ^b
Placebo (ms)	0.362	216	-1.32 to 1.98
Baseline (ms)	0.321	241	-1.31 to 1.72
Placebo/Baseline IIV ^c (ms ²)	3.62	34.5	–
Slope (ms/ng/mL)	13.4	26.7	6.90 to 21.9
Slope IIV ^c (ms/ng/mL) ²	118	37.1	–
Potency	0.140	48.7	-0.306 to 0.227
Residual Varianced (ms ²)	67.3	10.3	–

^a%SE (precision) of the parameter estimate = 100*SE/Mean; ^b95% CI based on Bootstrap Analysis; ^c Inter-individual variance; ^d Intra-individual (residual) variance.

parameters were generated. Precision of slope was very good, as evidenced by the low %SE (26.7). Precision of placebo and baseline was not precisely estimated given the rather high %SE (216 and 241, respectively). Residual error was low (67.3 ms², or 8.20 ms expressed as a standard deviation) and precisely estimated (%SE = 10.3). The 95% CI on slope (6.90 to 21.9) did not contain zero and is consistent with the good precision of the slope estimate. The 95% CI for placebo, baseline and potency parameters all enclosed zero, consistent with the large %SE associated with each of these parameters.

Figure 2 presents a plot of Δ QTcP interval versus unbound tolterodine and DD01 serum concentration,

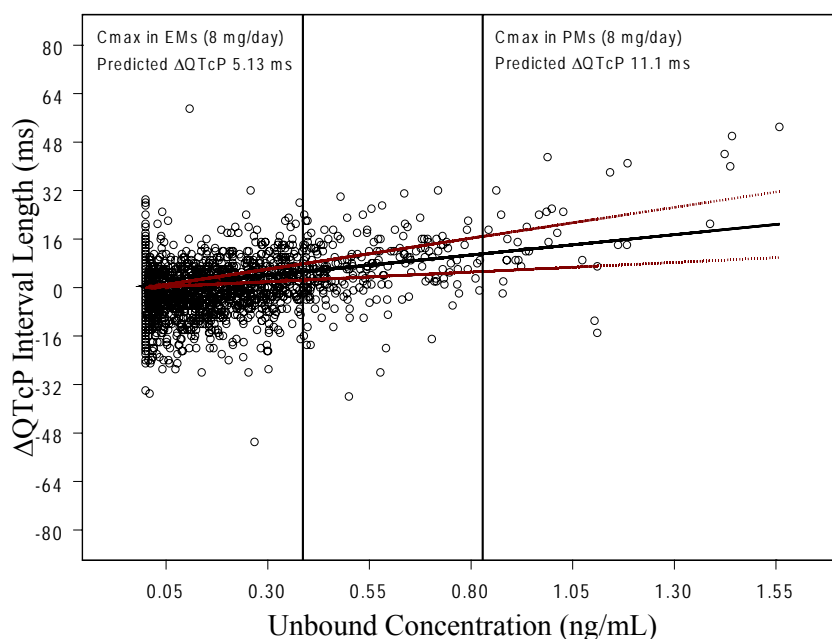


Figure 2. Population Δ QTcP interval versus unbound tolterodine/DD01 serum concentration following twice-daily oral administration of tolterodine immediate release tablets. Lines denotes NONMEM population model predicted slope and 95% CI estimates.

Table 2. Summary of mean unbound concentrations of tolterodine and DD01 metabolite and model-Predicted prolongation at T_{max} , by genotype and administered dose

Group	Unbound Tolterodine (ng/mL)	Unbound DD01 (ng/mL)	Normalized Concentration ^a (ng/mL)	Predicted Prolongation (ms)
EM 2 mg BID ^b	0.0790	0.814	0.193	2.59
EM 4 mg BID ^c	0.159	1.60	0.383	5.13
PM 2 mg BID ^d	0.392	0.102	0.406	5.44
PM 4 mg BID ^e	0.793	0.230	0.825	11.1
Study Population 2 mg BID ^f	–	–	–	3.90
Study Population 2 mg BID ^f	–	–	–	7.87

^a Unbound Tolterodine Concentration + POT*Unbound DD01 Concentration; ^b Extensive metabolizers administered 2 mg every 12 h (4 mg/day); ^c Extensive metabolizers administered 4 mg every 12 h (8 mg/day); ^d Poor metabolizers administered 2 mg every 12 h (4 mg/day); ^e Poor metabolizers administered 4 mg every 12 h (8 mg/day); ^f (Study population genotype-specific mean prolongation*respective number of individuals)/total number of individuals in the study.

including the 95% CI constructed about the slope estimate. In Figure 2, the vertical reference lines denote the mean unbound C_{max} in EMs and PMs receiving the tolterodine supratherapeutic dose, and the corresponding QTc prolongations are noted for each C_{max} . Table 2 presents mean tolterodine and DD01 unbound concentration by dose level and genotype (EM = extensive metabolizer, PM = poor metabolizer), along with estimates of predicted QTc interval at T_{max} . Additionally, prolongation estimates by dose group in

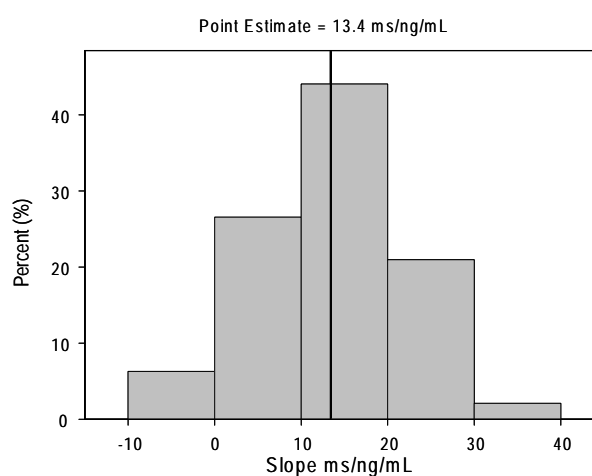


Figure 3. Population distribution of slopes from describing Δ QTcP interval versus unbound tolterodine/DD01 serum concentration following twice-daily oral administration of tolterodine immediate release tablets.

the pooled study population (enriched for PMs) were calculated.

A histogram distribution of slope across the 48 individuals in the study is presented in Figure 3. The range of slopes by genotype was as follows: EM, -7.66 to 27.7 ms/ng/mL; PM, 0.24 to 31.9 ms/ng/mL. The highest observed slopes were comparable in the EM and PM subgroups (31.9 ms/ng/mL and 27.7 ms/ng/mL, respectively). The similarity of slope ranges between EM and PM subjects suggested that there was

no difference by CYP2D6 genotype in sensitivity to tolterodine/DD01 with respect to QTc prolongation.

3.5. Δ QTcP simulation

A simulation of 250 trial replicates was performed and a limited predictive check was conducted using the simulated data as a measure of model performance. Final parameter estimates of the model were used to generate simulations of Δ QTcP interval values as a function of random noise and unbound concentration of tolterodine and DD01 metabolite. Five distributions of simulated maximum Δ QTcP were generated: EM subjects at the 2 and 4 mg BID dose level, PM

subjects at the 2 and 4 mg BID dose level, and placebo. The respective mean observed maximum DQTcP in the study was superimposed on each of the five distributions identified above. In each of the five groups, the observation of mean maximum Δ QTcP fell within the distribution: 11, 16, 16, 20 and 9 ms for the 2 mg BID EM, 4 mg BID EM, 2 mg BID PM, 4 mg BID PM and placebo subjects, respectively. Overall performance of the model as a Monte Carlo simulation tool was acceptable, but some over-prediction was evident for the placebo group. These distributions are presented in Figure 4.

Additionally, the simulation with uncertainty (250 trial replicates) was used to describe the expected

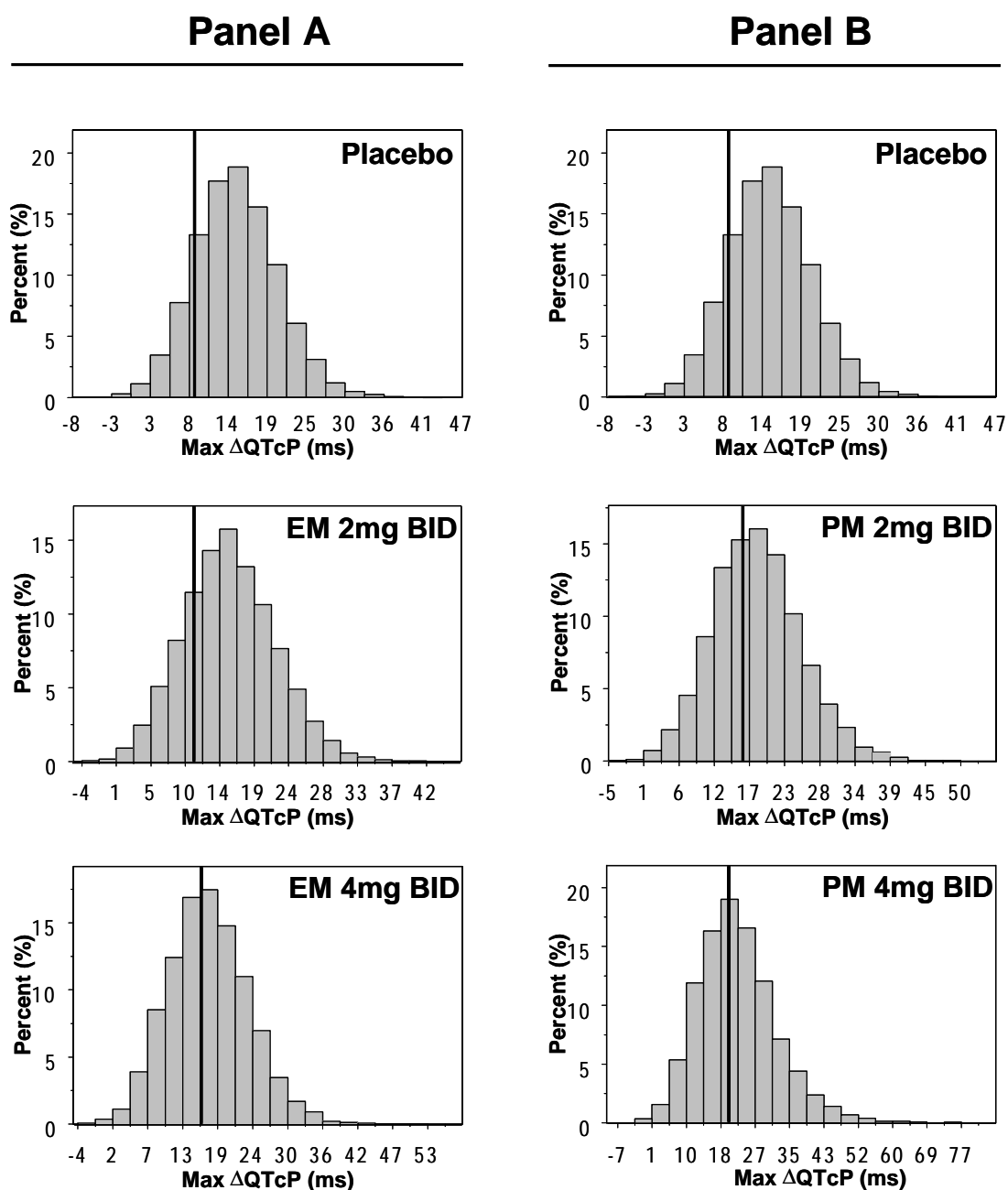


Figure 4. Simulated distributions and observed mean (solid line) maximum Δ QTcP interval by dose group and genotype following twice-daily oral administration of tolterodine immediate release tablets. Panel A: Extensive metabolizers. Panel B: Poor metabolizers.

Table 3. Trial simulation results for median percent (95% CI) of subjects predicted to exhibit prolongation, stratified by tolterodine dose level and genotype status

Dose Group	Genotype	% Subjects Predicted for Categorical Increases in Δ QTcP		
		Normal (≤ 30 ms)	Borderline (> 30 and ≤ 60 ms)	Prolonged (> 60 ms)
Placebo	EM/PM	100 (93.6 to 100)	0 (0 to 0)	0 (0 to 0)
2 mg BID	EM	100 (92.3 to 100)	1.92 (0.0962 to 3.75)	0 (0 to 0)
4 mg BID	EM	96.2 (88.5 to 100)	3.85 (0.192 to 7.50)	0 (0 to 0)
2 mg BID	PM	95.5 (81.8 to 100)	4.55 (0.227 to 8.86)	0 (0 to 0)
4 mg BID	PM	81.8 (63.6 to 95.5)	9.09 (0.455 to 17.7)	0 (0 to 4.55)

extreme responders in this study, under the derived model and point estimates. A categorical tabulation of median percent maximal prolongation with associated 95% CI by dose level and genotype was generated, with values less than or equal to 30 ms, greater than 30 and less than or equal to 60 ms, and greater than 60 ms reported. These simulated values were consistent with observations made during the conduct of the study. Results are presented in Table 3.

4. Discussion

A thorough QT study was conducted to investigate the potential effect on the QTc interval following oral administration of tolterodine (2 and 4 mg BID, 4 and 8 mg/day total dose, respectively). Based on the statistical analyses of the machine-read QTcF data for the pool of EM and PM subjects combined, a negative TQT conclusion could be made for both recommended and supratherapeutic doses of tolterodine (14). The modeling results also predicted only small increases in QTc interval following tolterodine administration and were consistent with the traditional statistical analysis. Concentration-QTc modeling approaches were used to further investigate the effects of tolterodine on QTc interval in EMs and PMs separately. An estimation approach was employed, using bootstrap estimates to make inference regarding model parameters.

The systemic exposures and pharmacokinetic profiles of tolterodine and DD01 were consistent with those previously reported in both EM and PM subjects, suggesting that the results of the PK/PD analysis of a potential QT effect would be indicative of the population at large (5). Additionally, exposure observed in PMs receiving twice the recommended daily dose (4 mg BID) approximated that observed in PMs administered the recommended daily dose (2 mg BID) allowing the concentration-response relationship to be descriptive of PMs whose tolterodine exposure is inadvertently increased by concomitant dosing with a potent CYP3A4 inhibitor. The moxifloxacin exposure in this study was consistent with values reported in the product label (18).

Four correction methods were investigated to eliminate the dependence of QT on heart rate. The

study-specific population method was determined to be the best method for generation of QTc data, as the Fridericia, Bazett and Individual methods retained some bias. Following appropriate correction of the observed QT data, Δ QTc data were generated using time-matched and period-specific Day 0 baseline data. The Δ QTcP data were used as the primary endpoint in this modeling analysis. A linear model characterized the relationship between Δ QTcP and concentration, accounting for placebo, baseline and drug effects. Since the DD01 metabolite is reported to be pharmacologically active, and there is an approximate 10-fold difference in unbound fraction when compared to tolterodine, the analysis was performed using unbound serum concentrations with a potency correction for DD01 metabolite based on observed differences in IKr channel blocking activity *in vitro*. A similar model was fitted to Δ QTcP interval *versus* moxifloxacin total plasma concentration data. The differences were that total concentration was used and no potency correction factor was necessary.

Results of the moxifloxacin analysis were consistent with generally accepted prolongation values, validating the sensitivity of study conduct. The global mean concentration of moxifloxacin was 3,610 ng/mL. The slope describing QTc prolongation in this study was 0.00300 ms/ng/mL, translating to an average prolongation of 10.8 ms. There was a high degree of confidence in this value since the 95% CI constructed about the moxifloxacin slope was relatively narrow and did not include zero (0.00207 to 0.00393 ms/ng/mL).

Results of the tolterodine/DD01 analysis indicated a population slope estimate (95% CI) of 13.4 (6.90 to 21.9) ms/ng/mL. This parameter was well-estimated as evidenced by the relative standard error of 26.7%. CI constructed about the placebo and baseline model parameters enclosed the null value, suggesting that these were essentially zero. Additionally, the potency parameter 95% CI also enclosed zero, but this was retained in the model as there are pre-clinical data supporting differences in HERG blockade between tolterodine and DD01 metabolite. This result was most likely due to the relatively small numbers of subjects in the study. Residual variability was low, 8.20 ms when expressed as a standard deviation.

The current analysis of tolterodine/DD01 data indicated that tolterodine administration elicited only a small effect on the QTc interval. However, since PM subjects exhibited higher concentrations of tolterodine, they potentially represent a group with greater QTc interval prolongation. Separating the population of subjects by genotype, an estimate of prolongation was determined for EM and PM subjects by dose level, by identifying the respective dose-specific mean C_{max} . Tolterodine appeared to cause a small QTc interval prolongation which is at or below the threshold of clinical significance in EM subjects, irrespective of dose (2.59 and 5.13 ms for the 2 and 4 mg BID doses, respectively). This statement is supported by the current ICH E14 concept paper suggesting that a mean change of "around 5 ms" in the QT/QTc interval is viewed as clinically not important (13).

PM subjects administered the recommended dose of tolterodine appeared to exhibit a small QTc interval prolongation (5.44 ms) which is at the threshold of clinical significance; the model-predicted magnitude of effect in EMs given the suprathreshold dose is similar to that in PMs given the recommended dose of tolterodine. The suprathreshold dose of tolterodine was predicted to prolong QTc interval in PM subjects by 11.1 ms. Although the effect in PMs receiving the suprathreshold tolterodine dose was above 5 ms, it remained well below the 20 ms threshold above which drugs have a substantially increased likelihood of being proarrhythmic, and might have clinical arrhythmic events captured during drug development (13,19). Overall, the results of this analysis support a conclusion that tolterodine administration at recommended doses (2 mg BID) to all subjects or twice the recommended dose to EM subjects appears to have a low potential for QT prolongation.

Model performance was assessed and validated by a predictive check. Essentially, this method of validation assessed the ability of the model to reproduce the observed data. A particular characteristic of the data, maximum $\Delta QTcP$ in this study, was summarized from both observed and simulated data. Concordance of these summaries is an indication of acceptable model performance. Following simulation of 250 trial replications, maximum $\Delta QTcP$ distributions by dose level and genotype were constructed. The respective mean observed maximum $\Delta QTcP$ was then superimposed onto each distribution. Since the observation of maximum $\Delta QTcP$ by dose level and genotype was positioned centrally in each distribution, the model performed very well, validating conclusions drawn from the modeling effort.

Lastly, simulations of expected extreme responders support above statements on prolongation potential. The categorical analysis of these data indicates that the median percentage of subjects predicted to exhibit borderline prolongation (> 30 and ≤ 60 ms) was small

following administration of the recommended dose of 2 mg BID, irrespective of genotype status (1.92% and 4.55% for EM and PM subjects, respectively). The percentage of EM subjects predicted to show borderline prolongation at the suprathreshold dose was also small (3.85%), indicating minimal prolongation potential. A somewhat greater percentage of PM subjects (9.09%) were predicted to have borderline prolongation upon administration of the suprathreshold dose. QTc interval prolongation of clinical concern (> 60 ms) was not predicted at either dose, irrespective of metabolizer status, as median percent of subjects predicted to exhibit prolongation was zero. Based upon these simulations, there appears to be minimal potential of any subject being classified as an extreme responder to tolterodine and DD01 metabolite.

In conclusion, the systemic exposures of tolterodine, its DD01 metabolite and moxifloxacin were consistent with previous reported results. Based on the exposure-response analysis of data collected from a thorough QT study, tolterodine appears to have a low potential for QT prolongation. Model-predicted mean changes in QTc for both tolterodine and moxifloxacin were consistent with the corresponding statistical estimates. Based on simulation of 250 trials, no subjects were predicted to have increase of > 60 ms; the predicted incidence of borderline QTc increases (> 30 but less than ≤ 60 ms) remained low at the suprathreshold tolterodine dose in both PMs and EMs. These analyses confirm our clinical experience that tolterodine does not have a clinically significant effect on QT interval.

Acknowledgements

Dr. Gastonguay is a paid consultant and Drs. Sweeney, Glue, Malhotra, Cronenberger and Benincosa are employees of Pfizer.

References

1. Nilvebrant L, Andersson KE, Gillberg PG, Stahl M, Sparf B. Tolterodine – a new bladder-selective antimuscarinic agent. *Eur J Pharmacol.* 1997; 327:195-207.
2. Rentzhog L, Stanton SL, Cardozo L, Nelson E, Fall M, Abrams P. Efficacy and safety of tolterodine in patients with detrusor instability: a dose-ranging study. *Br J Urol.* 1998; 81:42-48.
3. Guay DR. Clinical pharmacokinetics of drugs used to treat urge incontinence. *Clin Pharmacokinet.* 2003; 42:1243-1285.
4. Brynne N, Stahl MM, Hallén B, Edlund PO, Palmér L, Höglund P, Gabriellson J. Pharmacokinetics and pharmacodynamics of tolterodine in man: a new drug for the treatment of urinary bladder overactivity. *Int J Clin Pharmacol Ther.* 1997; 35:287-295.
5. Postlind H, Danielson A, Lindgren A, Andersson SH. Tolterodine, a new muscarinic receptor antagonist, is metabolized by cytochromes P450 2D6 and 3A in human liver microsomes. *Drug Metab Dispos.* 1998;

- 26:289-293.
6. Bertilsson L, Dahl ML. Polymorphic drug oxidation - relevance to the treatment of psychiatric disorders. *CNS Drugs*. 1996; 5:200-223.
 7. Brynne N, Dalen P, Alvan G, Bertilsson L, Gabrielsson J. Influence of CYP2D6 polymorphism on the pharmacokinetics and pharmacodynamic of tolterodine. *Clin Pharmacol Ther*. 1998; 63:529-539.
 8. Brynne N, Forslund C, Hallen B, Gustafsson LL, Bertilsson L. Ketoconazole inhibits the metabolism of tolterodine in subjects with deficient CYP2D6 activity. *Br J Clin Pharmacol*. 1999; 48:564-572.
 9. Nilvebrant L, Gillberg PG, Sparf B. Antimuscarinic potency and bladder selectivity of PNU-200577, a major metabolite of tolterodine. *Pharmacol Toxicol*. 1997; 81:169-172.
 10. Pharmacia & Upjohn Company. US product label for Detrol[®] (tolterodine tartrate tablets). 2006.
 11. Pharmacia & Upjohn Company. US product label for Detrol LA[®] (tolterodine tartrate extended release capsules). 2006.
 12. Kang J, Chen XL, Wang H, Ji J, Reynolds W, Lim S, Hendrix J, Rampe D. Cardiac ion channel effects of tolterodine. *J Pharmacol Exp Ther*. 2004; 308:935-940.
 13. The clinical evaluation of QT/QTc interval prolongation and proarrhythmic potential for non-antiarrhythmic drugs – ICH harmonised tripartite guideline E14 (2005). Available at: www.ich.org. (Accessed: September 11, 2007).
 14. Malhotra BK, Glue P, Sweeney K, Anziano R, Mancuso J, Wicker P. Thorough QT study with recommended and supratherapeutic doses of tolterodine. *Clin Pharmacol Ther*. 2007; 81:377-385.
 15. Hodges M. Rate correction of the QT interval. *Cardiac Electrophysiol Rev*. 1997; 3:360-363.
 16. Tozer T. Implications of altered plasma protein binding in disease states. In: Benet L, Massoud N, Gambertoglio J, eds. *Pharmacokinetic Basis for Drug Treatment*. Raven Press, New York, 1984.
 17. Pahlman I, Gozzi P. Protein binding of tolterodine and its major metabolites in human and several animal species. *Biopharm Drug Dispos*. 1999; 20:91-99.
 18. Bayer Pharmaceuticals Corporation. US product label for Avelox[®] (moxifloxacin tablets). 2004.
 19. Shah RR. Drug-induced QT dispersion: does it predict the risk of torsade de pointes? *J Electrocardiol*. 2005; 38:10-18.

(Received February 25, 2009; Revised November 5, 2009; Accepted November 17, 2009)

Drug Discoveries & Therapeutics

Guide for Authors

1. Scope of Articles

Drug Discoveries & Therapeutics mainly publishes articles related to basic and clinical pharmaceutical research such as pharmaceutical and therapeutical chemistry, pharmacology, pharmacy, pharmacokinetics, industrial pharmacy, pharmaceutical manufacturing, pharmaceutical technology, drug delivery, toxicology, and traditional herb medicine. Studies on drug-related fields such as biology, biochemistry, physiology, microbiology, and immunology are also within the scope of this journal.

2. Submission Types

Original Articles should be reports new, significant, innovative, and original findings. An Article should contain the following sections: Title page, Abstract, Introduction, Materials and Methods, Results, Discussion, Acknowledgments, References, Figure legends, and Tables. There are no specific length restrictions for the overall manuscript or individual sections. However, we expect authors to present and discuss their findings concisely.

Brief Reports should be short and clear reports on new original findings and not exceed 4000 words with no more than two display items. *Drug Discoveries & Therapeutics* encourages younger researchers and doctors to report their research findings. Case reports are included in this category. A Brief Report contains the same sections as an Original Article, but Results and Discussion sections must be combined.

Reviews should include educational overviews for general researchers and doctors, and review articles for more specialized readers.

Policy Forum presents issues in science policy, including public health, the medical care system, and social science. Policy Forum essays should not exceed 2,000 words.

News articles should not exceed 500 words including one display item. These articles should function as an international news source with regard to topics in the life and social sciences and medicine. Submissions are not restricted to journal staff - anyone can submit news articles on subjects that would be of interest to *Drug Discoveries & Therapeutics'* readers.

Letters discuss material published in *Drug Discoveries & Therapeutics* in the last 6 months or issues of general interest. Letters should not exceed 800 words and 6 references.

3. Manuscript Preparation

Preparation of text. Manuscripts should be written in correct American English and submitted as a Microsoft Word (.doc) file in a single-column format. Manuscripts must be paginated and double-spaced throughout. Use Symbol font for all Greek characters. Do not import the figures into the text file but indicate their approximate locations directly on the manuscript. The manuscript file should be smaller than 5 MB in size.

Title page. The title page must include 1) the title of the paper, 2) name(s) and affiliation(s) of the author(s), 3) a statement indicating to whom correspondence and proofs should be sent along with a complete mailing address, telephone/fax numbers, and e-mail address, and 4) up to five key words or phrases.

Abstract. A one-paragraph abstract consisting of no more than 250 words must be included. It should state the purpose of the study, basic procedures used, main findings, and conclusions.

Abbreviations. All nonstandard abbreviations must be listed in alphabetical order, giving each abbreviation followed by its spelled-out version. Spell out the term upon first mention and follow it with the abbreviated form in parentheses. Thereafter, use the abbreviated form.

Introduction. The introduction should be a concise statement of the basis for the study and its scientific context.

Materials and Methods. Subsections under this heading should include sufficient instruction to replicate experiments, but well-established protocols may be simply referenced. *Drug Discoveries & Therapeutics* endorses the principles of the Declaration of Helsinki and expects that all research involving humans will have been conducted in accordance with these principles. All laboratory animal studies must be approved by the authors' Institutional Review Board(s).

Results. The results section should provide details of all of the experiments that are required to support the conclusions of the paper. If necessary, subheadings may be used for an orderly presentation. All figures, tables, and photographs must be referred in the text.

Discussion. The discussion should include conclusions derived from the study and supported by the data. Consideration should be given to the impact that these conclusions have on the body of knowledge in which context the experiments were conducted. In Brief Reports, Results and Discussion sections must be combined.

Acknowledgments. All funding sources should be credited in the Acknowledgments section. In addition, people who contributed to the work but who do not fit the criteria for authors should be listed along with their contributions.

References. References should be numbered in the order in which they appear in the text. Cite references in text using a number in parentheses. Citing of unpublished results and personal communications in the reference list is not recommended but these sources may be mentioned in the text. For all references, list all authors, but if there are more than fifteen authors, list the first three authors and add "et al." Abbreviate journal names as they appear in PubMed. Web references can be included in the reference list.

Example 1:

Hamamoto H, Akimitsu N, Arimitsu N, Sekimizu K. Roles of the Duffy antigen and glycoprotein A in malaria infection and erythrocyte. *Drug Discov Ther.* 2008; 2:58-63.

Example 2:

Zhao X, Jing ZP, Xiong J, Jiang SJ. Suppression of experimental abdominal aortic aneurysm by tetracycline: a preliminary study. *Chin J Gen Surg.* 2002; 17:663-665. (in Chinese)

Example 3:

Mizuochi T. Microscale sequencing of N-linked oligosaccharides of glycoproteins using hydrazinolysis, Bio-Gel P-4, and sequential exoglycosidase digestion. In: *Methods in Molecular Biology: Vol. 14 Glycoprotein analysis in biomedicine* (Hounsell T, ed.). Humana Press, Totowa, NJ, USA, 1993; pp. 55-68.

Example 4:

Drug Discoveries & Therapeutics. Hot topics & news: China-Japan Medical Workshop on Drug Discoveries and Therapeutics 2007. <http://www.ddtjournal.com/hotnews.php> (accessed July 1, 2007).

Figure legends. Include a short title and a short explanation. Methods described in detail in the Materials and methods section should not be repeated in the legend. Symbols used in the figure must be explained. The number of data points represented in a graph must be indicated.

Tables. All tables should have a concise title and be typed double-spaced on pages separate from the text. Do not use vertical rules. Tables should be numbered with Arabic numerals consecutively in accordance with their appearance in the text. Place footnotes to tables below the table body and indicate them with lowercase superscript letters.

Language editing. Manuscripts submitted by authors whose primary language is not English should have their work proofread by a native English speaker before submission. The Editing Support Organization can provide English proofreading, Japanese-English translation, and Chinese-English translation services to authors who want to publish in *Drug Discoveries & Therapeutics* and need assistance before submitting an article. Authors can contact this organization directly at <http://www.iacmhr.com/iac-eso>.

IAC-ESO was established in order to facilitate manuscript preparation by researchers whose native language is not English and to help edit work intended for international academic journals. Quality revision, translation, and editing services are offered by our staff, who are native speakers of particular languages and who are familiar with academic writing and journal editing in English.

4. Figure Preparation

All figures should be clear and cited in numerical order in the text. Figures must fit a one- or two-column format on the journal page: 8.3 cm (3.3 in.) wide for a single column; 17.3 cm (6.8 in.) wide for a double column; maximum height: 24.0 cm (9.5 in.). Only use the following fonts in the figure: Arial and Helvetica. Provide all figures as separate files. Acceptable file formats are JPEG and TIFF. Please note that files saved in JPEG or TIFF format in PowerPoint lack sufficient resolution for publication. Each Figure file should be smaller than 10 MB in size. Do not compress files. A fee is charged for a color illustration or photograph.

5. Online Submission

Manuscripts should be submitted to *Drug Discoveries & Therapeutics* online at <http://www.ddtjournal.com>. The manuscript file should be smaller than 10 MB in size. If for any reason you are unable to submit a file online, please contact the Editorial Office by e-mail: office@ddtjournal.com

Editorial and Head Office

Wei TANG, MD PhD
Executive Editor
Drug Discoveries & Therapeutics
TSUIN-IKIZAKA 410,
2-17-5 Hongo, Bunkyo-ku,
Tokyo 113-0033, Japan.
Tel: 03-5840-9697
Fax: 03-5840-9698
E-mail: office@ddtjournal.com

Cover letter. A cover letter from the corresponding author including the following information must accompany the submission: name, address, phone and fax numbers, and e-mail address of the corresponding author. This should include a statement affirming that all authors concur with the

submission and that the material submitted for publication has not been previously published and is not under consideration for publication elsewhere and a statement regarding conflicting financial interests.

Authors may recommend up to three qualified reviewers other than members of Editorial board. Authors may also request that certain (but not more than three) reviewers not be chosen.

The cover letter should be submitted as a Microsoft Word (.doc) file (smaller than 1 MB) at the same time the work is submitted online.

6. Accepted Manuscripts

Proofs. Rough galley proofs in PDF format are supplied to the corresponding author *via* e-mail. Corrections must be returned within 4 working days of receipt of the proofs. Subsequent corrections will not be possible, so please ensure all desired corrections are indicated. Note that we may proceed with publication of the article if no response is received.

Transfer of copyrights. Upon acceptance of an article, authors will be asked to agree to a transfer of copyright. This transfer will ensure the widest possible dissemination of information. A letter will be sent to the corresponding author confirming receipt of the manuscript. A form facilitating transfer of copyright will be provided. If excerpts from other copyrighted works are included, the author(s) must obtain written permission from the copyright owners and credit the source(s) in the article.

Cover submissions. Authors whose manuscripts are accepted for publication in *Drug Discoveries & Therapeutics* may submit cover images. Color submission is welcome. A brief cover legend should be submitted with the image.

Revised April 20, 2009



Drug Discoveries & Therapeutics



Editorial Office

TSUIN-IKIZAKA 410,
2-17-5 Hongo, Bunkyo-ku,
Tokyo 113-0033, Japan

Tel: 03-5840-9697

Fax: 03-5840-9698

E-mail: office@ddtjournal.com

URL: www.ddtjournal.com

JOURNAL PUBLISHING AGREEMENT

Ms No:

Article entitled:

Corresponding author:

To be published in Drug Discoveries & Therapeutics

Assignment of publishing rights:

I hereby assign to International Advancement Center for Medicine & Health Research Co., Ltd. (IACMHR Co., Ltd.) publishing Drug Discoveries & Therapeutics the copyright in the manuscript identified above and any supplemental tables and illustrations (the articles) in all forms and media, throughout the world, in all languages, for the full term of copyright, effective when and if the article is accepted for publication. This transfer includes the rights to provide the article in electronic and online forms and systems.

I understand that I retain or am hereby granted (without the need to obtain further permission) rights to use certain versions of the article for certain scholarly purpose and that no rights in patent, trademarks or other intellectual property rights are transferred to the journal. Rights to use the articles for personal use, internal institutional use and scholarly posting are retained.

Author warranties:

I affirm the author warranties noted below.

- 1) The article I have submitted to the journal is original and has not been published elsewhere.
- 2) The article is not currently being considered for publication by any other journal. If accepted, it will not be submitted elsewhere.
- 3) The article contains no libelous or other unlawful statements and does not contain any materials that invade individual privacy or proprietary rights or any statutory copyright.
- 4) I have obtained written permission from copyright owners for any excerpts from copyrighted works that are included and have credited the sources in my article.
- 5) I confirm that all commercial affiliations, stock or equity interests, or patent-licensing arrangements that could be considered to pose a financial conflict of interest regarding the article have been disclosed.
- 6) If the article was prepared jointly with other authors, I have informed the co-authors(s) of the terms of this publishing agreement and that I am signing on their behalf as their agents.

Your Status:

I am the sole author of the manuscript.

I am one author signing on behalf of all co-authors of the manuscript.

Please tick one of the above boxes (as appropriate) and then sign and date the document in black ink.

Signature:

Date:

Name printed:

Please return the completed and signed original of this form by express mail or fax, or by e-mailing a scanned copy of the signed original to:

**Drug Discoveries & Therapeutics office
TSUIN-IKIZAKA 410, 2-17-5 Hongo,
Bunkyo-ku, Tokyo 113-0033, Japan
e-mail: proof-editing@ddtjournal.com
Fax: +81-3-5840-9698**

